SCHOOL OF CHEMISTRY

CARDIFF UNIVERSITY

DIHYDROFOLATE REDUCTASE AND THE PHYSICAL BASIS OF ENZYME CATALYSIS

A thesis submitted to Cardiff University for the degree of Doctor of Philosophy

by

Enas Mamdouh Behiry

Supervisor: Prof. Rudolf K. Allemann **2013**

DECLARATION

This work has not previously been accepted in substance for any degree and is not being concurrently submitted in candidature for any degree.

Signed…… (Candidate)
Date……

STATEMENT 1
This thesis is being submitted in partial fulfilment of the requirements for the degree of Doctor of Philosophy.

Signed…… (Candidate)
Date……

STATEMENT 2
This thesis is the result of my own independent work/investigation, except where otherwise stated. Other sources are acknowledged by explicit references.

Signed…… (Candidate)
Date……

STATEMENT 3
I hereby give consent for my thesis, if accepted, to be available for photocopying and for interlibrary loan, and for the title and summary to be made available to outside organisations.

Signed…… (Candidate)
Date……

DEDICATION

To my father & mother, brothers & sisters

To my husband Alaa

To my children, Yasmin, Nour & Abdulrahman

Acknowledgment

It is with pleasure that I would like to acknowledge and express particular thanks to my supervisor, Prof. Rudolf Allemann for giving me the opportunity to participate in this work and for his constant support, guidance, and patience throughout the course of my PhD. My extended thanks and gratitude are also due to Dr Mahmoud Akhtar for continous support and always being ready to help during the time of my study.

I express my sincere thanks to Dr Joel Loveridge for his guiding, precious suggestions and advice during the course of my study and for proof reading this thesis, thank you for everything. I am grateful to Dr Eric Tippmann and Dr Niklaas Buurma for the help and for the useful discussions during my *viva*.

Also I would like to thank all my colleagues in the DHFR project, especially Dr Rhiannon Evans, Dr Lai-Hock Tai and Dr Louis Luk, for all the help they offered. I extend my thanks to all my colleuges in the Allemann group for their input and support. A special thanks goes to Dr Verónica González for the help in the laboratory, and to Dr Robert Mart and Dr Juan Faraldos for helping in the synthetic part of this work. I also would like to thank all the chemistry academic staff and the technical staff in the School of Chemistry for their continued support and help.

Many thanks to Dr Christian Ludwig, Dr Sara Whittaker and Prof. Ulrich Günther (NMR facilities at School of Cancer Studies, University of Birmingham), I have had the pleasure of working with you.

I want to express my gratitude to my parents for helping me to reach this stage in my life. Also, I would like to thank all my family and my friends for their love, care and for always encouraging me to keep going. A special "Thank you" for my husband Dr Alaa El-Betany for his endless patience, sacrifice, understanding and encouragement throughout the course of this study. "Without you I would not do it".

Finally, this study could not have been completed without the help, guidance and inspiration of Allah; the Lord of the universe

Abstract

Dihydrofolate reductase (DHFR) is the enzyme that catalyses the reduction of 7,8-dihydrofolate (DHF) to 5,6,7,8-tetrahydrofolate (THF) in the presence of the cofactor reduced nicotinamide adenine dinucleotide phosphate (NADPH). The DHFR catalysed reaction has often been used to study enzymatic tunnelling and the contribution of protein dynamics to catalysis. To gain a better understanding of such phenomena and to investigate the key elements of structural adaptation in DHFR, in this thesis the hydride transfer reaction of DHFR from *Moritella profunda* (MpDHFR), a cold adapted enzyme, was studied and compared to the mesophilic and extensively studied enzyme from *Escherichia coli* (EcDHFR) and the thermophilic enzyme from *Thermotoga maritima* (TmDHFR). Chapter 1 gives a brief introduction to the thesis. Description of the materials and methods used in evaluating this work is reported in Chapter 2. In Chapter 3, the steady state and pre-steady state temperature dependences of the kinetic isotope effect (KIE) for the MpDHFR catalysed reaction was elevated, compared to data obtained for the mesophilic and the thermophilic DHFR homologues and the results interpreted according to the environmentally coupled tunnelling model. The work presented in Chapters 4 and 5 has investigated the role of dynamics during catalysis by DHFR using site directed mutagenesis. In Chapter 4, mutations were created in the GH loop for both EcDHFR and MpDHFR to elucidate the role of the occluded conformation during catalysis by DHFR. In Chapter 5, different MpDHFR and EcDHFR variants in the highly mobile M20 loop were generated and their temperature dependences of KIE were studied in addition to studying the two variants MpDHFR-G123V and MpDHFR-D124N in the catalytically important FG loop. The results obtained suggest that MpDHFR does not undergo the dynamical loop movements that have been recognized previously for EcDHFR in spite of following the same catalytic cycle. Further findings were found which contradict the current models that relate protein dynamics to catalysis efficiency, thus modifying these models has become essential. Chapter 6 has focused on studying the effect of different denaturants/salt concentrations on MpDHFR chemical step. Finally, a summary of the work presented in this thesis and future guidelines are provided in Chapter 7.

Abbreviations

A	absorption
A	Arrhenius pre-exponential factor
ADB	adenosine-binding domain
ADP	adenosine diphosphate
AMP	ampicillin
APS	ammonium persulfate
ATP	adenosine triphosphate
BaDHFR	dihydrofolate reductase from *Bacillus anthracis*
βME	β–mercaptoethanol
BsDHFR	dihydrofolate reductase from *Geobacillus stearothermophilus*
Conc.	concentration
CBD	cofactor binding domain
CD	circular dichroism spectroscopy
CV	column volume
D	deuterium
DAD	donor-acceptor distance
DCC	dicyclohexylcarbodiimide
DDF	5,10-dideazatetrahydrofolate
DEAE	diethylaminoethyl
Df	dilution factor
dH_2O	deionised water
DHF	7,8-dihydrofolate
DHFR	dihydrofolate reductase
DMF	dimethylformamide
DNA	deoxyribose nucleic acid
dNTP	deoxynucleotide triphosphate
dTMP	deoxythymidine monophosphate
DTT	dithiothreitol
dUMP	deoxyuridine monophosphate
E_a	activation energy

E	enzyme
$[E]_0$	total enzyme concentration
EDTA	ethylenediaminetetraacetic acid
ES	enzyme-bound substrate complex
EXP	Swain-Schaad exponent
F.C. term	Franck-Condon nuclear overlap term
FPLC	fast performance liquid chromatography
FRET	Förster/fluorescence resonance energy transfer
G	permeability of the barrier
Gdn-HCl	guanidine hydrochloride
H	Planck's constant = 6.626176 x 10-34 J s
$\hbar$	Planck's constant divided by 2π, $\hbar$ = 1.054588664 x 10^{-34} J s
H	hydrogen (protium)
HsDHFR	human dihydrofolate reductase
HOBt	hydroxybenzotriazole
HPLC	high pressure/performance liquid chromatography
IPTG	isopropyl-β-D-1-thiogalactopyranoside
KIE	kinetic isotope effect
K	rate constant
K_b	Boltzmann constant = 1.3806503×10^{-23} J K^{-1}
k_{cat}	steady state rate constant or the turnover number
K_M	Michaelis constant
K_S	substrate dissociation constant
k_{sc}	the semi-classical rate constant
k_{tun}	the rate of tunnelling
K_iPO_4	potassium phosphate
L	pathlength
LB	Luria-Bertani growth media
LcDHFR	dihydrofolate reductase from *Lactobacillus casei*
LD	loop domain
m_x	atomic mass
MaDHFR	dihydrofolate reductase from *Mycobacterium avium*
MES	morpholinoethanesulfonic acid

MpDHFR	dihydrofolate reductase from *Moritella profunda*
MtDHFR	dihydrofolate reductase from *Mycobacterium tuberculosis*
MmDHFR	dihydrofolate reductase from *Mus musculus* (mouse)
MyDHFR	dihydrofolate reductase from *Moritella yayanosii*
MTEN	MES Tris ethanolamine sodium chloride
MTX	methotrexate
NAD^+	oxidised nicotinamide adenine dinucleotide
NADase	nicotinamide adenine dinucleotide glycohydrolase
$NADP^+$	oxidised nicotinamide adenine dinucleotide phosphate
NADPD	$4R^{-2}H$ reduced nicotinamide adenine dinucleotide phosphate
NADPH	reduced nicotinamide adenine dinucleotide phosphate
NMR	nuclear magnetic resonance
OD	optical density
P	product
PAGE	polyacrylamide gel electrophoresis
PCR	polymerase chain reaction
PDB	protein data bank
PYR	Pyrimethamine
Q	gating coordinate
Q_{env}	the environmental free energy surface
Q_t	tunnelling correction
R	Reactant
R	general gas constant
RCF	relative centrifugal force
r_x	tunnelling distance for the transferring isotope
RNase	Ribonuclease
Rpm	revolutions per minute
S	Substrate
SBD	substrate-binding domain
SDS-PAGE	sodium dodecyl sulfate-polyacrylamide gel electrophoresis
SpDHFR	dihydrofolate reductase from *Streptococcus pneumoniae*
SvDHFR	dihydrofolate reductase from *Shewanella violacea*
T	absolute temperature

T	Tritium
TbADH	alcohol dehydrogenase from *Thermoanaerobacter brockii*
TMP	Trimethoprin
TS	thymidelate synthase
TS	transition state
TST	transition state theory
TEMED	N,N,N',N'-tetramethylenediamine
THF	5,6,7,8-tetrahydrofolate
TM	melting temperature
TmDHFR	dihydrofolate reductase from *Thermotoga maritime*
TMP	Trimethoprim
TRC	tunnelling ready conformation
Tris	tris(hydroxymethyl)aminomethane
TS	thymidylate synthase
TST	transition state theory
UV/Vis	ultraviolet/visible spectroscopy
ε	extinction coefficient
v_0	velocity of the reaction
V_{max}	maximal velocity
$(V_{max}/2)$	half maximum velocity
X	gating coordinate
ZPE	zero point energy
ΔG^o	reaction free energy
$\Delta G^{\ddagger}$	free activation energy of the reaction
$\Delta H^{\ddagger}$	activation enthalpy
$\Delta S^{\ddagger}$	activation entropy
λ	reorganisation energy
λ_B	de Broglie wavelength
$\upsilon_{H/D}$	vibrational frequency for hydrogen/deuterium
σ	standard deviation
σ_M	standard error of the mean
Θ	ellipticity in millideg

Θ_{MRE}	mean residue ellipticity
μ_x	reduced mass
υ_x	vibrational frequency of gating
ω_x	gating frequency
‡	the reactive configuration

Amino Acid	**1 letter code**	**3 letter code**
Alanine	A	Ala
Arginine	R	Arg
Asparagine	N	Asn
Aspartic acid	D	Asp
Cysteine	C	Cys
Glutamic acid	E	Glu
Glutamine	Q	Gln
Glycine	G	Gly
Histidine	H	His
Isoleucine	I	Ile
Leucine	L	Leu
Lysine	K	Lys
Methionine	M	Met
Phenylalanine	F	Phe
Proline	P	Pro
Serine	S	Ser
Threonine	T	Thr
Tryptophan	W	Trp
Tyrosine	Y	Tyr
Valine	V	Val

List of figures

List of tables

Table of contents

1

Introduction

1.1 Enzyme kinetics

Enzymes catalyze chemical reactions at rates that are astonishingly rapid relative to uncatalyzed reactions under the same conditions (typically from 10^5 up to 10^{22} fold faster). Thus, the catalytic rate enhancement imposed by enzymes has attracted the attention of chemists for more than a century. In the absence of enzymes, some chemicals would require 300 to 30,000,000 years to react. Therefore, enzymes are essential to maintain biological activity under physiological conditions.[1-3]

To elucidate the mechanism of enzymatic reactions, it is important to understand the specific interactions between the substrate and its enzyme environment and their effect on the reaction rate. Enzyme kinetics is the study of the rate at which an enzyme works. The field of enzyme kinetics has undergone significant growth over the past years, accompanied by the development of several models for enzyme catalysis, and a true understanding of the principles which motivate the resulting rate equations. As a result, it is possible to write equations for the velocity in the presence of all reactants, predict the effect of altering the concentration of any reactant and propose the kinetic mechanism from experimental data.[4-5]

Over the years, our understanding of enzymatic catalysis has evolved in parallel with the development of experimental tools to investigate chemical and kinetic mechanisms. In this thesis, steady state and pre-steady state kinetics and kinetic isotope effects were used to study the hydride transfer reaction catalysed by dihydrofolate reductase (DHFR). The theoretical bases of these techniques are discussed below.

1.1.1 Steady state and pre-steady state kinetics

Steady state kinetic studies can be used to determine the order of addition and release of reactants and products and where the major rate limiting steps are in a mechanism. However, to determine the intrinsic rate constants and to characterize intermediates, usually pre-steady state experiments are used.[6] For example, the chemical step during catalysis by DHFR can be measured at physiological pH only under pre-steady state conditions and not steady state conditions where product release is the rate limiting step.[7]

The initial rate of a given reaction is described mathematically by a rate equation. An enzyme catalysed reaction can described by the mechanism given below

$$E + S \underset{k_{-1}}{\overset{k_1}{\rightleftharpoons}} ES \xrightarrow{k_2} P \qquad (1.1)$$

Equation 1.1 describes the conversion of the substrate (S) into product (P), *via* the enzyme-bound substrate complex (ES). Substrate binds to enzyme with the second order rate constant k_1. It can then dissociate with first order rate constant k_{-1} to give free enzyme, or it can be converted to product with first order rate constant k_2.

Enzyme catalysed reactions are typically assumed to be at steady state, where the rates of formation and decay of the intermediates are equal.[8] We can consider this situation in terms of Equation 1.1. When k_{-1} is greater than k_2, then the relative concentrations of free substrate [S], free enzyme [E] and the enzyme-substrate complex [ES] can be described by the substrate dissociation constant K_S, expressed in Equation 1.2.

$$K_S = \frac{k_{-1}}{k_1} = \frac{[E][S]}{[ES]} \qquad (1.2)$$

For an enzymatic reaction, at the beginning of the reaction the concentration of the enzyme-substrate complex rises from zero to its steady state value. During this time the steady state approximation is not applicable as the rate of formation of products is not equal to the rate of consumption of substrate (Equation 1.3). This brief period of time is known as "pre-steady state". The pre-steady state kinetics are simply defined as the enzyme kinetics that take place during the short time before the enzymes and reactants are able to reach the steady state (Figure 1.1).

$$\frac{\delta[S]}{\delta t} \neq \frac{\delta[P]}{\delta t} \qquad (1.3)$$

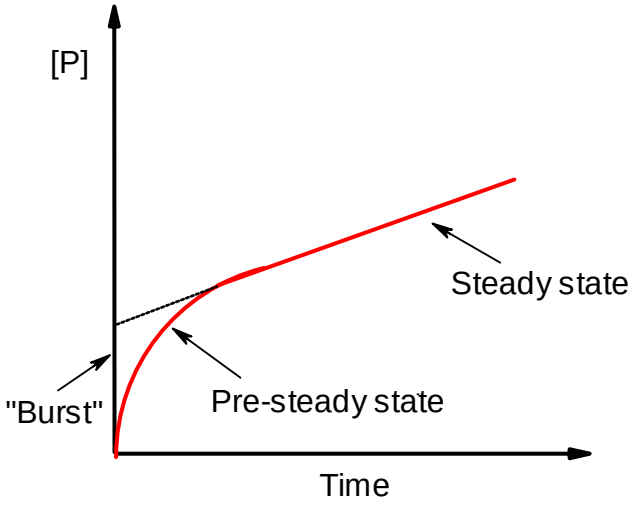

Figure 1.1: *Graphical description showing the change in product concentration over the reaction time. The initial burst represents the pre-steady state region that takes place before the reaction reaches the steady state conditions.*

When carrying out pre-steady state kinetic experiments, precautions are taken to work under pseudo first order conditions. These can be obtained when the enzyme concentration is much greater than the reactant concentrations. For experimental measurements of the pre-steady state rate constant, techniques that allow spectra of chromophoric reaction components to be collected in the millisecond time regime, such as stopped flow and rapid quench techniques, can be used (Figure 1.2). Quench-flow and stop-flow are designed to mix enzyme and reactants very rapidly to start the enzymatic reaction, and then quench it after a certain time. The reaction time ranges from about five milliseconds to several seconds. When studying catalysis by DHFR, only stopped flow kinetics were used. The quench-flow is used when the enzymatic reaction does not involve a component that can be spectrally monitored in real time.[6]

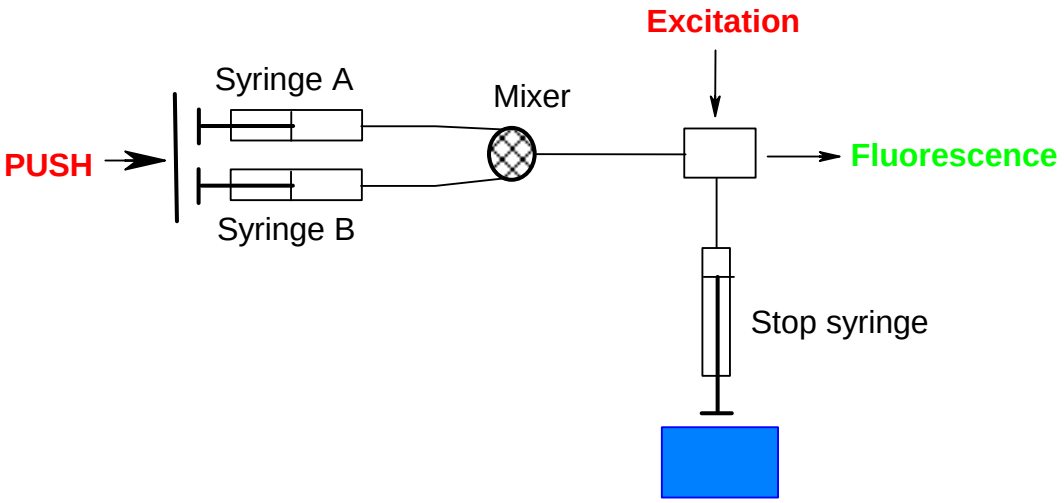

Figure 1.2: *Stopped flow / quenched flow spectrophotometer*

On the other hand, the steady state course can be reached when the rate of formation of product is equal to the rate of consumption of substrate (Equation 1.4) and can be studied using the methods of Michaelis and Menten.

$$\frac{\delta[ES]}{\delta t} = 0 \qquad (1.4)$$

Under steady state conditions, the rate of consumption of substrate or the rate of formation of product should change in a linear fashion (Figure 1.1). This can be obtained experimentally by making the concentrations of the substrates much greater than the concentration of the enzyme; such conditions will maintain a linear change in the substrate concentration over a longer period of time.

The steady state rate constant or the turnover number (k_{cat}) of the reaction can be calculated from the reaction velocity, as a function of the concentration of enzyme (Equation 1.5).

$$V_{max} = k_{cat}[E]_0 \qquad (1.5)$$

where V_{max} is the maximal velocity of the reaction, and $[E]_0$ is the total enzyme concentration. The simplest treatment of the steady state rate equation was provided by the Michaelis-Menten equation (Equation 1.6).

$$v_0 = \frac{[E]_0[S]k_{cat}}{K_M + [S]} \qquad (1.6)$$

where v_0 is the velocity of the reaction, $[E]_0$ is the total enzyme concentration, k_{cat} is the steady state rate constant, K_M is the Michaelis constant. This can be illustrated by plotting the substrate concentration against the enzyme velocity (Figure 1.3). At low substrate concentration the velocity of the reaction increases linearly with increasing substrate concentration [S]. At high substrate concentration, the velocity of the reaction will reach V_{max}, the maximal velocity of the reaction (Equation 1.5), and K_M can obtained by determining the substrate concentration at half maximum velocity ($V_{max}/2$) (Figure 1.3).

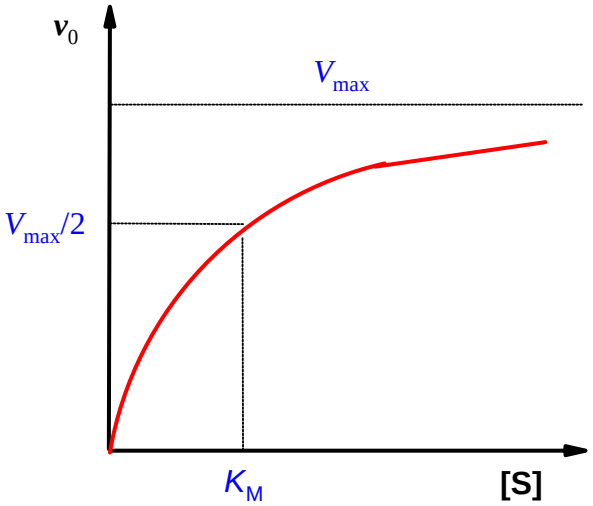

Figure 1.3: *A graphical representation of the Michaelis-Menten plot showing the relation between the reaction velocity (v_0) and substrate concentration [S]. The maximum velocity (V_{max}) and Michaelis constant (K_M) are shown on the graph.*

1.2 The physical basis of enzyme catalysis

Many years of research in enzymology have determined that enzymes undergo numerous conformational fluctuations during the catalytic cycle.[9-10] The questions discussed in this thesis mainly cover physical phenomena such as how enzyme dynamics and electrostatics contribute to enzyme catalysis, by evaluating the temperature dependency of kinetic isotope effects in hydride transfer reactions using different DHFR homologues.

In 1894 Emil Fischer proposed the lock-and-key enzyme model. Since that time, various explanations for the catalytic power of enzymes have been proposed.[11-12] In 1935, Eyring initiated the development of modern theories of the activated transition-state complex,[13] which was modified by Pauling ten years after.[14] Soon thereafter, Koshland proposed the "induced fit" mechanism, which is a modification of the lock and key model derived by Fischer.[15] More recently, hydrogen tunnelling was proposed to explain enzyme catalysis.[1-2,16-17] In recent years, many researchers have focused on exploring how enzyme dynamics contribute to catalysis.[10,18-19]

1.2.1 Kinetic isotope Effects (KIEs)

Isotope effects are powerful tools for studying the physical and biological basis of enzymatic reactions and are used to aid the understanding of reaction kinetics, mechanisms, and solvent effects. Kinetic isotope effects (KIEs) are measured by comparing the ratio of the rate of the reaction between two isotopologues, *i.e*. molecules that differ only in their isotopic composition. Primary (1˚) isotope effects are due to isotopic substitution at a site of bond breaking/forming in the rate determining step of a reaction while secondary (2˚) isotope effects occur at sites more distant from the reactive centre.[20] For instance, the primary kinetic isotope effect can be measured during the DHFR reaction by replacing the transferred (*pro*-R) hydrogen at C4 on the nicotinamide ring of the cofactor NADPH with deuterium, and comparing the relative rate constants with the different isotopically labelled cofactors (k_H/k_D).[21] A secondary KIE can be measured, for example, by isotopically substituting the *pro*-S hydrogen of NADPH.[22] In this work, only primary KIEs have been investigated.

1.2.2 Hydrogen Tunnelling in Enzymatic Reactions

A main concept of quantum mechanics is treating a particle in terms of its location and momentum as a wave of energy ('wave-particle duality').[23] Equation (1.7) is showing that the position and momentum of the particle depend on its mass,[24] defined by the de Broglie wavelength. In terms of

this expression, the lighter the particle in mass, the greater the uncertainty of its position and the higher its de Broglie wavelength.

$$\lambda_B = \sqrt{h/2mE} \qquad (1.7)$$

where λ_B is the uncertainty of the position of the transferred particle, *h* is the Planck's constant, *m* is the mass of the transferred particle and *E* is its energy.

Quantum mechanical tunnelling is the physical phenomenon by which a particle transfers through a reaction energy barrier by means of its wave-like properties (Figure 1.4).[25] The de Broglie wavelength is an important pattern to take into account when describing the tunnelling of particles through the energy barrier. For example, for light particles with small wavelengths such as the H-nucleus, assuming an energy of 20 kJ mol^{-1}, the de Broglie wavelength is calculated to be 0.63 Å for protium (H) and 0.45 A° for deuterium (D).[26] They are transferred over a similar distance (<1 Å) along a reaction coordinate, and have a positional uncertainty that gives a significant tunnelling probability.[26]

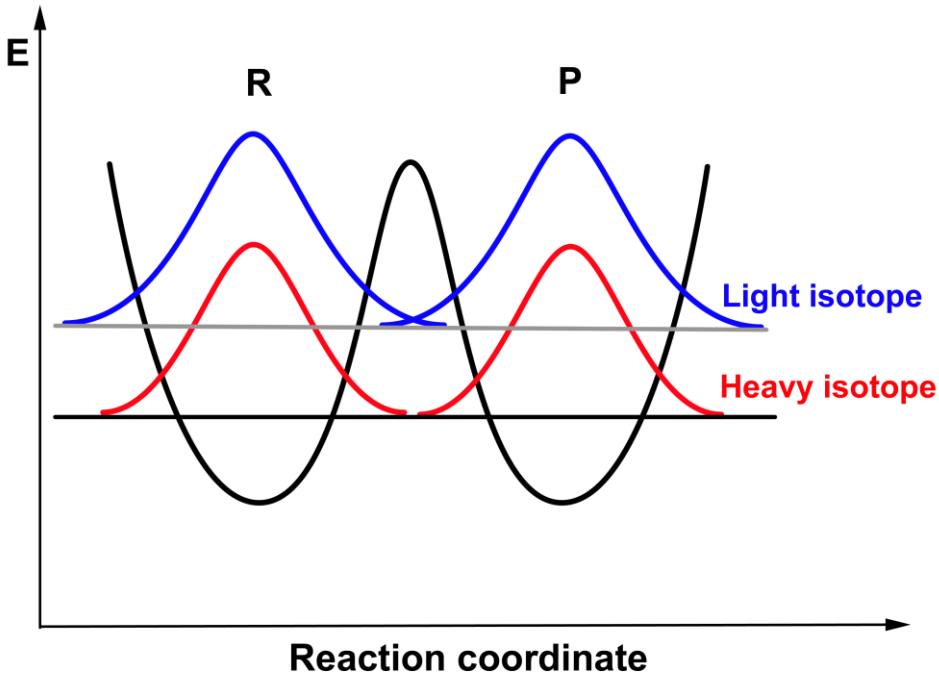

Figure 1.4: *Illustration of the tunnelling phenomenon along the reaction coordinate. The reactant well (R) is on the left and the product well (P) is on the right. The probability of finding the light and the heavy isotopes in the reactant or the product wells are shown in blue and red, respectively. More*

overlap between the probability functions of the reactants and products causes higher tunnelling probability.[27]

The tunnelling probability is also affected by many factors including certain properties of the particle, the distance between the donor and acceptor (donor-acceptor distance, DAD) and the symmetry of the reactant (R) and the product (P) wells.[28] A light isotope has a higher zero point energy and and its probability function is less localized in its well (more diffuse wavefunction), thus it has a higher tunnelling probability (Figure 1.4). Consequently, KIEs are useful tools for studying tunnelling.[29]

Analyzing the temperature dependence of KIEs using the Arrhenius equation is powerful experimental approach to examine the physical nature of H transfer reactions. According to the Arrhenius equation, the rate constant of the reaction is exponentially proportional to the activation energy and the inverse absolute temperature,

$$k = Ae^{\frac{-\Delta E_a}{RT}} \tag{1.8}$$

where k is the rate constant, A is the Arrhenius pre-exponential factor, and E_a is the reaction activation energy. Using the Arrhenius equation, the relationship between the KIE ($\frac{k_l}{k_h}$) and the absolute temperature (T) are represented in Equation 1.9.

$$KIE = \frac{k_l}{k_h} = \frac{A_l e^{\frac{-\Delta E_{al}}{RT}}}{A_h e^{\frac{-\Delta E_{ah}}{RT}}} = \frac{A_l}{A_h} e^{\frac{-\Delta E_{a(h-l)}}{RT}} \tag{1.9}$$

where k_x is the rate constant, A_x is the Arrhenius pre-exponential factor, and E_{ax} is activation energy for the transfer of isotope x. x=h and x=l represent the heavy and light isotopes, respectively. $E_{a(h\text{-}l)}$ represents the difference in activation energies for the reaction with heavy and light isotopes.

When ln(KIE) is plotted as a function of 1/T, the plot is typically linear. The slope is the difference in activation energies between two isotopes divided by the general gas constant ($\frac{-\Delta E_{a(h-l)}}{R}$), and the y-

axis intercept represents the logarithm of the ratio of Arrhenius pre-exponential factor for the light and heavy isotopes ($\ln A_l/A_h$). According to Equation 1.9, the temperature dependence/independence of KIEs corresponds to the difference in the energy of activation for the two isotopes (ΔE_a). Some of the models that have been proposed to explain the experimental results on the temperature dependence of KIEs are presented below.

1.2.2.1 Semi-classical models

Traditional literature treats enzyme catalyzed reactions, including hydrogen transfer, in terms of transition state theory (TST).[2] Almost all of the current discussions of isotope effects in chemical reactions are based on TST.[27,29] TST assumes that the reaction coordinate may be described by a minimum in free energy representing the reactant well and a maximum in free energy representing the saddle point or transition state (TS) leading to the formation of product (Figure 1.5). Semi-classically, a KIE is defined in terms of transition state theory by Equation 1.10.[29]

$$KIE = \frac{k_l}{k_h} = \frac{A_l}{A_h} e^{\left(\frac{\frac{1}{2}h\nu_l - \frac{1}{2}h\nu_h}{RT}\right)} \qquad (1.10)$$

where k_l and k_h are the rate constants for the light and heavy isotopic substrates, respectively and are expressed in Equation 1.11.

$$k_x = A_x e^{-\left(\frac{\Delta G^o - \frac{1}{2}h\nu_x}{RT}\right)} \qquad (1.11)$$

where ΔG^o is the free energy barrier, h is Planck's constant and υ_x is the particle vibrational frequency, A_x is a pre-exponential factor and x can be the light or the heavy isotopes. R is the general gas constant and T is the absolute temperature.

In H transfer reactions, the transferable hydrogen is labelled with one of the three isotopes of hydrogen, *i.e.*, protium (^{1}H, or H), deuterium (^{2}H, or D), or tritium (^{3}H, or T), taking into consideration that lighter isotopes have a higher zero point energy ($ZPE = ½\ h\upsilon$) than heavier isotopes (Figure 1.5). Therefore, the KIEs can be measured as k_H/k_T (H/T), k_H/k_D (H/D), or k_D/k_T (D/T). In the cases addressed here, the KIE significantly depends on the zero point energy of the transferred particle and neglects motions in the transition state.[29-30] Based on the semi-classical

models, a primary H/D KIE for C-H cleavage at 298 K is calculated to be 6.9 based on the stretching frequencies of a C-H bond and a C-D bond. Similarly, k_H/k_T is predicted to be 18. This arises because the stretching frequencies of a C-H bond, C-D bond and C-T bond are ~3000 cm^{-1}, 2200 cm^{-1} and 1800 cm^{-1}, respectively. Such models are not able to explain temperature independent KIE values or small KIEs with sharp temperature dependency.[26,31]

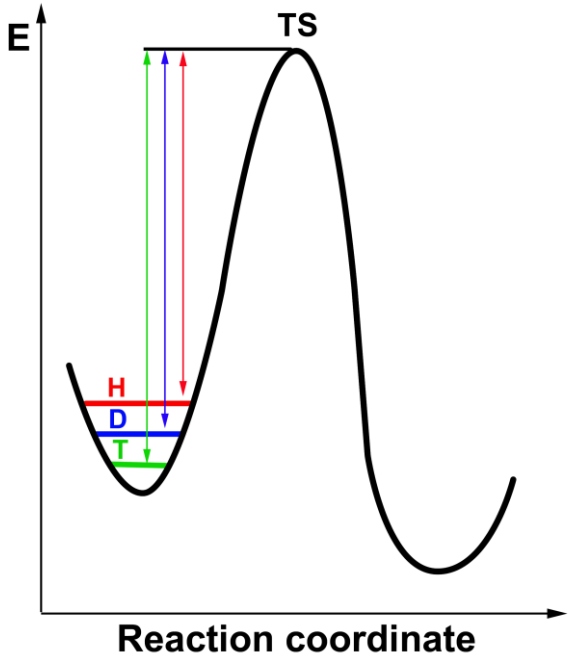

Figure 1.5: *Illustration of the energy barrier to an enzymatic reaction from a semi-classical point of view with the path of transfer for the three isotopes of hydrogen indicated.*

In 1958 Swain *et al*. proposed an equation that explains the kinetic relationships between reaction rate constants for the three hydrogen isotopes according to the differences in the zero-point energy. The Swain-Schaad exponential relationships (*EXP*) are the semi-classical corrections among the hydrogen three isotopes.[32] They can be represented using H as a reference,

$$\frac{k_H}{k_T} = \left(\frac{k_H}{k_D}\right)^{EXP_{HD}} \tag{1.12}$$

or using T as a reference,

$$\frac{k_H}{k_T} = \left(\frac{k_D}{k_T}\right)^{EXP_{DT}} \tag{1.13}$$

where *k* is the rate constant for each hydrogen isotope, and *EXP* represents the Swain-Schaad exponent, which is calculated based on differences in the zero-point energy between two hydrogen isotopes. EXP_{HD} and EXP_{DT} are for the relationship for H/T *vs*. H/D, and H/T *vs*. D/T, respectively. Each *EXP* is calculated from the following equations:[29]

Using hydrogen as a reference,

$$EXP_{HD} = \frac{\ln\left(\frac{k_H}{k_T}\right)}{\ln\left(\frac{k_H}{k_D}\right)} = \frac{\frac{1}{\sqrt{\mu_H}} - \frac{1}{\sqrt{\mu_T}}}{\frac{1}{\sqrt{\mu_H}} - \frac{1}{\sqrt{\mu_D}}} = \frac{\frac{1}{\sqrt{m_H}} - \frac{1}{\sqrt{m_T}}}{\frac{1}{\sqrt{m_H}} - \frac{1}{\sqrt{m_T}}} \tag{1.14}$$

And using tritium as a reference,

$$EXP_{HD} = \frac{\ln\left(\frac{k_H}{k_T}\right)}{\ln\left(\frac{k_D}{k_T}\right)} = \frac{\frac{1}{\sqrt{\mu_H}} - \frac{1}{\sqrt{\mu_T}}}{\frac{1}{\sqrt{\mu_D}} - \frac{1}{\sqrt{\mu_T}}} = \frac{\frac{1}{\sqrt{m_H}} - \frac{1}{\sqrt{m_T}}}{\frac{1}{\sqrt{m_D}} - \frac{1}{\sqrt{m_T}}} \tag{1.15}$$

where μ_x is the reduced mass and m_x is the atomic mass for the hydrogen isotope (x). The EXP_{HD} was calculated as a value of 1.44 using atomic masses[33] whereas based on reduced mass it is a value of 1.42. The calculated EXP_{DT} is 3.34 from reduced mass, and 3.26 from atomic mass.[34]

The Swain-Schaad ratio can be used as indicator of tunnelling if the step in the catalytic cycle giving rise to the isotope effect is fully rate limiting. Deviations from the values mentioned above could be due to kinetic complexity, when more than one step is rate limiting under the reaction conditions or the rate determining step is not well isolated and this will lead to a smaller KIE.

1.2.2.2 Bell Model

The Bell model is a tunnelling correction model of the semi-classical theory, in which tunnelling of light particles is described through the energy barrier of the reaction around the transition state

(Figure 1.6). According to this model, tunnelling occurs below the energy of the transition state (*i.e.*, for the reaction to proceed to products, the difference in energy between the ground state and the transition state does not have to be realised) (Figure 1.6). The potential for this tunnelling to occur is dependent on certain properties of the particle, such as particle mass, and also on the width of the energy barrier or length of the reaction coordinate.[28]

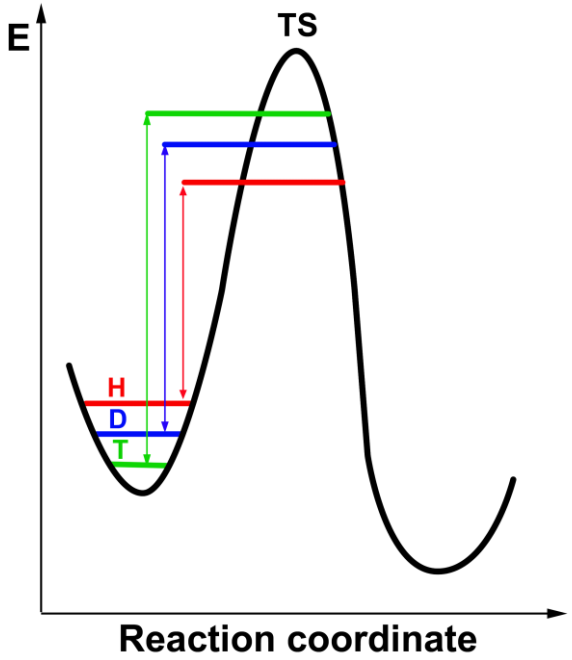

Figure 1.6: *Representation of the energy barrier to an enzymatic reaction according to Bell's tunnelling correction model with the path of transfer for the three isotopes of hydrogen indicated.*

The Bell Model for Tunnel Effect Correction is presented in Equations 1.16 and 1.17

$$k = Q_t k_{SC} \tag{1.16}$$

$$Q_t = \frac{1}{k_b T} e^{\frac{E}{k_b T}} \int G(W) e^{-\frac{W}{k_b T}} dW \tag{1.17}$$

where Q_t is a tunnelling correction, and k_{sc} is the semi-classical rate constant. G is the probability that the particle shall cross the barrier (often described as the permeability of the barrier), and is a function of the particle's mass, width of barrier and the barrier height. W represents the energy of the particle, and k_b is the Boltzmann constant. According to this, a greater probability of tunnelling can occur in the presence of small particle mass, narrow barrier width and small barrier height. This in

turn leads to higher 1° KIE than the semi-classically predicted value with pre-exponential ratio (A_l/A_h) <1, and to a large difference in the activation energies (ΔE_a), exceeding the semi-classical limit of 5.4 kJ mol^{-1} (the difference in ZPE at 300 K of the H and D hydrogen isotopes).[30]

Following the arrhenius equation (equation 1.8) and Bell model for tunnelling correction [29,35], the temperature dependence of the rate constants (k) and the KIE can presented as in Figure 1.7, where ln$k$ and lnKIE are plotted versus the inverse temperature. In the high temperature region (Figure 1.7, cyan region), the temperature dependence of the KIE reflects the difference in the activation energies (ΔE_a) of the light and heavy isotopes. Under these conditions, thermal energy is available and contribution of tunnelling to the rate is minimal (no tunnelling region). Therefore, at infinite temperature, the KIE should be close to unity with (A_l/A_h) ≈ 1. On the other hand, at very low temperatures, due to the lack of thermal energy, tunnelling contributions dominate the reaction rates (extensive tunnelling region) (Figure 1.7, orange region). As a result, the rates of the reaction become temperature independent accompanied by temperature independent and large KIE values, with A_l/A_h larger than unity. In the middle temperature range (Figure 1.7, yellow region), the contribution of H tunnelling to the rate is significant, but the contribution of tunnelling is only for the light isotope, in contrast to the extensive tunnelling region which includes tunnelling of both isotopes. In the moderate tunnelling region, the KIE on A_l/A_h is smaller than unity, which has been taken as one of the proofs for tunnelling.

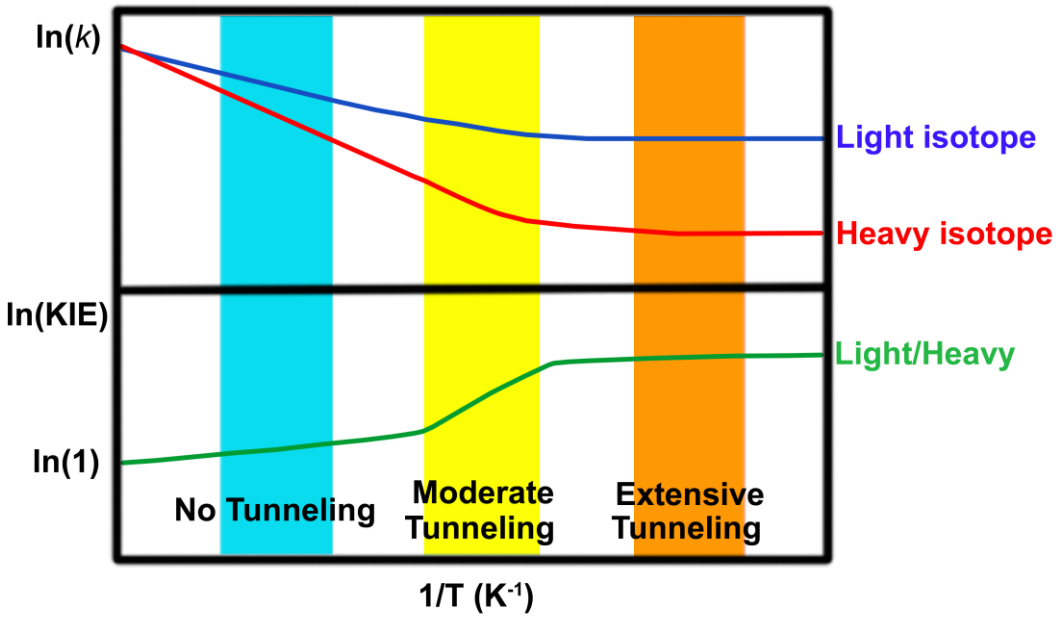

Figure 1.7: *Arrhenius plot of a hydrogen transfer reaction for TST models with a tunnelling correction showing rate constants for the light (blue) and heavy (red) isotopes and the*

corresponding KIEs versus the inverse absolute temperature. This figure is adapted from reference [27].

In the last four decades, the temperature dependences of the KIEs have been determined for a wide range of enzymes. Many of those reports could not be fully described by the Bell tunnelling correction model. For example, KIEs for soybean lipoxygenase greatly exceeded the semi-classical limit with a value of ~80 and A_l/A_h exceeded unity, which should suggest it fits the extensive tunnelling region in Figure 1.7. However, if this is the case the KIE should be at least six orders of magnitude higher than the semi-classical limit, which is not the case.[36] For other systems a high activation energy (E_a) for the H transfer process was obtained along with a high KIE, with no temperature dependence of the KIE, which is incompatible with the predictions made above in Figure 1.7.[31] As a one-dimensional potential surface, the Bell tunnelling correction model gives an explanation for systems with temperature dependent KIEs, and temperature independent KIEs with no energy of activation for the isotopically sensitive step. However, that model fails to explain temperature independent KIEs with significant energies of activation. Therefore, the development of an assumption that can elucidate more understanding of such a phenomenon is still an ongoing challenge. Recent treatments of hydrogen transfer reactions pay attention to the motion(s) of the heavy atom environment that modulate the potential surface of the reaction, and the multidimensional nature of hydrogen tunnelling.

1.2.2.3 Dynamical treatment of enzyme catalysis

In contrast to the static lock and key model proposed by Fischer in 1894, the "induced fit" mechanism proposed by Koshland pays attention to the important of enzyme flexibility.[15] However, while the induced fit model takes into account the dynamic nature of enzymes, it omits fluctuation between different sub-states during the catalytic cycle.

As mentioned previously, the Bell model fails to explain systems that have temperature independent KIEs with significant activation energies *(vide supra)*. Marcus-like models are derived from Marcus theory for electron transfer and can accommodate both temperature dependent and temperature independent KIEs, whether the activation barrier for the reaction is significant or not *(vide infra)*. Various modifications have been added to these models under different names such as 'vibrationally enhanced tunnelling',[37] 'rate-promoting vibrations',[38] and 'environmentally coupled tunnelling',[39] to explain hydrogen transfer in an enzymatic system.

1.2.2.3.1 Marcus-like models

Many researchers have developed models to explain hydrogen transfer reactions in enzymatic systems using Marcus theory.[37,40-42] These models tried to explain the contribution of dynamics to hydrogen transfer reactions and proposed that environmental reorganization assists to form an optimal conformation of the transition state for tunnelling, known as the tunnelling ready conformation (TRC).[26,43] Different terms are used in all of those models, but all of them share two common basic concepts that are required for well-organized tunnelling. One is a short average donor-acceptor distance (DAD) or arrangement of hydrogen donor and acceptor into an orientation from which hydrogen tunnelling would be efficient, and the other is degeneracy of the reactant and product energy levels or modulation of hydrogen transfer along the environmental coordinate as represented in Figure 1.8. There are different definitions for such motions in the literature, but generally they are recognised to be active ("gating") or re-organisational motions, and passive or pre-organisational motions respectively.[23]

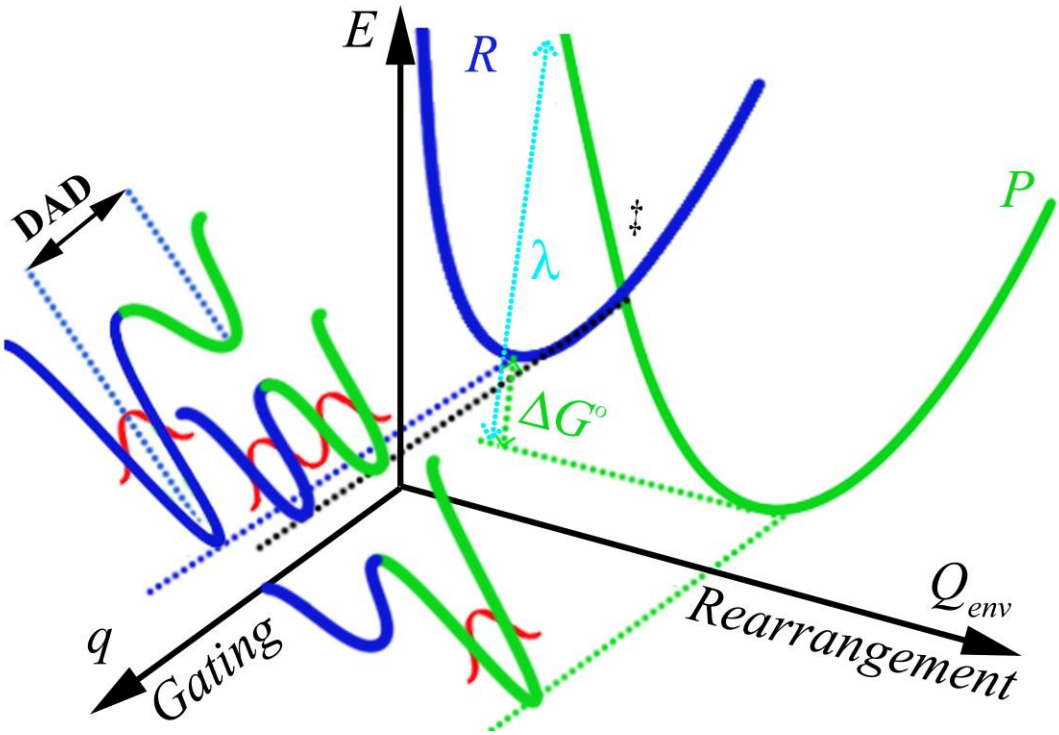

Figure 1.8: *Three dimensional representation of a Marcus-like model of the energy surface of environmentally coupled hydrogen tunneling. Two orthogonal coordinates are presented:* Q_{env} *is the environmental free energy surface for the reactants (R: blue) and the products (P: green) with free energy of reaction (*ΔG^o*), reorganisation energy (*λ*) and ‡ represents the reactive configuration, and q is the gating coordinate along which modulation of the donor acceptor distance (DAD) occurs. The*

red lines represent the hydrogen's probability wave-function. The figure is adapted from reference [44].

The Marcus-like model is mathematically represented as

$$k_{tun} = Ce^{-\frac{(\Delta G^o + \lambda)^2}{4\lambda RT}}(F.C.\,term) \tag{1.18}$$

where k_{tun} is the rate of tunnelling, C is a temperature and isotope independent constant, ΔG_o is the free energy difference between the reactants and the products (the driving force for the reaction), λ is the reorganization energy,[42] R is the gas constant and T is the absolute temperature.

In Equation 1.18, the first exponential is the Marcus term. This term is mostly isotopically insensitive and corresponds to reorganization along the environmental free energy coordinate to adjust the relative energy levels of the reactants and the products to the TRC. The F.C. or Franck-Condon term is the tunnelling term and is described in Equation 1.19

$$F.C.\,term = \int_{DAD1}^{DAD0} e^{\left(-\frac{m_H \omega_H r_H^2}{2\hbar}\right)} e^{\left(-\frac{E_x}{k_b T}\right)} dDAD \tag{1.19}$$

The F.C. term is an exponential function consisting of two terms. The first term is the integrated tunnelling probability of all of the relevant donor–acceptor distances (DAD) as a function of the isotopic mass (m_x) and frequency (ω_x). This term is DAD and isotope dependent. The second term is an exponential function of the energy involved in reaching each DAD (E_X). This term is the expression of the DAD fluctuations, namely the conformational space and is often defined as 'gating' which is temperature as well as isotope sensitive. E_X can defined as shown in Equation 1.20.

$$E_x = \frac{1}{2} \times \frac{h}{2\pi} \omega_x X^2 = \frac{1}{2} m_x \omega_x^2 r_x^2 \tag{1.20}$$

where h is Planck's constant, ω_x is the gating frequency, m_x is the mass of the gating unit, r_x is the tunnelling distance for the transferring isotope and X is the gating coordinate. The gating coordinate (X) is related to the gating frequency (ω_x), the tunnelling distance for the transferring isotope (r_x), and its mass (m_x) as showing in Equation 1.21

$$X = r_x \sqrt{\frac{m_x \omega_x}{\hbar}} \tag{1.21}$$

where $\hbar$ is the Planck's constant divided by 2π

Using Equation 1.18, the kinetic isotope effect can describe by the F.C. term as shown in Equation 1.21, since all other terms cancel each other out.

$$KIE = \frac{(F.C.\,term)_H}{(F.C.\,term)_D} = \frac{\int_{DAD_1}^{DAD_0} e^{\left(-\frac{m_H \omega_H r_H^2}{2\hbar}\right)} e^{\left(-\frac{E_x}{k_b T}\right)} dDAD}{\int_{DAD_1}^{DAD_0} e^{\left(-\frac{m_D \omega_D r_D^2}{2\hbar}\right)} e^{\left(-\frac{E_x}{k_b T}\right)} dDAD} \tag{1.22}$$

According to the Marcus-like model, a system will have temperature independent KIEs when the first exponential of Equation 1.18 dominates and the activation energies for H and D are similar. This happens when the enzyme's conformational distribution, controlled through 'passive dynamics', is the important feature and the tunnelling ready configuration (TRC) is optimized. Alternatively, when the second exponential of Equation 1.19 (the gating term) dominates, 'active dynamics' are the major contributing factor, temperature-dependent KIEs are observed and the values of A_H/A_D decrease and may approach unity.[26,29,45]

Studies of the temperature dependence of the KIE cannot clearly separate the contribution of each term to the tunnelling reaction. Different studies have shown that dynamics does not enhance enzyme catalysis.[40,46-47] However, other theoretical and experimental studies have established an important role for protein dynamics in enzyme catalysis.[38,48-50] For further understanding of the relation between protein dynamics and the rate of enzymatic reaction, in this thesis, hydride transfer reaction and kinetic isotope effect of dihydrofolate reductase have been studied using DHFR homologues from bacteria living over a wide range of temperature environments, namely, the psychrophilic DHFR from *Moritella profunda* (MpDHFR), the mesophilic DHFR from *Escherichia coli* (EcDHFR) and the thermophilic DHFR from *Thermatoga maritima* (TmDHFR).

1.3 Dihydrofolate reductase

1.3.1 Dihydrofolate reductase in biochemistry

Dihydrofolate reductase (DHFR) catalyzes the stereospecific reduction of 7,8-dihydrofolate (DHF) to 5,6,7,8-tetrahydrofolate (THF) in the presence of reduced nicotinamide adenine dinucleotide phosphate (NADPH). During the DHFR reaction, the *pro*-R hydrogen of C4 of NADPH transfers to the C6 atom of the pterin ring of DHF with simultaneous protonation at N5 (Figure 1.9).

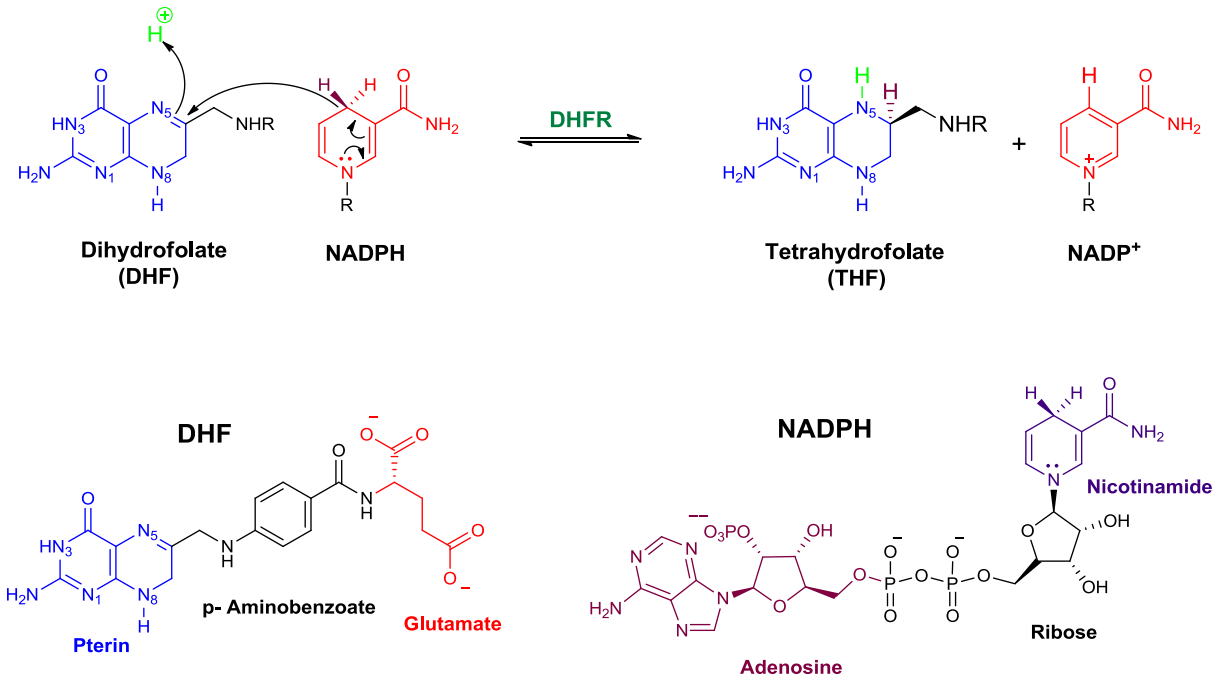

Figure 1.9: *The reaction catalysed by DHFR and the structure of the cofactor (NADPH) and substrate (DHF).*

DHFR is important for maintaining the intracellular pool of THF, a cofactor involved in many biological reactions that require transfer of a one carbon unit such as biosynthesis of thymidylate, purines and some amino acids (Figure 1.10). As a result of the biological and pharmacological importance of DHFR, for many years researchers have been working towards a detailed picture of how this enzyme works and it has become a subject of intensive kinetic and structural investigations.

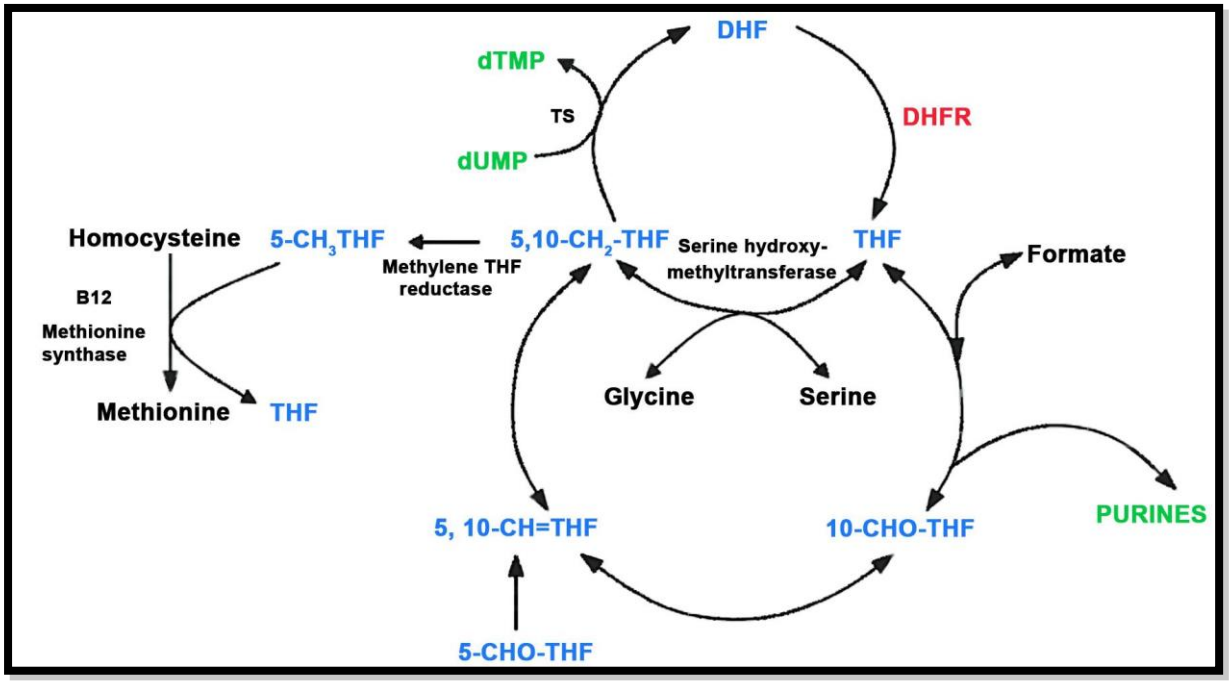

Figure 1.10: *A selection of biological reactions that use different THF derivatives as a cofactor during one carbon transfer reactions. THF is converted to 5,10-methylene-THF. The 5,10-methylene-THF is then converted to 5-methyl-THF by reduction with NADPH. The methyl group is in turn transferred to homocysteine generating methionine in the presence of cobalamin (Vit B12). The 5,10-methylene-THF is also used in the presence of thymidylate synthase (TS) to methylate the pyrimidine base uracil in deoxyuridine monophosphate (dUMP) to thymine to produce deoxythymidine monophosphate (dTMP) which is essential for DNA synthesis. 5,10-methylene-THF and 5-formyl-THF can be converted into 5,10-methenyl-THF which is in turn converted to 10-formyl-THF which acts as a cofactor during purine biosynthesis.*[51-52]

THF, the product of the DHFR catalysed reaction, is essential for cell growth and proliferation. Hence DHFR is a major target for anticancer and antibacterial drugs.[7] More than 50 years ago, studies of methotrexate (MTX), an anticancer drug that is used as a treatment of leukemias, lymphomas and also rheumatoid arthritis, led to the discovery of DHFR.[53] Figure 1.11 shows a variety of drugs that target DHFR.

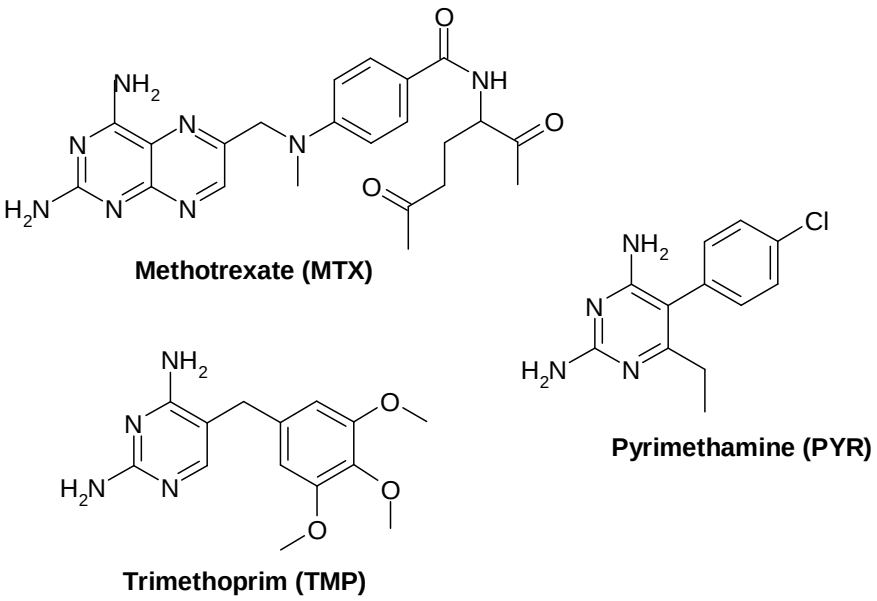

Figure 1.11: *Structures of some DHFR inhibitors. Methotrexate (MTX) is a famous anticancer drug. Trimethoprim (TMP), which binds tightly to bacterial DHFRs, is an important antibacterial agent. Pyrimethamine (PYR) is an antimalarial agent that targets DHFR from Plasmodium falciparum.*[54-55]

1.3.2 The three dimensional structure of DHFR

Due to the biological important of DHFR, it has been characterised from all of the three kingdoms and has prompted numerous structural studies. The first crystal structure of DHFR was published in 1977 [56] and soon after a huge variety of DHFRs in complex with various ligands were reported. To date, more than 200 structures for DHFR isolated from different organisms can be found in the Protein Data Bank (PDB) bound to a wide range of ligands.

All the chromosomally encoded DHFRs are relatively small enzymes normally ranging from 18,000 to 25,000 in molecular weight and they all adopt similar secondary and tertiary structure arrangements. The general structure of DHFRs (Figure 1.12) consists of four α-helices, eight β-sheets and three structural subdomains that surround the active site cleft. These subdomains are the cofactor binding domain (CBD) (residues 38-88 in EcDHFR) where the adenosine moiety of NADP(H) binds, the substrate binding domain (SBD) (residues 23-37 in EcDHFR) where DHF binds to the enzyme and the loop domain (LD). The loop domain forms approximately 40-50% of the major subdomains and is dominated by a set of three loops on the ligand binding face that surround the active site. These loops are the M20 loop (residues 9-24), FG loop (residues 116-132), and GH loop (residues 142-150) (Figure 1.12).[57-58]

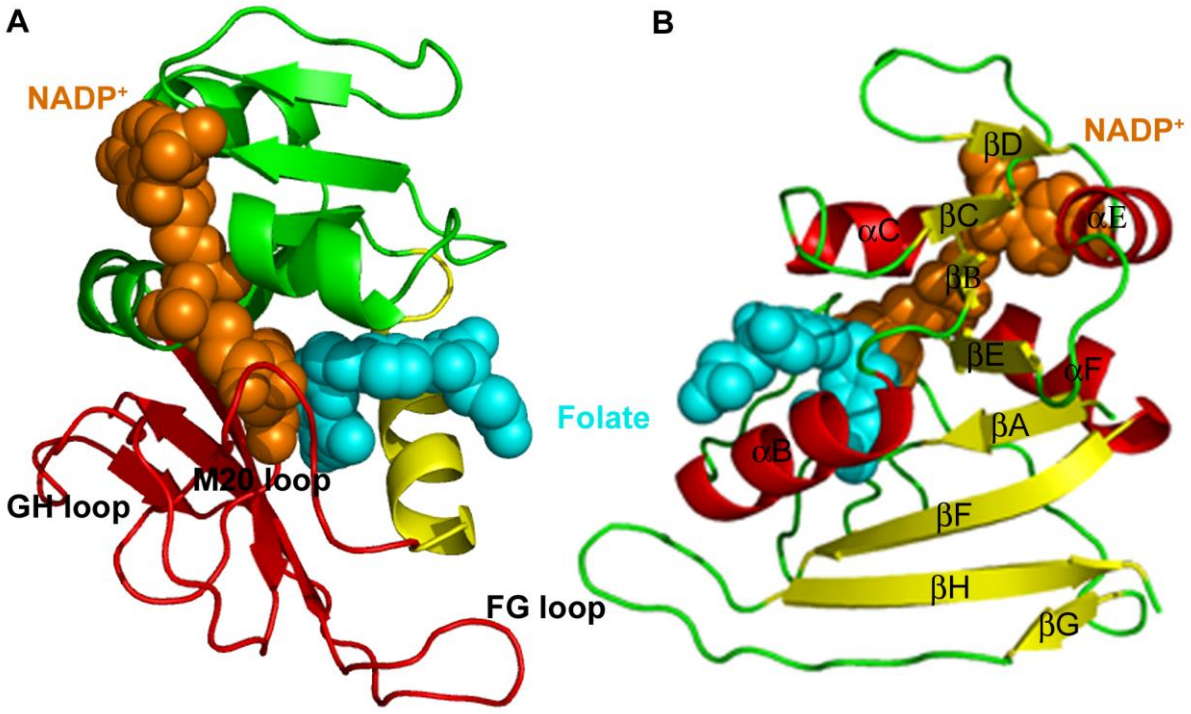

Figure 1.12: *Cartoon representation of EcDHFR (PDB 1RX2)*[59] *showing (A) the substrate binding domain (yellow), the cofactor binding domain (green) and the loop domain (red), and (B) the secondary structural elements; α-helices (red), β-strands (yellow) and connecting loops (green). Folate (cyan) and NADP*$^+$ *(orange) are shown as spheres. Rotation between (A) and (B) is 180°.*

Prokaryotic organisms live at wide range of temperatures starting below 0 °C and extending up to at least 113 °C.[60] The comparative analysis of a series of enzyme homologs across this range of temperature allows further understanding of their enzymatic molecular strategies, structural flexibility and stability. In this thesis three DHFRs have been used as a model system: DHFR isolated from *Moritella profunda* (MpDHFR), a psychrophilic and moderately piezophilic bacterium isolated from deep sea at high pressure and 2 °C;[60] the mesophilic and the extensively studied DHFR from *Escherichia coli* (EcDHFR); and DHFR from *Thermotoga maritima* (TmDHFR), a hyperthermophilic and anaerobic bacterium with an optimal growth temperature of 80 °C.[61] The amino acid sequences for the three enzymes are shown in Figure 1.13.

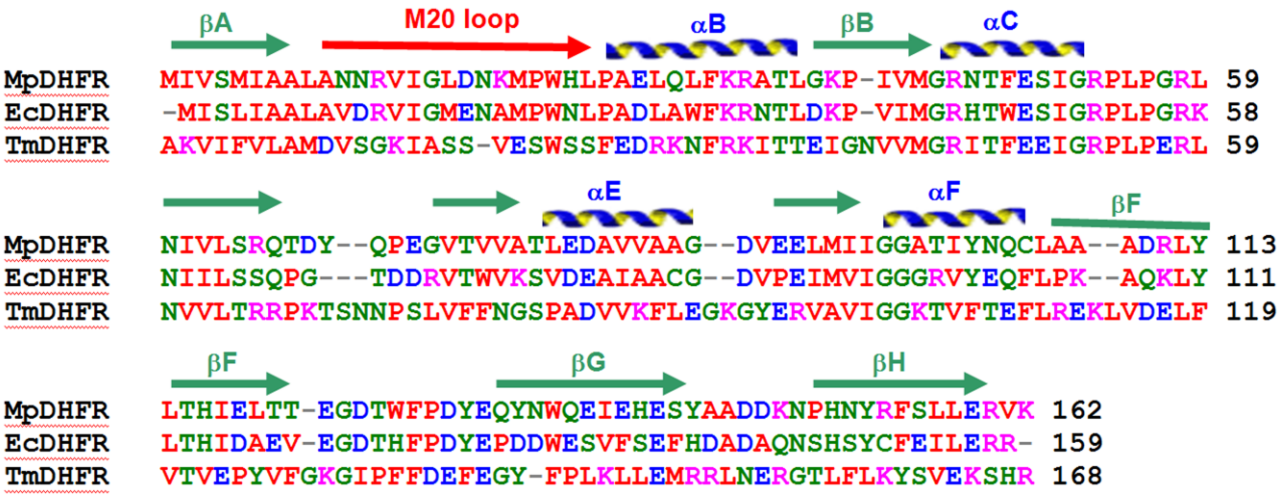

Figure 1.13: *Sequence alignment of the psychrophilic MpDHFR, the mesophilic EcDHFR and the thermophilic TmDHFR.*

The crystal structures for all of the three enzymes have been reported previously.[59,62-63] In general, the overall folded structures of the psychrophilic, mesophilic and thermophilic DFHR homologues are similar, and residues involved in catalysis are highly conserved (Figure 1.13 and Table 1.1). However, MpDHFR and EcDHFR are monomeric enzymes, as are most chromosomal DHFRs, whereas TmDHFR is the only characterised DHFR which forms a stable homodimer and its dimerization interface involves the catalytically important M20 and FG loops[63] (Figure 1.14). Therefore, TmDHFR adopt a rigid structure which was thought to be the reason for the poor catalytic efficiency for this enzyme.[64] However, the monomeric version of this enzyme did not show significant change in the hydride transfer rate constant.[65]

Table 1.1: Sequence identity and similarity scores for EcDHFR, MpDHFR and TmDHFR

Enzymes	Identity (%)	Similarity (%)	Non-identity (%)
Ec and Tm	23.67	21.89	54.44
Ec and Mp	53.70	19.75	26.55
Mp and Tm	26.32	20.47	53.21

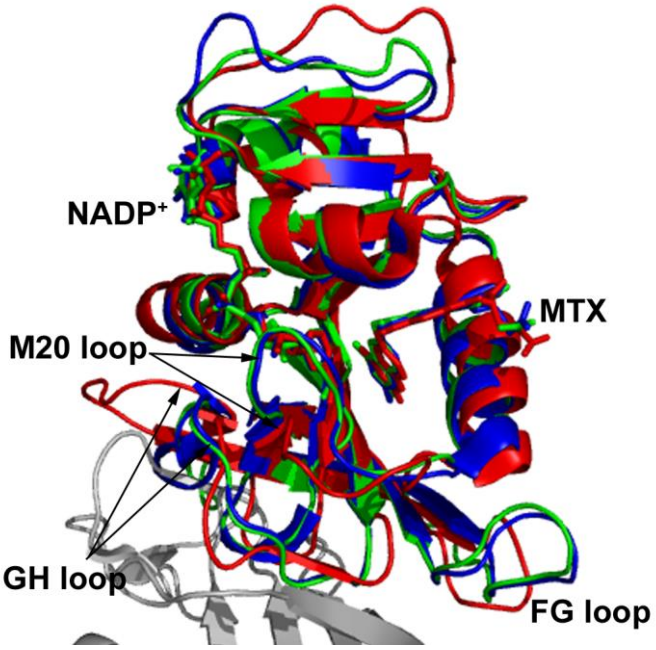

Figure 1.14: *Cartoon representation showing the alignment of the crystal structures of MpDHFR (blue, PDB 3IA4)[62], EcDHFR (green, PDB 1DRE)[59] and TmDHFR (red, PDB 1D1G)[63] in complex with $NADP^+$ and methotraxate.(MTX). Part of the dimeric interface of TmDHFR is shown in gray, $NADP^+$ and MTX are shown as sticks.*

1.3.3 The catalytic cycle of DHFR

Over the years, DHFR from different sources have been a paradigm for extensive structural and mechanistic studies. The full kinetic schemes have been reported for DHFR from different organisms,[66-70] including EcDHFR[7] (Figure 1.15). Under steady-state turnover conditions the catalytic cycle of EcDHFR was found to follow a specific pathway through five kinetically observable intermediates: the holoenzyme E:NADPH; the Michaelis complex E:DHF:NADPH and the product complexes E:THF:$NADP^+$, E:THF, and E:THF:NADPH (Figure 1.15). The binding kinetics suggest that during the EcDHFR catalytic cycle, product dissociation after the chemical step follows a specific preferred pathway in which tetrahydrofolate (THF) dissociation occurs after NADPH replaces $NADP^+$ in the product ternary complex. This is the rate-limiting step for steady-state turnover at physiological pH. However, hydride transfer becomes the rate limiting step at higher pH values.[7]

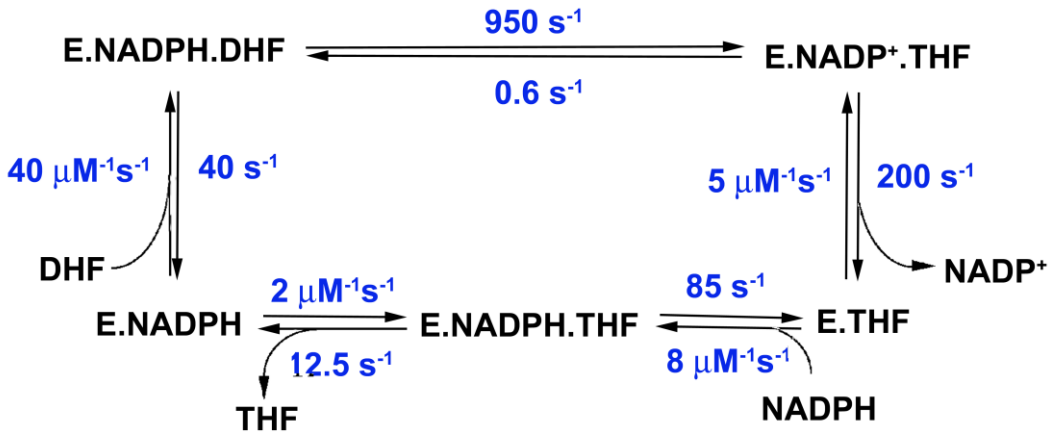

Figure 1.15 *The EcDHFR catalytic cycle at pH 7 and 25 °C. E, dihydrofolate reductase; DHF, dihydrofolate; THF, tetrahydrofolate; NADPH, reduced nicotinamide adenine dinucleotide phosphate and NADP$^+$, oxidized nicotinamide adenine dinucleotide phosphate.*[7,71]

1.3.4 Loop motions in DHFR

Extensive X-ray studies of DHFRs from different organisms have given valuable information on how the enzyme binds to its substrate and cofactor in various ligand complexes. The substrate and cofactor bind in the deep hydrophobic cleft of the active site in close proximity to one another, which allows van der Waals contact between the hydride donor atom (C4 of NADPH) and hydride acceptor atom (C6 of the pterin ring of DHF).[72] Previous studies have shown the role of the loop domain in such contact and in maintaining the active site geometry.[73-76] The M20 loop sits directly over the active site, protecting it from solvent and forms stabilizing hydrogen bonding with the neighbouring FG and GH loops (*vide infra*). X-ray studies of EcDHFR have shown that the M20 loop can adapt four characteristic conformations according to the bound ligand, occluded, closed, open, and disordered.[59] The first two conformations have been observed in solution NMR experiments.[77-78] The open M20 loop conformation has been seen for both EcDHFR[59] and MpDHFR[62,79] only in the absence of ligands.[59] In the open conformation the substrate binding cleft is widened significantly, combined with an 8 Å opening to the nicotinamide binding site. Thus this conformation was seen in the apoenzyme for EcDHFR and MpDHFR.[62] The fourth conformation or the 'disordered state', in which the loop's motions are unclear crystallographically, is thought to be a result of fluctuations between the occluded and closed conformations.[59,72,75]

As mentioned previously, the conformation of the active site loops depends on the ligands bound in the substrate and cofactor binding sites.[59] Binding of the nicotinamide ribose moiety of the cofactor within its binding pocket leads to formation of the closed conformation. However, when the substrate

site is occupied, DHFR adopts the occluded conformation. Thus, loop movement is coordinated with the stages of the catalytic cycle.

1.3.5 Loop movements during the DHFR catalytic cycle

Movement of the M20 loop of EcDHFR has been proposed to be important for the catalytic cycle. Sawaya and Kraut[59] showed that, during the EcDHFR catalytic cycle, the M20 loop adopts either the closed or the occluded conformation according to the binding ligand. The crystal structures provided for the five key intermediates of EcDHFR suggest that the enzyme switches between the two conformations during the catalytic cycle (Figure 1.16).

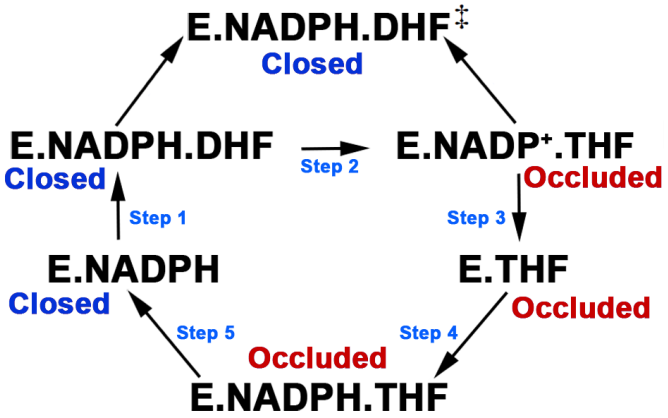

Figure 1.16: *Schematic representation of the catalytic pathway of EcDHFR. In the holoenzyme E:NADPH, the Michaelis complex E:NADPH:DHF and the transition state complex E.NADPH.THF‡, the Met20 loop adopts the closed conformation. In the three product complexes, E:NADP+, E:THF and E:NADPH:THF, the Met20 loop is in the occluded conformation.[59] In the steady state, product release from E:NADPH:THF ternary complex (Step 5) is the rate limiting step, but hydride transfer becomes the rate limiting step at pH higher than 8.4.[7]*

The M20 loop is in the closed conformation in the holoenzyme (E.NADPH), the Michaelis complex (E.NADPH.DHF), and the transition state (E.NADPH.THF)‡, packing against NADPH and preventing solvent access to the active site. On the other hand, this loop occludes the nicotinamide binding pocket in the three product complexes: E:THF:NADP+, E.THF and E:THF:NADPH (Figure 1.16). In the Michaelis complex and transition state, the nicotinamide-ribose moiety occupies its binding pocket within the active site, in close proximity to the pterin ring of the substrate. However, in the occluded product complexes, this moiety projects into the solvent.[59]

The occluded and closed conformations differ in structure in the middle part of the Met20 loop. In the closed conformation (Figure 1.17), the M20 loop (residues 16 to 19 in EcDHFR) extends across the active site forming a short antiparallel β-sheet and a hairpin turn, which effectively seals the active site by forming a hydrogen bond between Asn18 in the hairpin and His45. In this conformation Met16 and Glu17 in the active side are flipped out allowing nicotinamide binding, while the side chains of Asn18 and Met20 sit behind the bound substrate and cofactor. In the occluded state, the central region of the Met20 loop forms a 3_{10}-helix, with Met16 and Glu17 sitting into the active site and occluding the cofactor binding site. In this conformation, the M20 loop prevents the nicotinamide group from entering the active site and it instead sticks out into solution.[59] It was found that only in the closed conformation are the cofactor and substrate reactive centres in close proximity within the active site pocket. This was seen in the structures of the E.$NADP^+$.folate and E.NADPH.MTX complexes, which are good models of the Michaelis complex and transition state, respectively.[59] Movement between the closed and occluded conformations is thought to be important for ligand affinity and progression through the catalytic cycle.[59]

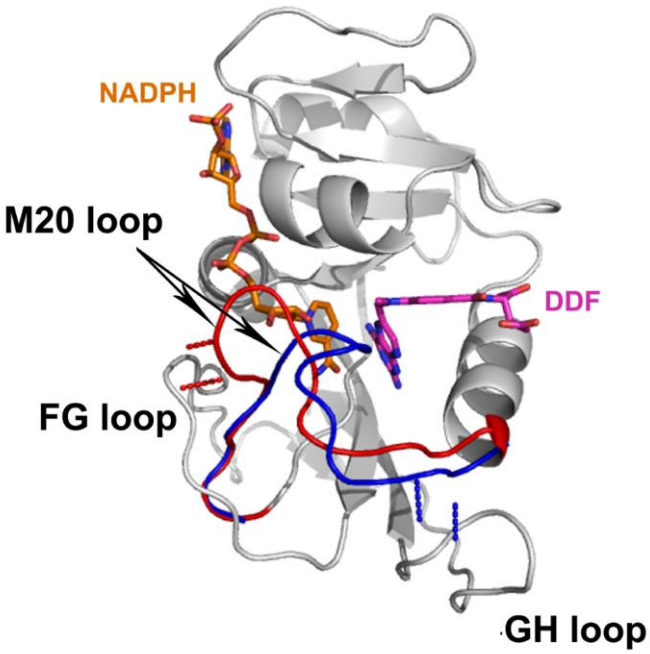

Figure 1.17: *Cartoon representation of EcDHFR highlighting the positioning of the M20 loop in the closed conformation (red, PDB 1RX2), and occluded conformation (blue, PDB 1RX6). DDF is shown in magenta and NADPH in orange.*[59]

The closed conformation is stabilized by pairs of hydrogen bonds between residues in the M20 loop and the FG loop (residues 116 to 132 in EcDHFR), namely Gly15(O) to Asp122(HN) and

Glu17(HN) to Asp122(Oδ2) (Figure 1.18).[7,59] In the product binary and ternary complexes, on the other hand, the loop switches to the occluded conformation, therefore the two hydrogen bonds between the M20 loop and FG loop that stabilize the closed conformation are not formed and instead the occluded conformation is stabilized by two hydrogen bonds between Asn23 (O and HN) in the M20 loop and Ser148 (HN and γO2) in the GH loop (residues 142 to 149 in EcDHFR) (Figure 1.18).[7,59]

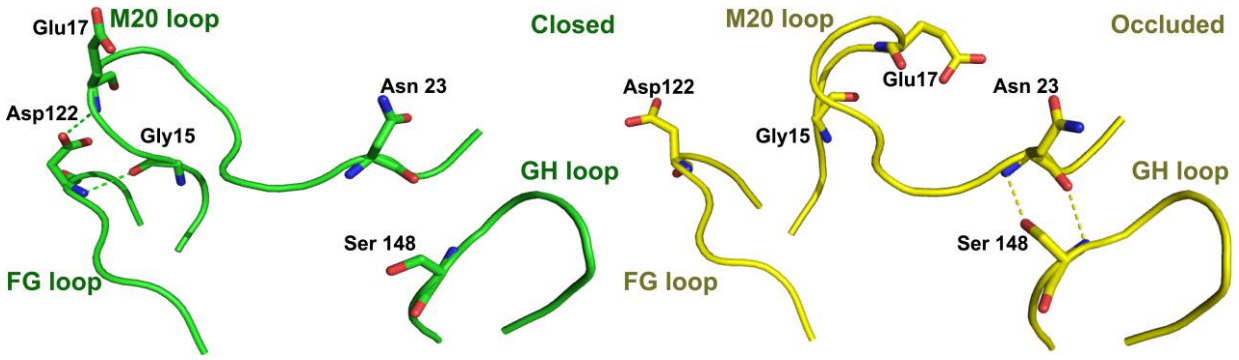

Figure 1.18: *Cartoon representation of EcDHFR showing details of the M20 loop, FG loop and GH loop and the residues participating in the hydrogen bonds which stabilizes the closed (left, green, PDB 1RX2) and the occluded conformation (right, yellow, PDB 1RX6).*[59]

1.4 General Research Aims

Several kinetic, NMR and stimulation studies have been applied to DHFR in order to understand the relation between enzyme dynamic and catalysis. Studying catalysis by DHFR should in general enhance our understanding of enzyme catalysis and help answering the questions such as how enzyme dynamics couple to the reaction coordinate? Are enzyme dynamics important for improving enzyme efficiency? These questions, in turn, may lead to advances in enzymology and other aspects of chemical catalysis in the broadest sense.

The general aims of this thesis are to study the hydride transfer reaction catalysed by the cold adaptive enzyme MpDHFR. And compare it to the mesophilic and the thermophilic homologues, EcDHFR and TmDHFR. The rate constants and KIE will be determined as a function of temperature, pH and salt concentration, and denaturant concentration to examine their effect on the chemical step in catalysis by DHFR. Comparing DHFR homologues across a wide temperature range, and study their ability to function at different temperatures should develop our understanding of the role of protein motions and tunnelling of the transferred hydride in the chemical step of the different homologues, and give deeper insight into the structural elements that present the specific adaptations

of each homologue.

A ^{15}N labelled cofactor, $NADP^+$ will be synthesised and used to record ^{1}H-^{15}N HSQC NMR spectra with various DHFRs to provide information on how the cofactor binds to the enzyme in different complexes. In addition, different MpDHFR and EcDHFR variants in the catalytically important loops, viz the M20, FG and GH loop, will be created and studied to investigate the role of loop dynamics on catalysis by DHFR and how it can affect the chemical step.

2

Materials and Methods

2.1 Materials

NAD^+, $NADP^+$ and NADPH were purchased from Melford. All other chemicals used in this work were purchased from Sigma Aldrich or Fisher Scientific unless otherwise stated. Restriction enzymes were purchased either from Promega or New England Biolabs. Oligonucleotides were purchased from Eurofins.

2.2 Media and buffers

2.2.1 Luria-Bertani (LB) medium

For 1 L LB medium, 10 g Tryptone, 5 g yeast extract and 10 g NaCl were dissolved in 950 mL of deionized water and the pH taken to 7.4 with 5 M NaOH. The volume was taken to 1 L and sterilized by autoclave for 20 minutes at 121 ºC. The medium was used immediately after cooling down or stored at 4 ºC.

2.2.2 LB-Agar medium

1.5 g agar was added to 100 mL LB medium (Section 2.2.1) and sterilized by autoclave for 20 minutes at 121 ºC. The solution was allowed to cool to approximately 50 ºC and ampicillin was added if required. The sterilized LB-agar medium was poured into sterile petri dishes, left to set then stored at 4 ºC.

2.2.3 Ampicillin

100 mg L^{-1} ampicillin was added to culture media before use. Ampicillin (300 mg) was dissolved in 1.5 mL sterile water, and then 250 μL of this solution was added to 500 mL LB medium. For overnight cultures 10 mg ampicillin was added directly to 100 mL of LB medium.

2.2.4 Isopropyl-β-D-1-thiogalactopyranoside (IPTG) (240 mg mL^{-1})

IPTG (360 mg) was dissolved in 1.5 mL sterile water and used at a working concentration of 120 mg mL^{-1} by adding 250 μL of this solution to 500 mL culture medium.

2.2.5 Dithiothreitol (DTT) (10 mM)

DTT (154 mg) was dissolved in 100 mL deionised water. The solution was sterilised using a 0.2 μm syringe filter and stored at 4 °C. DTT was used at a working concentration of 1 mM for enzyme storage (Section 2.2.14).

2.2.6 Ethylenediaminetetraacetic acid (EDTA) (10 mM, pH 8)

EDTA (1.46 g) was added to 450 mL deionised water. The pH was adjusted with 5 M NaOH to dissolve the solid, the total volume was taken to 500 mL with deionised water and the solution was sterilised using a 0.2 μm syringe filter. The stock solution was stored at room temperature and used at a working concentration of 0.1 mM for enzyme storage (Section 2.2.14).

2.2.7 dNTP solution

dNTPs were purchased from Promega at a concentration of 100 mM each. 10 mM stock solution of each dNTP was prepared using sterile deionised water, aliquoted and stored at -20 °C. dNTPs were used at a working concentration of 200 μM.

2.2.8 Buffers used for preparation of ultra-competent cells

The following solutions were prepared, sterilised using a 0.2 μm syringe filter and stored at 4 ºC.

2.2.8.1 Rubidium chloride solution 1 (Rb1) (30 mM KOAc, 100 mM RbCl, 10 mM $CaCl_2$, 50 mM $MnCl_2$, 15% (v/v) glycerol, pH 5.8)

Potassium acetate (294 mg), rubidium chloride (1.21 g), calcium chloride (111 mg), manganese chloride (692 mg) and glycerol (15 mL) were dissolved in 80 mL deionised water and the pH was adjusted with dilute acetic acid (0.1 M). The total volume was taken to 100 mL with deionised water.

2.2.8.2 Rubidium chloride solution 2 (Rb2) (10 mM MOPS, 75 mM $CaCl_2$, 10 mM RbCl, 15% (v/v) glycerol, pH 6.5)

3-(N-morpholino)propanesulfonic acid (MOPS) (209 mg), calcium chloride (832 mg), rubidium chloride (121 mg) and glycerol (15 mL) were dissolved in 80 mL deionised water and the pH was adjusted with dilute NaOH (0.1 M). The total volume was taken to 100 mL with deionised water.

2.2.9 Buffers used for protein purification method 1

2.2.9.1 Buffer A (50 mM Tris-HCl, pH 8)

Tris base (6.1 g) was dissolved in 950 mL of deionised water and the pH was adjusted with 6 M HCl. The volume was then taken to 1 L with deionised water and the buffer was filtered and degassed *via* vacuum pump (Vacuubrand GmbH + CO KG, MD4C, Werthein, Germany). The

buffer was stored at room temperature and 10 mM 2-mercaptoethanol (1.4 mL) was added immediately before use.

2.2.9.2 Buffer B (50 mM Tris-HCl, 1 M NaCl, pH 8)

Tris base (6.1 g) and sodium chloride (58.44 g) were dissolved in 950 mL deionised water and the pH was adjusted with 6 M HCl. The volume was then taken to 1 L with deionised water and the buffer was filtered and degassed *via* vacuum pump (Vacuubrand GmbH + CO KG, MD4C, Werthein, Germany). The buffer was stored at room temperature. 10 mM 2-mercaptoethanol (1.4 mL) was added immediately before use.

2.2.9.3 Buffer C (50 mM Tris-HCl, 1 M NaCl, 5 mM sodium folate, pH 8)

0.11 g folic acid was dissolved in the smallest amount of 0.1 M sodium hydroxide. The volume was taken to 50 mL with Buffer B (Section 2.2.9.2) and the pH adjusted using 6 M HCl. The buffer was prepared immediately before use.

2.2.10 Buffers used for protein purification method 2

2.2.10.1 Buffer A (50 mM potassium phosphate, pH 7)

HK_2PO_4 (5.4 g) and H_2KPO_4 (2.6 g) were dissolved in 950 mL deionised water and the pH was adjusted using 6 M HCl. The volume was taken to 1 L, the buffer was filtered and degassed by vacuum pump (Vacuubrand GmbH + CO KG, MD4C, Werthein, Germany) and stored at room temperature. 10 mM of 2-mercaptoethanol (1.4 mL) was added immediately before use.

2.2.10.2 Buffer B (50 mM potassium phosphate, 1 M NaCl, pH 7)

HK_2PO_4, (5.4 g), H_2KPO_4 (2.6 g) and sodium chloride (58.44 g) were dissolved in 950 mL deionised water and the pH was adjusted using 6 M HCl. The volume was taken to 1 L, the buffer was filtered and degassed by vacuum pump (Vacuubrand GmbH + CO KG, MD4C, Werthein, Germany) and stored at room temperature. 10 mM mercaptoethanol (1.4 mL) was added immediately before use.

2.2.11 Buffers used for cofactor purification

2.2.11.1 Buffer A (20 mM Tris-HCl, pH 9)

Tris base (1.21 g) was dissolved in 950 mL deionised water, the pH was adjusted with 6 M HCl and the volume was taken to 1 L with deionised water. The buffer was filtered, degassed and stored at room temperature.

2.2.11.2 Buffer B (20 mM Tris-HCl, 1 M NaCl, pH 9)

Tris base (1.21 g) and sodium chloride (58.44 g) were dissolved in 950 mL of deionised water, the pH was adjusted with 6 M HCl and the volume was taken to 1 L with deionised water. The buffer was filtered, degassed and stored at room temperature.

2.2.12 Buffers used for tetrahydrofolate (THF) purification

2.2.12.1 Buffer A (200 mM Tris-HCl, pH 8)

Tris base (12.1 g) was dissolved in 450 mL deionized water, the pH was adjusted with 6 M HCl and the volume was taken to 0.5 L with deionized water. The buffer was filtered, degassed, saturated with argon and used immediately.

2.2.12.2 Buffer B (5 mM Tris-HCl, pH 8)

12.5 mL of Buffer A (Section 2.2.12.1) was taken to 0.5 L with deionized water and the pH was adjusted using 6 M HCl before the buffer was filtered and degassed. The buffer was saturated with argon before use.

2.2.13 SDS-PAGE

The following solutions were prepared, stored at room temperature and used for SDS-PAGE analysis:

2.2.13.1 Sodium Dodecyl Sulfate (SDS) (10% w/v)

10 g SDS was dissolved in 100 mL deionized water and stored at room temperature.

2.2.13.2 Bromophenol blue (0.5% w/v)

50 mg bromophenol blue dye was dissolved in 10 mL deionized water and stored at room temperature.

2.2.13.3 Gel buffer (3 M Tris-HCl, 10 mM SDS, pH 8.45)

Tris base (36.42 g) was dissolved in 95 mL deionised water and 3 mL of 10% SDS stock solution (Section 2.2.13.1) was added. The pH was adjusted using 6 M HCl and the volume taken to 100 mL with deionised water.

2.2.13.4 Loading buffer (780 mM Tris-HCl, 34.7 mM SDS, 10% (v/v) glycerol, 1% (v/v) 2-mercaptoethanol, 0.01% (w/v) bromophenol blue, pH 6.8)

Tris base (0.95 g) was added to 7 mL deionised water and 1 mL 10% SDS stock solution (Section 2.2.13.1), 1 mL glycerol, 100 μL 2-mercaptoethanol and 200 μL 0.5% bromophenol blue stock solution (Section 2.2.13.2) were added. The pH was adjusted using 6 M HCl and the volume taken to 10 mL with deionized water.

2.2.13.5 Anode buffer (200 mM Tris-HCl, pH 8.9)

Tris base (24.28 g) was dissolved in 950 mL deionised water. The pH was adjusted using 6 M HCl and the volume taken to 1 L with deionised water.

2.2.13.6 Cathode buffer (100 mM Tris-HCl, 100 mM tricine, 3.5 mM SDS, pH 8.4)

Tris base (12.14 g) and tricine (17.92 g) were dissolved in 950 mL deionised water and 10 mL 10% SDS stock solution (Section 2.2.13.1) was added. The pH was adjusted using 6 M HCl and the volume was taken to 1 L with deionised water.

2.2.13.7 Staining solution

0.25% (w/v) Coomassie blue dye was added to 45% (v/v) methanol and 10% (v/v) glacial acetic acid in deionised water and filtered.

2.2.13.8 Destaining solution

45% (v/v) methanol and 10% (v/v) glacial acetic acid in deionised water.

2.2.14 Protein storage buffer

MpDHFR was stored in a solution containing 1 mM DTT, 0.1 mM EDTA and 20% sterile glycerol using the stock solutions prepared in Sections 2.2.5 and 2.2.6.

2.2.15 TAE buffer

TAE buffer stock solution (50x) was prepared by dissolving Tris base (242 g) in 800 mL deionised water containing 57.1 mL glacial acetic acid and 100 mL of EDTA solution (0.5 M, pH 8). EDTA solution (0.5 M, pH 8) was prepared immediately prior to use by dissolving EDTA (14.61 g) in 50 mL deionised water, adjusting the pH with 5 M NaOH, and taking the volume to 100 mL with

deionised water. The working solution of TAE buffer (1x) was made by diluting the stock solution 50-fold with deionised water. Final solute concentrations are 40 mM Tris acetate and 1 mM EDTA.

2.2.16 Agarose gel

Agarose (1-2 g) was added to 100 mL 1x TAE buffer (Section 2.2.15) and the mixture heated in the microwave until fully dissolved. The gel was poured into a casting block and allowed to set. Gels were run at constant amplitude of 80 V for 45 minutes then stained with 200 mL of dilute ethidium bromide solution (Section 2.2.21) and visualized using a Syngene GeneFlash UV light box (Syngene, Cambridge, UK).

2.2.17 Phosphate Buffers

1 M stock solutions of monobasic and dibasic potassium phosphate were prepared by separately dissolving 68.1 g and 87.1 g of monobasic and dibasic potassium phosphate respectively in 450 mL deionised water. The total volume of each was taken to 0.5 L with deionised water. The stock solutions were used in the ratios shown below (Table 2.1) to prepare potassium phosphate buffers of varying pH, and diluted accordingly for required buffer concentrations. pD of the deuterated phosphate buffers used for SKIE measurements was calculated from the relation: pD = pH meter reading + 0.41.[80]

Table 2.1: *Phosphate buffer stock solutions.*

pH	% 1 M K_2HPO_4	% 1 M KH_2PO_4
5.8	8.5	91.5
6	13.2	86.8
6.2	19.2	80.8
6.4	27.8	72.2
6.6	38.1	61.9
6.8	49.1	50.3
7.0	61.5	38.5
7.2	71.7	28.3
7.4	80.2	19.8
7.6	86.6	13.4
7.8	90.8	9.2
8.0	94.0	6.0

2.2.18 Urea stock solution (8 M)

Urea (210.21 g) was dissolved in 200 mL deionised water. After the crystals dissolved completely, ion exchange resin was added to deionise the solution. The stock solution was stirred overnight at room temperature, filtered and stored at 4 °C.

2.2.19 Kinetic buffers

2.2.19.1 100 mM phosphate buffer, 100 mM NaCl, 10 mM βME

For kinetic experiments at physiological pH, 100 mM phosphate buffer was used. 12.3 mL of monobasic potassium phosphate 1 M stock solution was added to 7.7 mL of dibasic potassium phosphate 1 M stock solution (Section 2.2.17) and the volume was taken to 190 mL with deionised water, and NaCl (1.16 g) and β–mercaptoethanol (140 μL) were added. The pH was adjusted to 7 and the volume was taken to 200 mL with deionised water.

2.2.19.2 MTEN buffer (25 mM MES, 50 mM Tris, 25 mM ethanolamine, 100 mM NaCl, 10 mM 2-mercaptoethanol)

For pH values between 9 and 5, MTEN buffer was used. 2-(N-morpholino)ethanesulfonic acid (0.49 g), Tris base (0.61 g) and NaCl (0.58 g) were dissolved in 90 mL deionised water containing ethanolamine (150.9 μL) and 2-mercaptoethanol (140 μL). The volume was taken to 100 mL and the pH was adjusted at the experimental temperature prior to use.

2.2.19.3 Urea/phosphate buffers

Kinetic experiments were performed in urea/phosphate buffers to explore the effect of different concentrations of urea on DHFR catalysis. 7 M urea was prepared by adding 12.3 mL of 1 M monobasic potassium phosphate stock solution, 7.7 mL of 1 M of dibasic potassium phosphate stock solution (Section 2.2.17), NaCl (1.16 g) and β–mercaptoethanol (140 μL) to 175 mL of the deionised urea stock solution (Section 2.2.18), The pH was adjusted to 7 and the volume was taken to 200 mL with deionised water. To prepare phosphate buffers containing different dilutions of urea, the solution was diluted using 100 mM potassium phosphate containing 100 mM NaCl and 10 mM βME (Section 2.2.19.1) and the pH of each serial dilution was adjusted to 7 before running kinetics.

2.2.19.4 Guanidinium hydrochloride (Gdn-HCl)/phosphate buffers

2 M stock solution of Gdn-HCl was prepared by dissolving 19.1 g of guanidinium hydrochloride in 90 mL of 100 mM phosphate buffer containing 100 mM NaCl and 10 mM βME (Section 2.2.19.1). The pH was adjusted to 7 and the volume was taken to 100 mL with 100 mM phosphate buffer and the pH was adjusted to 7. To make phosphate buffers containing serial dilutions of Gdn-HCl, the stock solution was diluted using 100 mM potassium phosphate (pH 7) containing 100 mM NaCl and 10 mM βME (Section 2.2.19.1) and the pH of each serial dilution was adjusted to 7 before running kinetics.

2.2.19.5 Various salt/phosphate buffers

2 M stock solutions of NaCl, KCl and KI were made by dissolving 5.844 g, 7.46 g and 16.6 g of NaCl, KCl and KF, respectively, in 45 mL of 100 mM potassium phosphate containing 10 mM βME (Section 2.2.19.1). The pH of each stock solution was adjusted to 7 and the volume was taken to 50 mL with 100 mM phosphate buffer (Section 2.2.19.1). To prepare phosphate buffers containing different concentrations of each salt, the stock solutions were diluted using 100 mM potassium phosphate (pH 7) containing 10 mM βME (Section 2.2.19.1) and the pH of each serial dilution was adjusted to 7 before running kinetics.

2.2.20 Protein dialysis buffer (5 mM potassium phosphate, 10 mM 2-mercaptoethanol, pH 7)

1 M monobasic potassium phosphate (12.3 mL), 1 M dibasic potassium phosphate (7.7 mL) (Section 2.2.17) and 2-mercaptoethanol (2.8 mL) were added to 3.95 L deionised water. The pH was adjusted to 7.0 and the total volume was taken to 4 L with deionised water. The buffer was used immediately and dialysis was performed at 4 °C.

2.2.21 Plasmid DNA purification buffers

The following buffers were prepared and stored at room temperature except buffer P1:

2.2.21.1 Buffer P1 (suspension buffer) (50 mM Tris-HCl, 10 mM EDTA, 50 µg/mL RNase A pH 8)

Tris-HCl (157.6 mg), EDTA (58.5 mg) and RNase A (50 µg/mL final concentration) were dissolved in 15 mL deionised water. The pH was adjusted to 8.0 and the total volume taken to 20 mL with deionised water. The solution was stored at 4 °C.

2.2.21.2 Buffer P2 (lysis buffer) (0.2 M NaOH, 1% (w/v) SDS)

NaOH (4 g) and SDS (5 g) were dissolved separately in 200 mL deionised water, the total volumes were taken to 250 mL and the solutions stored at room temperature. Immediately prior to use the two solutions were mixed 1:1.

2.2.21.3 Buffer N3 (neutralization and binding buffer) (4 M guanidine hydrochloride, 0.5 M potassium acetate, pH 4.2)

Guanidine hydrochloride (7.6 g) and potassium acetate (0.98 g) were dissolved in 15 mL deionised water. The pH was adjusted with 6 M HCl and the total volume taken to 20 mL with deionised water.

2.2.21.4 Buffer PB (wash buffer) (5 M Guanidine hydrochloride, 20 mM Tris-HCl, 38% (v/v) ethanol, pH 6.6)

Guanidine hydrochloride (9.5 g) and Tris-HCl (63.0 mg) were dissolved in 7.4 mL deionised water. Ethanol (7.6 mL) was added, the pH adjusted to 6.6 and the total volume taken to 20 mL with deionised water.

2.2.21.5 Buffer PE (wash buffer) (2 mM Tris-HCl , 20 mM NaCl, 80% (v/v) ethanol, pH 7.5)

NaCl (23.4 mg) and Tris-HCl (6.3 mg) were dissolved in 2 mL deionised water. Ethanol (16 mL) was added, the pH adjusted to 7.5 and the total volume taken to 20 mL with deionised water.

2.2.21.6 Buffer EB (elution buffer) (10 mM Tris-HCl, pH 8.5)

Tris-HCl (32 mg) was dissolved in 15 mL deionised water. The pH was adjusted to 8.5 and total volume taken to 20 mL.

2.2.22 Ethidium bromide solution (25 mM)

Ethidium bromide (8.1 g) was dissolved in 100 mL deionised water. The solution was wrapped in foil and stored in the dark at 4 °C. The solution was used at a working concentration of 6 μM, by adding 48 μL to 200 mL deionised water immediately prior to gel staining.

2.3 Methods

2.3.1 SDS-PAGE protocol

10 mL 4% stacking gel and 5 mL 10% running gel were prepared by mixing the following components (Table 2.2)

Table 2.2: *SDS-PAGE gel compositions*

Ingredient	**Stacking gel (4%)**	**Running gel (10%)**
30% Acrylamide/Bis-acrylamide, 29:1	0.67 mL	3.33 mL
Gel Buffer	1.25 mL	3.33 mL
Glycerol (50% (v/v))	-	2.60 mL
Sterile H_2O	3.00 mL	0.62 mL
APS and TEMED were added immediately prior to pouring the gel		
10% APS	50 μL	100 μL
TEMED	20 μL	20 μL

APS and TEMED were added to the running gel, mixed gently, and the gel was poured carefully between the two gel casting plates. A layer of isopropanol was added at the top of the gel to remove air bubbles and the gel was left for 20 minutes to polymerize. After complete polymerization, the isopropanol was removed and absorbed from the top of the gel with tissue and the stacking gel was poured carefully. A comb was added and the gel was left for an additional 20 minutes for complete polymerization. The gel was either used immediately or wrapped in wet tissue then wrapped with foil and stored at 4 °C.

2.3.2 Plasmid purification

After transforming cells (Section 2.3.9.2) with the desired plasmid, one colony was picked from an ampicillin selective plate, inoculated in 10 mL of ampicillin selective LB medium and incubated overnight at 37 °C and 150 rpm in an Innova® 43 shaker (New Brunswick Scientific, Hertfordshire, UK). Cells were harvested by centrifugation for 5 minutes at 4000 RCF (Eppendorf centrifuge 5415R). Then pure plasmid was isolated using a QIAprep spin miniprep kit (QIAGEN, Crawley, UK) *via* alkaline lysis of the bacterial cells. After that DNA was adsorbed onto a silica membrane in the presence of a high salt concentration, washed and eluted following the manufacturer's instructions (see Section 2.2.20 for purification buffers used).

2.3.3 DNA sequencing

The concentration of pure plasmid DNA isolated from the appropriate cloning strain of competent cells was measured by Nanodrop spectrophotometer and sent for sequencing in a concentration of 50-100 ng/μL by the DNA sequencing core, School of Biosciences, Cardiff University.

2.3.4 Synthesis of dihydrofolate (DHF)[81-82]

Ascorbic acid (8 g) was dissolved in 80 mL H_2O and the pH adjusted to 6.0. Folic acid (400 mg) was dissolved in a minimal volume of 0.1 M NaOH, added, and any fluctuation in pH adjusted back to pH 6.0. The mixture was stirred whilst purging with N_2 and sodium dithionite (4.4 g) was added. The reaction was cooled on ice for 5 min and the pH slowly taken to 2.8 *via* drop-wise addition of 1 M HCl. The precipitate was decanted and centrifuged at 4 °C, 27000g for 5 minutes. The solid pellet was added to another 80 mL of 10% ascorbic acid solution (pH 6.0), cooled on ice and the pH decreased to 2.8 by dropwise addition of 1 M HCl. The centrifugation step was repeated and the solid pellet re-suspended in ~20 mL acetone and centrifuged again. This washing step was carried out twice with acetone and once with diethyl ether. The sample tube containing the product was purged with N_2, wrapped in foil and stored at -20 °C. The product was dissolved in NaOD and D_2O for analysis of purity by proton NMR.

2.3.5 Synthesis of tetrahydrofolate (THF)[82-83]

Tetrahydrofolate was synthesized enzymatically from dihydrofolate using excess EcDHFR in the presence of alcohol dehydrogenase from *Thermoanaerobacter brockii* (TbADH), isopropanol and $NADP^+$. The reaction was incubated at 37 °C for 1-2 hours, then the product was purified using Dionex ICS3000 FPLC and eluted using a linear gradient of 0.2 M Tris buffer (Section 2.2.12.1). The peak of interest was collected, freeze dried, aliquoted and stored at -20 °C under argon. The concentration of THF was determined using the UV spectrometer at 297 nm using the extinction coefficient of 28000 M^{-1} cm^{-1}.

2.3.6 Enzymatic preparation of 4R-^{2}H-nicotinamide adenine dinucleotide phosphate reduced form (NADPD).[84-85]

Synthesis of NADPD relies on the 4R stereospecific reduction of $NADP^+$ TbADH, with d_8-isopropanol as the substrate.

$NADP^+$ (10 mg) was dissolved in ~1 mL 25 mM Tris buffer (pH 9.0) and 0.2 mL d_8-isopropanol was added. The volume was taken to 2 mL with the same buffer, and the reaction started by adding

6 units of TbADH. The reaction was incubated at 40 °C with stirring for 30 minutes. The reaction solution was purified by Dionex ICS3000 FPLC on a SAX10 anion exchange column eluting with a 0 to 0.75 M NaCl gradient over 14 min, then the eluted NADPD was flash frozen, wrapped in foil and stored at -20 °C.

2.3.7 Synthesis of ^{15}N-labelled NADP$^+$

2.3.7.1 Synthesis of ^{15}N-nicotinamide:

^{15}N-labelled nicotinamide was synthesized according to a literature protocol.[86] First the reaction was performed with unlabelled ammonium chloride to adjust the reaction conditions.

1 equivalent of nicotinic acid (123.1 mg, 1.0 mmol) was mixed with 1.5 equivalent of dicyclohexylcarbodiimide (DCC), (309.5 mg, 1.5 mmol) in dimethylformamide (DMF; 4 mL) and stirred at room temperature for 5 minutes. 1.5 equivalent of hydroxybenzotriazole (HOBt), 202.7 mg, 1.5 mmol), 4 equivalent of ^{15}N-NH_4Cl (215.6 mg, 4 mmol) and diisopropylethylamine (2 mL) were added. The reaction was stirred overnight at room temperature, then the solvent was evaporated under vacuum and an excess of water was added to the crude product to precipitate the co-product dicyclohexylurea, excess DCC and HOBt. The last step was repeated until no further precipitate formed, then the water was evaporated under vacuum and the crude product was dissolved in 2 mL deionised water and separated by preparative HPLC using a flow rate of 10 mL/min and monitoring the eluent at 254 nm, with a mixture of (99/1 v/v) aqueous formic acid (0.1%) and methanol.

2.3.7.2 Incorporation of ^{15}N-nicotinamide into NADP$^+$:

The ^{15}N-labelled nicotinamide was exchanged into NADP$^+$ using porcine brain NADase as described below.[87-88]

The labeled nicotinamide (250 mg) was incorporated into NADP$^+$ (80 mg) using porcine brain NADase (120 mg of 0.1 unit/mg) in 12 ml of 20 mM phosphate buffer pH 7.5 at 37 ºC. The exchange reaction was monitored by UV spectrometer by following the change in the absorbance at 340 nm after adding excess alcohol dehydrogenase from *Thermoanaerobacter brockii* (TbADH) and isopropanol. 5% trichloroacetic acid was added to the reaction mixture after 2 days to denature the NADase and the reaction mixture was centrifuged. ^{15}N-labeled NADP$^+$ was precipitated from the

supernatant with 5 volumes of cold acetone and used for NMR experiments without further purification.

All the NMR experiments were performed on Varian INOVA 800 MHz spectrometer at 20 °C in 50 mM phosphate buffer containing 1 mM of NaCl and 10 mM BME. 10% D_2O was added to all the NMR samples before being acquired. ^{15}N(AM)-$NADP^+$ was added to 2 fold excess of either DHFR/folate or DHFR/THF. The pH of the samples was adjusted carefully using 1M HCl and 1M KOH. Spectra were processed using the MATLAB based software package NMRLab/MetaboLab.[89]

2.3.8 Site directed mutagenesis

The following primers were used for site directed mutagenesis of EcDHFR and MpDHFR. The MpDHFR-G123V variant was created by Dr Rhiannon Evans.[90] The bases that have been replaced are underlined.

Ec-N23PP -Fwd- 5'-GAAAACGCCATGCCGTGGCCGCCGCTGCCTGCCGATCTCGCC-3'
Bwd- 5’-GGCGAGATCGGCAGGCAGCGGCGGCCACGGCATGGCGTTTTC-3’

Ec-M16L- Fwd- 5’-GATCGCGTTATCGGCCTGGAAAACGCCATGCCG-3’
Bwd- 5’-CGGCATGGCGTTTTCCAGGCCGATAACGCGATC-3’

Ec A19K-Fwd- 5’-GGCATGGAAAACAAAATGCCGTGGAACCTG-3’
Bwd- 5’-CAGGTTCCACGGCATTTTGTTTTCCATGCC-3’

Ec-M16L/A19K-Fwd- 5’-GATCGCGTTATCGGCCTGGAAAACAAAATGCCGTGGAAC-3’
Bwd- 5’-GTTCCACGGCATTTTGTTTTCCAGGCCGATAACGCGATC-3’

Ec-S148A -Fwd- 5'-GCGCAGAACGCTCACAGCTATTGC-3'
Bwd- 5’-GCAATAGCTGTGAGCGTTCTGCGC -3’

Ec-S148P -Fwd- 5’-GCTGATGCGCAGAACCCTCACAGCTATTGC-3’
Bwd- 5’-GCAATAGCTGTGAGGGTTCTGCGCATCAGC-3’

Mp-H24N -Fwd- 5’-GATAATAAGATGCCGTGGAATTTACCTGCTG-3’
Bwd- 5’-CAGCAGGTAAATTCCACGGCATCTTATTATC -3’

Mp-L16M- Fwd- 5'-CCGCGTGATTGGTATGGATAATAAGATGCCG-3'
Bwd- 5'-CGGCATCTTATTATCCATACCAATCACGCGG-3'

Mp-K19A- Fwd- 5'-GATTGGTTTAGATAATGCGATGCCGTGGCAT-3'
Bwd- 5'-ATGCCACGGCATCGCATTATCTAAACCAATC-3'

Mp-L16M/K19A-Fwd- 5'-AACCGCGTGATTGGTATGGATAATGCGATGCCGTGGCAT-3'
Bwd- 5'-ATGCCACGGCATCGCATTATCCATACCAATCACGCGGTT-3'

Mp-D124N- Fwd- 5'-GAATTAACCACCGAAGGGAATACTTGGTTC -3'
Bwd- 5'-GAACCAAGTATTCCCTTCGGTGGTTAATTC -3'

Mp-G123V- Fwd 5'-GAATTAACCACCGAAGTGGATACTTGGTTC-3'
Bwd 5'-GAACCAAGTATCCACTTCGGTGGTTAATTC-3'

Mp-P150S-Fwd- 5'-GCGGCAGATGATAAAAACTCGCATAATTACCGC-3'
Bwd- 5'-GCGGTAAT TATGCGAGTTTTTATCATCTGCCGC -3'

For EcDHFR-S148P, MpDHFR-H24N and MpDHFR-P150S, the Finnzymes Phusion® site directed mutagenesis kit was used. Several dilutions of template DNA were made and the required components were added (Table 2.3). The PCR cycle was set up as outlined in Table 2.4.

Table 2.3: *Components required for the site directed mutagenesis reactions.*		
Component	50 μL reaction	Final conc.
H_2O	To 50 μL	
5x Phusion® HF Buffer	10 μL	1x
20 mM dNTPs	0.5 μL	200 μM each
Fwd primer	1 μL	0.5 μM
Bwd primer	1 μL	0.5 μM
Template DNA	1 μL	-
DMSO	1.5 μL	3 %
$MgCl_2$	1 μL	1 mM
Phusion® DNA Polymerase	0.5 μL	0.02 U/μL

Table 2.4: *Temperatures and durations of the PCR cycle used in site directed mutagenesis.*			
Cycle step	Temperature	Time	Cycles
Initial denaturation	98 °C	1 m	1
Denaturation	98 °C	30 s	35
Annealing	70 °C	30 s	
Extension	72 °C	1m 40 s	
Final extension	72 °C	5 m	1
	4 °C	Hold	

For all other variants, the *Pfu* site directed mutagenesis kit was used. The components of the PCR reaction and the reaction cycles used are outlined in Tables 2.5 and 2.6.

Table 2.5: *Components required for the site directed mutagenesis reactions.*

Component	50 μL reaction	Final conc.
H_2O	To 50 μL	
10 x *Pfu* polymerase Buffer	5 μL	1x
20 mM dNTPs	0.5 μL	200 μM each
Fwd primer	2 μL	0.5 μM
Bwd primer	2 μL	0.5 μM
Template DNA	1 μL	-
Pfu DNA Polymerase	1 μL	0.02 U/μL

Table 2.6: *Temperatures and durations of the PCR cycle used in site directed mutagenesis.*

Cycle step	Temperature	Time	Cycles
Initial denaturation	95 °C	3 min	1
Denaturation	95 °C	1 min	16
Annealing	55-60 °C	2 min	
Extension	72 °C	12 min	
Final extension	72 °C	12 min	1
	4 °C	Hold	

2.3.9 Protein preparation

The bacterium *M. profunda* was purchased from the Belgian Co-ordinated Collections of Microorganisms – Laboratory of Microbiology Ghent University (BCCM-LMG).*Moritella profunda* chromosomal DNA was isolated, amplified and cloned in a PET expression vector by Dr Rhiannon Evans.[90] Primers were designed using the gene sequence for *M. profunda* (EMBL ID-AJ487535, UniProtKB/TrEMBL entry Q70YQ6), which was submitted in 2002 to the EMBL/GenBank/DDBJ databases by Xu and coworkers.[60]

2.3.9.1 Preparation of ultra-competent cells

Competent cells were prepared by streaking a glycerol stock of the cells on non-selective agar plates and ampicillin plates (as a negative control) and incubating at 37 °C overnight. A single colony from the agar plate was inoculated in non-selective LB medium (10 mL) and incubated at 37 °C until an optical density at 600 nm of 0.6 was reached after which the cells remained on ice. Cells were harvested by centrifugation at 5000 RPM, 4 °C for 5 minutes and the supernatant solution discarded. Cells were resuspended in 5 mL Rb1 solution (Section 2.2.8.1) and incubated on ice for 20 minutes, centrifugation step repeated. Then cells were resuspended in 6 mL of Rb2 solution (Section 2.2.8.2) then aliquoted (100 µL) into sterile Eppendorff tubes and flash frozen in liquid nitrogen for storage at -80 °C.

2.3.9.2 Transformation

Ultra-competent *E. coli* BL21 CodonPlus®(DE3) and *E. coli* BL21 CodonPlus®(DE3)RIL cells were used for plasmids harbouring EcDHFR and MpDHFR respectively.

A solution of the required plasmid (1-2 µL) was added to 100 µL ultra-competent cell suspension previously defrosted on ice. The cells were held on ice for 30 min and heat shocked in a water bath at 42 °C for 40 seconds. Preheated LB medium (250 µL) was then added to the cell suspension and the solution was incubated at 37 °C and 150 rpm for 30 min. The cells were plated on preheated agar plates containing ampicillin (100 mg/L). Inverted plates were incubated overnight at 37 °C and stored at 4 °C.

2.3.9.3 Expression

A single colony from a plate of freshly transformed cells was picked and inoculated in 100 mL LB medium (containing 100 mg/L ampicillin) overnight at 37 °C and 180 rpm. This overnight culture (60 mL) was used to inoculate 3000 mL of LB medium (containing 100 mg/L ampicillin) and the cells were then grown at 37 °C and 150 rpm until the OD_{600} was 0.6. Then temperature was taken to

16 °C, IPTG (120 mg/L) was added and protein was expressed at 16 °C overnight. The cells were then harvested *via* centrifugation in a Sorvall RC 6 Plus centrifuge (Thermo Fisher Scientific, Inc, MA, USA) using an SLA-3000 rotor at 6090 RCF for 20 minutes and the pellet either used immediately for purification or stored at -80 °C.

2.3.10 Protein purification

The harvested cells were re-suspended in a minimal volume of Buffer A (either 50 mM Tris buffer, pH 8.0 (Section 2.2.9.1) or 50 mM potassium phosphate buffer, pH 7 (Section 2.2.5.1), according to the purification method used). The suspension was sonicated three times for 5 min on ice and re-centrifuged at 17065 RCF for 30 minutes in a Sorvall RC 6 Plus centrifuge (Thermo Fisher Scientific, Inc, MA, USA) using an F21S-8x50 rotor to pellet cell debris. The supernatant solution was used for subsequent purification.

2.3.10.1 Protein purification method 1

2.3.10.1.1 Affinity chromatography (MTX)

The supernatant solution was applied to a methotrexate/agarose column equilibrated with Buffer A (Section 2.2.9.1). The column was washed with three coloum volumes of Buffer A then with one column volume of Buffer B (Section 2.2.9.2). Methotrexate is a specific reversible inhibitor of DHFR; therefore any DHFR present in the supernatant will bind the ligand and remain on the column. DHFR was eluted from the methotrexate column with 50 mL of 5 mM sodium folate (Buffer C, Section 2.2.9.3). Folic acid is the enzyme's substrate, which therefore competes with the methotrexate for the active site, releasing the enzyme from the column matrix. The eluent was dialysed overnight against 4 L of 5 mM potassium phosphate buffer at pH 7 (Section 2.2.18).

2.3.10.1.2 Anion exchange chromatography (DEAE)

The protein solution was applied to DEAE-Sepharose equilibrated with Buffer A. Bound proteins were eluted with a gradient from 0 to 1 M NaCl and used immediately for pre-steady state kinetics. For steady state kinetics the protein was either used fresh or exchanged into 2.5 mM potassium phosphate buffer (pH 7), 20 % glycerol, 0.1 mM EDTA, 1 mM DTT (Section 2.2.14), flash frozen and stored at -20°C.

2.3.10.2 Protein purification method 2

2.3.10.2.1 Anion exchange chromatography (Q-sepharose)

The supernatant solution (~30 mL) was applied to Q-sepharose column with column volume of 70 mL equilibrated with Buffer A (Section 2.2.5.1). The column was washed with 3-4 column volumes of Buffer A (Section 2.2.5.1) before eluting the protein with gradient from 0 to 1 M NaCl (using Buffer B (Section 2.2.5.2)) over 3 column volumes.

2.3.10.2.2 Size exclusion chromatography (Superdex 75)

The volume of the eluted protein was taken to 10 mL with Amicon and injected into Superdex 75 sixe exclusion column with column volume of 320 mL, equiliberated with Buffer A (Section 2.2.5.1). The enzyme was eluted with 1.5 column volume of Buffer A (Section 2.2.5.1).

2.3.11 Enzyme concentration determination

The concentration of the pure enzyme was determined by measuring the absorption at wavelengths of 210, 215 and 220 nm using equation (2.1)

$$Concentration(mg/mL) = \left(\left(\frac{A_{210}}{\varepsilon_{210}} + \frac{A_{215}}{\varepsilon_{215}} + \frac{A_{220}}{\varepsilon_{220}} \right) \times df \right) / 3 \qquad (2.1)$$

where *df* is the dilution factor, A_{210}, A_{215}, A_{220} and ε_{210}, ε_{215}, ε_{220} are the absorptions and the excitation coefficients at 210, 215 and 220 nm respectively. ε_{210} = 20 $ml.mg^{-1}.cm^{-1}$, ε_{215} =15 $ml.mg^{-1}.cm^{-1}$ and ε_{220} = 11 $ml.mg^{-1}.cm^{-1}$.

To express the concentration into μM, the concentration in mg/mL was divided by the enzyme molecular weight (18000 for EcDHFR and 18291 for MpDHFR) and multiplied by 10^6 (equation 2.2).

$$Concentration(\mu M) = \frac{Conc._{mg/mL}}{M.wt} \times 10^6 \qquad (2.2)$$

2.3.12 Kinetic assay

2.3.12.1 Steady state kinetics

Steady state turnover numbers (k_{cat}) were measured under saturating conditions by monitoring the linear decrease in the absorbance of the reduced cofactor NADPH at 340 nm with time *via* UV spectroscopy. For all the steady state kinetics reported in this work, 8-50 nM DHFR was incubated with NADPH/NADPD (100 μM) in the appropriate assay buffer for 60 seconds at the experimental temperature, to avoid hysteresis,[7] prior to the addition of DHF (100 μM) to initiate the reaction. Each data point was measured at least three times then the total rate of formation the product in $\mu M.s^{-1}$ was calculated using the expression:

$$Velocity\,(\mu M.s^{-1}) = \left(\frac{\delta AU \,\min^{-1} cm^{-1}}{\varepsilon \times 60} \right) \times 10^{6} \qquad (2.3)$$

Where ε is the molar absorbance change at 340 nm during the DHFR catalysed reaction, 11800 M^{-1} cm^{-1}.[80]

2.3.12.2 Measuring the Michaelis constant (K_M)

Michaelis constants were measured following the same method as k_{cat} (Section 2.3.12.1), except that an enzyme concentration of 10-20 nM was used. The concentration of NADPH was varied from 0.1 to 200 μM, and of the concentration of DHF was varied from 0.1 to 100 μM. When the concentration of one substrate was varied, that of the other was maintained at 100 μM. Each data point is the result of three independent measurements. The Michaelis-Menten equation was fit to the change in initial rate with concentration using SigmaPlot 10.

2.3.12.3 Pre-steady state (stopped-flow) kinetics

Pre-steady state kinetic experiments were performed on an Applied Photophysics stopped-flow spectrophotometer. Hydride transfer rate constants were measured following the fluorescence resonance energy transfer from the protein to the reduced cofactor NADPH. The reaction mixture was excited at 292 nm and the emission was measured using an output filter with a cut-off at 400 nm. DHFR (20-40 μM syringe concentration) was incubated with NADPH or NADPD (10-20 μM) at the experimental temperature for at least 3 minutes to avoid hysteresis. Then the reaction was started by rapidly mixing with an equal volume of dihydrofolate (200-400 μM).

2.3.12.4 Measurements of THF dissociation rates

The dissociation rates of THF were measured using stop flow apparatus by monitoring the decrease in the fluorescence signals at 340 nm following excitation at 292 nm. Different binary and ternary complexes were rapidly mixed with an excess of methotrexate.

2.3.12.5 pH dependence kinetics

Steady state and pre-steady state pH dependences were examined in MTEN buffer (Section 2.2.19) in the range between 5 and 9 for steady state catalysis either at room temperature or at 5 °C. The pH of the buffer was adjusted carefully at the experimental temperature before use. For all the experiments performed in deuterated buffers, pD was calculated from the relation: pD = pH meter reading + 0.41.[80]

2.3.13 Circular Dichroism spectroscopy

All circular dichroism spectroscopy was carried out using a Chirascan^{TM} spectrometer (Applied Photophysics Limited, UK).

2.3.13.1 Buffers for thermal denaturation experiments

5 mM potassium phosphate buffer (pH 7) was used to record the thermal melting temperature of the various enzymes used. The buffer was sterilised with a 0.2 μm syringe filter and degassed *via* vacuum pump. A blank run was always taken of the buffer alone before starting the experiment.

2.3.13.2 Calculation of Mean Residue Ellipticity (MRE)

The signal obtained from CD experiments was converted into mean residue ellipticity (Θ_{MRE}) using Equation 2.4.

$$\Theta_{MRE} = \Theta / 10.n.c.l \qquad (2.4)$$

where: Θ = CD signal in millideg, n = number of backbone peptide bonds (*i.e.* number of amino acid residues - 1), c = molar concentration of sample, and l = pathlength of cuvette used in cm.

Typically a 1 mm pathlength cuvette was used to monitor the CD spectrum of DHFR from 190-400 nm using ~10 μM enzyme.

2.3.14 Errors and propagations

2.3.14.1 Standard deviation and standard error of the mean

The errors in this work are reported as the standard error of the mean (σ_M) as in Equation 2.5 which is defined as the standard deviation (Equation 2.6) of the values in the sample divided by the square root of the sample size.

$$\sigma_M = \frac{\sigma}{\sqrt{n}} \tag{2.5}$$

where X is each value measured in the sample, M is the mean of the sample and n is the sample size.

$$\sigma = \sqrt{\frac{\Sigma(X-M)^2}{(n-1)^2}} \tag{2.6}$$

2.3.14.2 Propagation of errors

In this thesis the effect of the uncertainty of values directly measured experimentally (X or Y) on the uncertainty of a function based up on them (Z) was calculated using Equations 2.7-10. The equation used is dependent on the treatment of X and Y in order to obtain the value of Z.

If Z = X + Y or Z = X – Y then

$$\Delta Z = \sqrt{\Delta X^2 + \Delta Y^2} \tag{2.7}$$

If Z = X * Y or Z = X / Y then

$$\Delta Z = Z\sqrt{\left(\frac{\Delta X}{X}\right)^2 + \left(\frac{\Delta Y}{Y}\right)^2} \tag{2.8}$$

If Y = ln X then

$$\Delta Y = \frac{\Delta X}{X} \tag{2.9}$$

$Y = e^X$ then

$$\Delta Y = \Delta X \times e^X \tag{2.10}$$

where X and Y are independently measured values, ΔX and ΔY are their errors or uncertainty, and Z is the calculated value and ΔZ is its propagated error.

Results and Discussion

3

Hydride transfer catalysed by a cold adapted dihydrofolate reductase

3.1 Preface

DHFRs from the mesophilic bacterium *Escherichia coli* (EcDHFR) and the thermophilic bacterium *Thermotoga maritima* (TmDHFR) have been extensively studied. Studying a psychrophilic DHFR is important to expand the temperature range over which they have been analysed. The main target is to compare DHFR homologues across a wide temperature range, and to study their ability to function at different temperatures. This should give more information about the role of protein motions and tunnelling of the transferred hydride in the chemical step of the different homologues, and give deeper insight into the structural elements that present the specific adaptations of each homologue.

DHFR from the psychrophilic bacterium *Moritella profunda* (MpDHFR) has a very similar crystal structure to EcDHFR[91] and the two enzymes are monomers and exhibit 55% sequence identity.[92] On the other hand, DHFR from the hyperthermophilic bacterium *Thermotoga maritima* (TmDHFR) is the only DHFR shown to be dimeric so far, although it is likely that other DHFRs from the genus *Thermotoga* are also dimeric.[93-94] In spite of the dimeric structure of TmDHFR, this enzyme maintains a very similar tertiary structure to that of monomeric DHFRs[63] with 23% sequence identity with EcDHFR and 26% with MpDHFR.

In this chapter, hydride transfer catalysed by the cold adapted dihydrofolate reductase from *Moritella profunda* (MpDHFR) and kinetic isotope effect (KIE) in the steady and pre-steady state are reported. The data obtained is compared with hydride transfer data for the mesophilic EcDHFR and the hyperthermophelic TmDHFR.

3.2 Measurements of hydride transfer catalysed by MpDHFR

Hydride transfer rate constants for MpDHFR were measured under single-turnover conditions using an Applied Photophysics stopped-flow spectrophotometer. Reduction of the fluorescence resonance energy transfer (FRET) from the enzyme to NADPH during the reaction was observed by exciting the sample at 292 nm and measuring the emission at 450 nm (Figure 3.1).

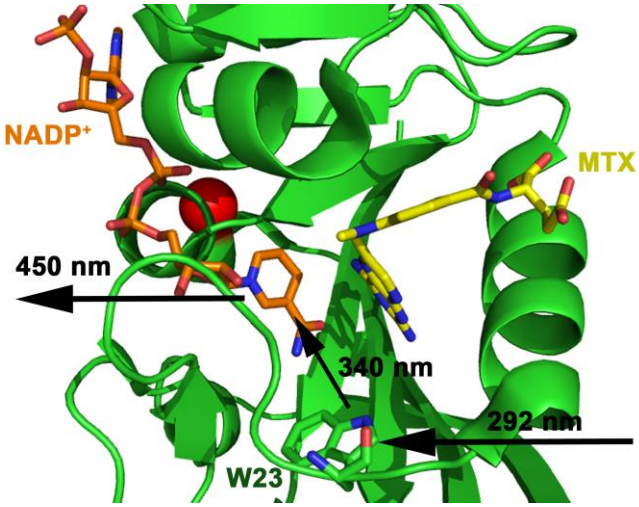

Figure 3.1: *Cartoon representation of MpDHFR (PDB 3IA4)[62] illustrating fluorescence resonance energy transfer (FRET) from W23 in the active site to the cofactor (NADPH). The position of C105 is shown as a red sphere.*

Unlike in EcDHFR, hydride transfer could not be measured in MpDHFR purified using buffers containing only 5 mM β-mercaptoethanol. MpDHFR has only one cysteine residue in position 105, (phenylalanine in EcDHFR), close to the cofactor-binding site (Figure 3.1), which might become oxidised, causing the poor stopped flow signals. Therefore, either 10 mM β-mercaptoethanol or 5 mM DTT were added to all of the purification and kinetic buffers in order to measure hydride transfer by MpDHFR to prevent the enzyme oxidation during the purification and the measurements.

A recent NMR study in our group for MpDHFR in the ternary complex E.$NADP^+$.Folate showed a doubling of resonance for the residues around C105 related to the reduced and the oxidized enzyme. Such doubling of resonances was not observed for the cysteine residues in EcDHFR in the same complex under the same conditions.[95] Hydrogen-deuterium exchange experiments gave evidence that MpDHFR is more flexible than EcDHFR, which might in turn make MpDHFR more exposed to oxidation than its mesophilic counterpart.[96] The two variants MpDHFR-C105A and C105S have been created and studied before, but both mutants showed remarkably different kinetics to the wild-type enzyme and no additional studies were performed.[90,95] To avoid enzyme oxidation, argon saturated buffers were used for preparing all the NMR samples.[95]

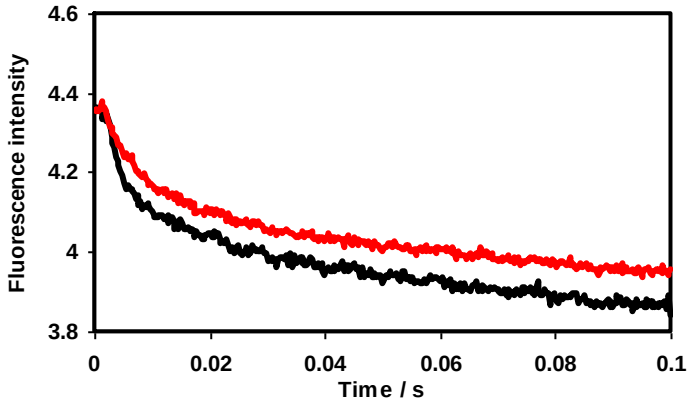

Figure 3.2: *Stopped flow traces of hydride (black) and deuteride (red) transfer catalysed by MpDHFR at 20 °C.*

The stopped flow trace was different when deuteride was transferred in comparison to hydride (Figure 3.2). An initial burst phase was observed for both NADPH and NADPD, but with NADPD the change in signal amplitude was to some extent lower than that of NADPH across the whole time of the measurement.

3.2.1 Temperature dependences of hydride transfer from MpDHFR

The temperature dependences for hydride and deuteride transfer were measured for MpDHFR at temperatures between 5 and 30 ^{o}C, at pH 7 in H_2O (Figure 3.3 and Table 3.1) and D_2O (Table 3.1). A wider temperature range could not be used due to the low melting temperature for MpDHFR as measured by CD spectroscopy (~37 °C).[79]

At pH 7 and under the temperature range used, k_H was significantly higher than k_{cat} (k_{cat} = 14.78 ± 0.79 s^{-1} at 20 ˚C)[79], which is in good accordance with the reported value of the steady state primary hydrogen kinetic isotope effect (KIE) (KIE = 1.05 ± 0.04 at 20 ˚C)[79] and indicates that k_{cat} is reflecting a physical step of the catalytic cycle. Similar observations were reported for EcDHFR as k_{cat} is representing THF release from the ternary product complex E.NADPH.THF.[7] In contrast the thermophilic enzyme, TmDHFR, has a contribution from the chemical step to the steady state rate at physiological pH with a KIE of 3.5.[64] Comparing the rate constants obtained for MpDHFR in both H_2O and D_2O with those obtained for EcDHFR and TmDHFR, shows an increase in the efficiency of hydride transfer with decreasing thermophilicity (Tables 3.1, 3.2 and 3.3). The psychrophilic enzyme, MpDHFR, and mesophilic enzyme, EcDHFR, have hydride transfer rate constants of similar magnitude (100-1000 s^{-1}), whilst that for the thermophilic TmDHFR is reduced in

comparison, at around 1-10 s^{-1}.[96-98] The hydride transfer rate constants were predicted for the three DHFRs, by linear extrapolation from the Arrhenius plots, at the typical operating temperatures and were found to be 255.0 ± 6.4, 317.3 ± 1.6 and 8.2 ± 0.1 s^{-1} for MpDHFR at 2 ºC, EcDHFR at 37 ºC and TmDHFR at 90 ºC, respectively.[96]

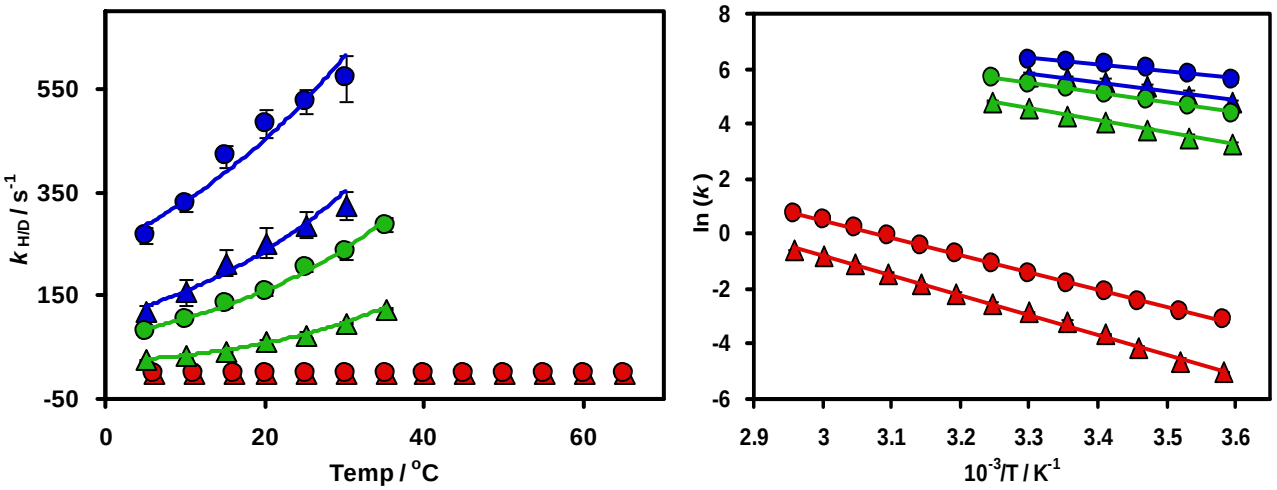

Figure 3.3: *Temperature dependence (left) and Arrhenius plots (right) of the pre-steady state rate constants for hydride (k_H, circles) and deuteride (k_D, triangles) transfer during catalysis by TmDHFR[98] (red), EcDHFR[98] (green) and MpDHFR (blue) at pH 7.*

In D_2O, similar to the mesophilic and the thermophilic enzyme (Tables 3.2 and 3.3),[98] a significant increase in the rate constants for both hydride and deuteride transfer was seen with MpDHFR (Table 3.1). An apparent inverse solvent KIE of 0.63 ± 0.04 for hydride transfer and 0.63 ± 0.06 for deuteride transfer was determined for the MpDHFR catalysed reaction at 20 ºC compared to 0.41 ± 0.05 and 0.42 ± 0.02 for hydride transfer and 0.25 ± 0.12 and 0.45 ± 0.05 for deuteride transfer for the mesosphilic and the thermophilic homologs at the same temperature,[98] respectively. Measurement of hydride transfer rates at varying pH in D_2O for MpDHFR catalysed reaction (Figure 3.4 and Table 3.4) is showing that the increase in k_H is a result of a D_2O-induced pK_a shift (to 7.13 ± 0.13, a shift of 0.60 ± 0.03 pH units) rather than affecting the chemistry of the reaction.[99]

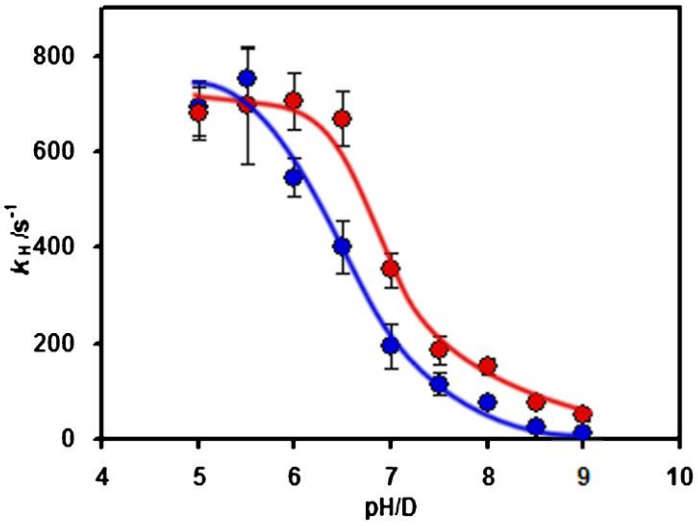

Figure 3.4: *The pH/D dependence for the MpDHFR catalyzed reaction in MTEN buffer at 5 ºC.*

Table 3.1: *Temperature dependence of the pre-steady-state rate constants for hydride (k_H) and deuteride (k_D) transfer during catalysis by MpDHFR at pH 7 in H_2O and D_2O.*

	H_2O		D_2O	
T (^oC)	k_H (s^{-1})	k_D (s^{-1})	k_H (s^{-1})	k_D (s^{-1})
5	267.6 ± 14.4	118.9 ± 14.5	400.0 ± 57.8	231.6 ± 35.5
10	327.2 ± 14.4	157.2 ± 25.6	545 ± 54.6	307.4 ± 52.7
15	420.3 ± 21.3	213.9 ± 25.1	698.0 ± 66.9	381.7 ± 36.9
20	484.4 ± 28.0	253.0 ± 30.4	773.2 ± 79.6	403.5 ± 43.2
25	526.8 ± 23.2	288.0 ± 24.8	815.5 ± 138.1	420.7 ± 76.5
30	570.5 ± 44.1	323.5 ± 26.9	871.6 ± 142.3	421.7 ± 80.8

Table 3.2: *Temperature dependence of the pre-steady-state rate constants for hydride (k_H) and deuteride (k_D) transfer during catalysis by EcDHFR in H_2O and D_2O at pH 7.*[a]

	H_2O		D_2O	
T (^oC)	k_H (s^{-1})	k_D (s^{-1})	k_H (s^{-1})	k_D (s^{-1})
5	81.9 ± 1.7	26.9 ± 1.9	141.4 ± 10.8	68.9 ± 13.1
10	106.3 ± 3.1	34.1± 3.4	198.5 ± 12.2	121.3 ± 13.6
15	135.3 ± 5.6	44.6± 3.7	246.3 ± 22.4	153.3 ± 22.0
20	159.8 ± 7.9	60.2 ± 4.1	386.3 ± 5.8	239.1 ± 51.9
25	203.7 ± 7.4	75.1 ± 5.4	506.3 ± 22.6	234.1 ± 3.0
30	235.4 ± 13.8	98.5 ± 2.8	597.8 ± 12.0	408.8 ± 9.6
35	287.9 ± 12.0	125.9 ± 3.5	767.0 ± 39.4	535.5 ± 17.6

[a] Data measured by Dr Joel Loveridge and Dr Richard Swanwick[98]

Table 3.3: *Temperature dependence of the pre-steady-state rate constants for hydride (k_H) and deuteride (k_D) transfer during catalysis by TmDHFR in H_2O and D_2O at pH 7.*[a]

T (^oC)	H_2O		D_2O	
	k_H (s^{-1})	k_D (s^{-1})	k_H (s^{-1})	k_D (s^{-1})
6	0.044 ± 0.001	0.0066 ± 0.0002	0.090 ± 0.006	0.015 ± 0.001
11	0.060 ± 0.003	0.010 ± 0.001	0.126 ± 0.013	0.022 ± 0.001
16	0.087 ± 0.002	0.016 ± 0.001	0.191 ± 0.011	0.037 ± 0.003
20	0.122 ± 0.003	0.027 ± 0.001	0.266 ± 0.020	0.063 ± 0.003
25	0.169 ± 0.002	0.042 ± 0.003	0.379 ± 0.017	0.093 ± 0.011
30	0.242 ± 0.005	0.060 ± 0.002	0.581 ± 0.049	0.147 ± 0.010
35	0.341 ± 0.006	0.082 ± 0.005	0.812 ± 0.035	0.181 ± 0.015
40	0.488 ± 0.010	0.116 ± 0.007	1.126 ± 0.033	0.270 ± 0.026
45	0.668 ± 0.015	0.161 ± 0.003	1.518 ± 0.081	0.389 ± 0.028
50	0.932 ± 0.036	0.245 ± 0.011	2.058 ± 0.095	0.510 ± 0.030
55	1.253 ± 0.057	0.336 ± 0.015	2.868 ± 0.198	0.775 ± 0.043
60	1.654 ± 0.093	0.444 ± 0.019	3.634 ± 0.219	1.034 ± 0.034
65	2.120 ± 0.159	0.575 ± 0.013	4.467 ± 0.272	1.290 ± 0.113

[a] Data measured by Dr Joel Loveridge[98]

Table 3.4: *Rate constants for hydride transfer (k_H) for the MpDHFR catalyzed reaction in MTEN buffered H_2O and D_2O at 5 ºC.*

pH	k_H in H_2O / s^{-1}	k_H in D_2O / s^{-1}
5	690.9 ± 59.1	678.8 ± 54.9
5.5	752.2 ± 63.1	698.2 ± 122.8
6	545.7 ± 40.6	705.6 ± 60.4
6.5	401.6 ± 54.8	669.2 ± 56.1
7	195.4 ± 47.1	353.7 ± 35.3
7.5	115.3 ± 23.4	184.0 ± 29.6
8	75.3 ± 5.5	153.0 ± 16.1
8.5	25.2 ± 5.2	75.7 ± 10.1
9	14.0 ± 3.2	48.7 ± 8.9

3.2.2 Temperature dependence of the kinetic isotope effect (KIE) for the reaction catalyzed by MpDHFR

The pre-steady state rate constants with both NADPH and NADPD for the MpDHFR catalysed reaction were measured in both H_2O and D_2O. The primary KIE of the hydride transfer event was determined by dividing the rate constant with NADPH by that of NADPD at the same temperature (Table 3.5). The data was compared with the KIE for the mesophilic and the thermophilic enzyme (Figure 3.5).

In H_2O, MpDHFR has a similar temperature dependence of the KIE to that observed for EcDHFR[98] (Figure 3.5). The activation energy for MpDHFR-catalyzed hydride transfer was found to be 21.6 ± 2.2 $kJ.mol^{-1}$, compared to 28.1 ± 2.5 $kJ.mol^{-1}$ for deuteride transfer, The KIE is temperature dependent with a ΔE_a of 6.6 ± 3.4 $kJ.mol^{-1}$ (Figure 3.4 and Table 3.6). The activation energy (and activation enthalpy) for the hydride transfer reaction was most favorable for MpDHFR and least favorable for TmDHFR (Table 3.11).

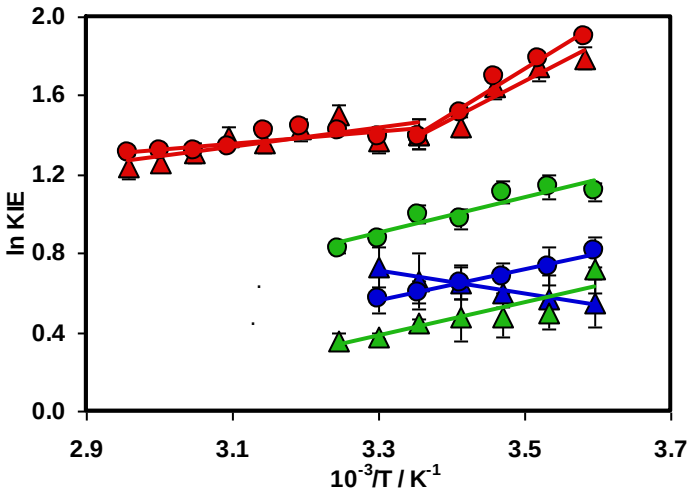

Figure 3.5: *The temperature dependence of the KIEs, plotted on a logarithmic scale against the inverse temperature, during catalysis by MpDHFR (blue), EcDHFR[98] (green) and TmDHFR[98] (red), measured in H_2O (circles) and D_2O (triangles) under single turnover conditions at pH 7.*

In D_2O, MpDHFR has a different temperature dependence of the KIE to that reported for EcDHFR (Figure 3.5). However, the isotope effects in EcDHFR at pH 7 were interdependent with KIE values lower than those of H_2O; KIEs in D_2O for MpDHFR (Table 3.6) were very similar within experimental error to those in H_2O (Table 3.5), as seen previously for TmDHFR.[98]

Unlike MpDHFR and EcDHFR, the temperature dependence of the KIE for TmDHFR, in both H_2O and D_2O, was shown to have a breakpoint at 25 ˚C with the KIE being temperature dependence below the breakpoint and temperature independent above.[100] However, the breakpoint disappeared when the salt bridges in the dimer interface were removed[93] and in high concentration of sucrose,[100] which was proposed to apply specific effects at the dimer interface, suggesting that the breakpoint in the temperature dependence of the KIE for TmDHFR is most probably related to the dimer interface.[93,100]

***Table 3.5**: Temperature dependence of the pre-steady state KIE during catalysis by MpDHFR, EcDHFR and TmDHFR in H_2O at pH 7*

T (^oC)	MpDHFR	EcDHFR [a]	TmDHFR[a]
5	2.25 ± 0.13	3.04 ± 0.22	nd
6	nd	nd	6.67 ± 0.25
10	2.08 ± 0.17	3.12 ± 0.32	nd
11	nd	nd	6.19 ± 0.71
15	1.96 ± 0.13	3.03 ± 0.28	nd
16	nd	nd	5.44 ± 0.36
20	1.91 ± 0.13	2.65 ± 0.22	4.52 ± 0.20
25	1.83 ± 0.10	2.71 ± 0.22	4.02 ± 0.29
30	1.76 ± 0.11	2.39 ± 0.16	4.03 ± 0.16
35	nd	2.29 ± 0.11	4.16 ± 0.26
40	nd	nd	4.21 ± 0.27
45	nd	nd	4.15 ± 0.12
50	nd	nd	3.80 ± 0.23
55	nd	nd	3.73 ± 0.24
60	nd	nd	3.73 ± 0.26
65	nd	nd	3.69 ± 0.29

[a] Data measured by Dr Joel Loveridge[98]

***Table 3.6**: Temperature dependence of the pre-steady state KIE during catalysis by MpDHFR, EcDHFR and TmDHFR in D_2O at pH 7*

T (^oC)	MpDHFR	EcDHFR [a]	TmDHFR [a]
5	1.7 ± 0.2	2.05 ± 0.42	nd
6	nd	nd	5.96 ± 0.53
10	1.8 ± 0.2	1.64 ± 0.21	nd
11	nd	nd	5.77 ± 0.60
15	1.8 ± 0.1	1.61 ± 0.27	nd
16	nd	nd	5.11 ± 0.50
20	1.9 ± 0.2	1.62 ± 0.35	4.24 ± 0.36
25	1.9 ± 0.3	1.56 ± 0.07	4.07 ± 0.53
30	2.1 ± 0.3	1.46 ± 0.05	3.95 ± 0.42
35	nd	1.43 ± 0.09	4.48 ± 0.42
40	nd	nd	4.16 ± 0.42
45	nd	nd	3.90 ± 0.35
50	nd	nd	4.03 ± 0.30
55	nd	nd	3.70 ± 0.33
60	nd	nd	3.52 ± 0.24
65	nd	nd	3.46 ± 0.37

[a] Data measured by Dr Joel Loveridge[98]

***Table 3.7**: Pre steady state activation energies during catalysis by MpDHFR and EcDHFR at pH 7 in H_2O.*

Enzyme		E_a^H ($kJ.mol^{-1}$)	E_a^D ($kJ.mol^{-1}$)	ΔE_a ($kJ.mol^{-1}$)
MpDHFR		21.55 ± 2.18	28.11 ± 2.55	6.56 ± 3.35
EcDHFR[a]		29.42 ± 0.71	37.02 ± 0.58	7.60 ± 0.92
TmDHFR[a]	(< 25 ºC)	49.95 ± 1.68	69.28 ± 3.69	19.32 ± 4.05
	(> 25 ºC)	53.55 ± 0.44	56.03 ± 0.84	2.49 ± 0.95

[a] rate constants measured by Dr Joel Loveridge[98]

***Table 3.8**: Pre-steady state activation energies during catalysis by MpDHFR and EcDHFR at pH 7 in D_2O.*

Enzyme		E_a^H (kJ.mol^{-1})	E_a^D (kJ.mol^{-1})	ΔE_a (kJ.mol^{-1})
MpDHFR		21.0 ± 3.5	16.17 ± 3.74	-4.85 ± 5.13
EcDHFR[a]		40.79 ± 1.77	47.62 ± 2.28	6.83 ± 2.89
TmDHFR[a]	(< 25 ºC)	53.29 ± 1.34	68.90 ± 3.77	15.61 ± 4.00
	(> 25 ºC)	51.79 ± 0.93	55.66 ± 1.16	3.87 ± 1.49

[a] rate constants measured by Dr Joel Loveridge[98]

***Table 3.9**: Pre-steady state Arrhenius prefactors (A) during catalysis by MpDHFR and EcDHFR at pH 7 in H_2O.*

Enzyme		A_H (s^{-1})	A_D (s^{-1})	A_H/A_D
MpDHFR		(3.17 ± 0.19) x 10^6	(2.44 ± 0.15) x 10^7	0.13 ± 0.09
EcDHFR[a]		(2.82 ± 0.05) x 10^7	(2.34 ± 0.03) x 10^8	0.12 ± 0.002
TmDHFR[a]	(< 25 ºC)	(9.47 ± 0.36) x 10^7	(5.65 ± 0.35) x 10^{10}	0.002 ± 0.001
	(> 25 ºC)	(4.11 ± 0.03) x 10^7	(2.67 ± 0.04) x 10^8	1.54 ± 0.36

[a] rate constants measured by Dr Joel Loveridge[98]

***Table 3.10**: Pre steady state Arrhenius prefactors (A) during catalysis by MpDHFR and EcDHFR at pH 7 in D_2O.*

Enzyme		A_H (s^{-1})	A_D (s^{-1})	A_H/A_D
MpDHFR		(4.01 ± 0.38) x 10^6	(2.88 ± 0.36) x 10^5	13.94 ± 0.2
EcDHFR[a]		(6.58 ± 0.21) x 10^9	(6.75 ± 0.25) x 10^{10}	0.098 ± 0.005
TmDHFR[a]	(< 25 ºC)	(8.20 ± 0.22) x 10^8	(1.11 ± 0.07) x 10^{11}	0.007 ± 0.006
	(> 25 ºC)	(4.79 ± 8.42) x 10^8	(5.31 ± 0.12) x 10^8	0.90 ± 0.56

[a] rate constants measured by Dr Joel Loveridge[98]

***Table 3.11**: Activation parameters for hydride transfer catalyzed by MpDHFR, EcDHFR and TmDHFR at pH 7.*

Parameter	MpDHFR	EcDHFR[99]	TmDHFR[101]
$\Delta H^{\ddagger}_{H}$ / kJ mol^{-1}	19.2 ± 2.2	27.4 ± 0.6	50.9 ± 0.5 [b]
$\Delta H^{\ddagger}_{D}$ / kJ mol^{-1}	25.7 ± 2.6	35.3 ± 0.6	53.4 ± 0.8 [b]
$\Delta S^{\ddagger}_{H}$ / J mol^{-1}	-128.6 ± 1.4	-109.0 ± 2.5	-88.9 ± 1.2 [b]
$\Delta S^{\ddagger}_{D}$ / J mol^{-1}	-111.6 ± 1.2	-90.3 ± 1.8	-92.4 ± 2.3 [b]
$\Delta G^{\ddagger}_{H}$ / kJ mol^{-1} [a]	57.5 ± 2.2	59.9 ± 0.6	77.4 ± 0.5
$\Delta G^{\ddagger}_{D}$ / kJ mol^{-1} [a]	59.0 ± 2.6	62.2 ± 0.6	80.9 ± 0.8

[a] At 25 °C; [b] Above 25 ºC.

3.3 Measuring hydride transfer using steady state kinetics

The complete kinetic cycle for EcDHFR has been reported in 1987 by Benkovic and co-workers.[7] They give evidence that product release is the rate determining step for EcDHFR in the steady state at physiological pH. However, hydride transfer becomes the rate-determining step above pH 8.4.[7,102] Hence, hydride transfer rates were measured under steady-state conditions at pH 9.5 for EcDHFR where the steady-state rate reflects the rate of the chemical step only.[103] The steady state rate for the MpDHFR catalysed reaction was determined at pH 9, not pH 9.5 as for EcDHFR, due to high errors on the catalytic rate at pH 9.5. For TmDHFR the steady state measurements were determined at pH 7, where hydride transfer is partially rate limiting.[64]

The temperature dependences of the steady state turnover rates during EcDHFR catalysis (Table 3.13) was reported previously.[103] In this part, the temperature dependences of the steady state turnover rates for the reduction of DHF with NADPH and NADPD during MpDHFR (Table 3.12) and TmDHFR (Table 3.14) catalysis (Figure 3.6) were determined in H_2O and D_2O from the decrease in the absorbance at 340 nm due to the oxidation of the cofactor using UV/vis spectroscopy.

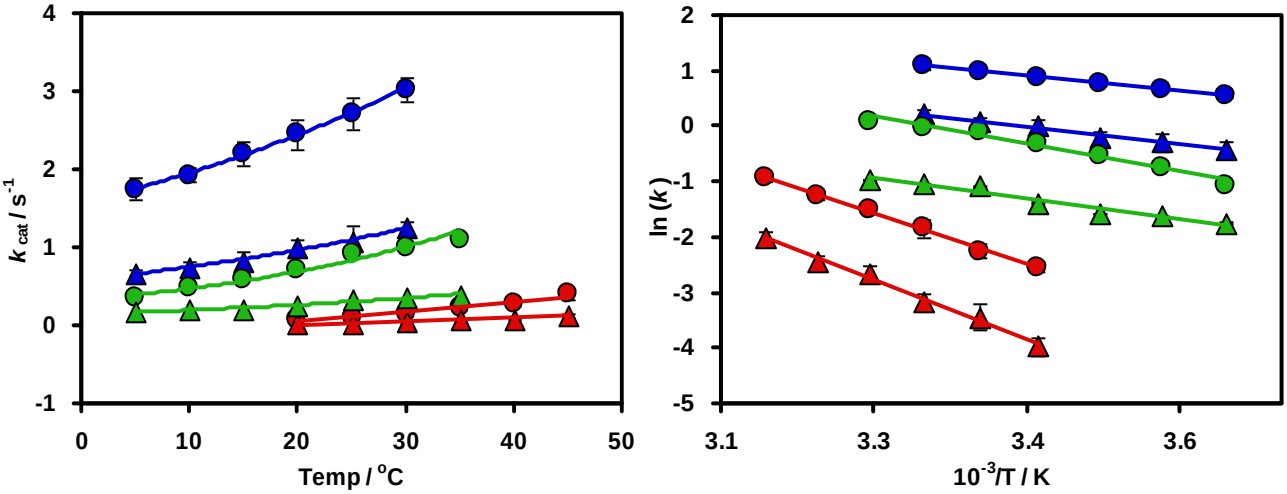

Figure 3.6: *Temperature dependence (left) and Arrhenius plots (right) of the steady state rate constants for hydride (k_{cat}^{H}, circles) and deuteride (k_{cat}^{D}, triangles) transfer during catalysis by TmDHFR (red), EcDHFR[103] (green) and MpDHFR (blue) in H_2O at pH 7, 9.5 and 9 respectively.*

Similar to the pre-steady state kinetics, the rate constants obtained in D_2O were higher than those in H_2O (Tables 3.12, and 3.14). The KIE for hydride/deuteride transfer in H_2O and D_2O was determined by dividing the rate of H transfer by the rate of D transfer (Figure 3.7).

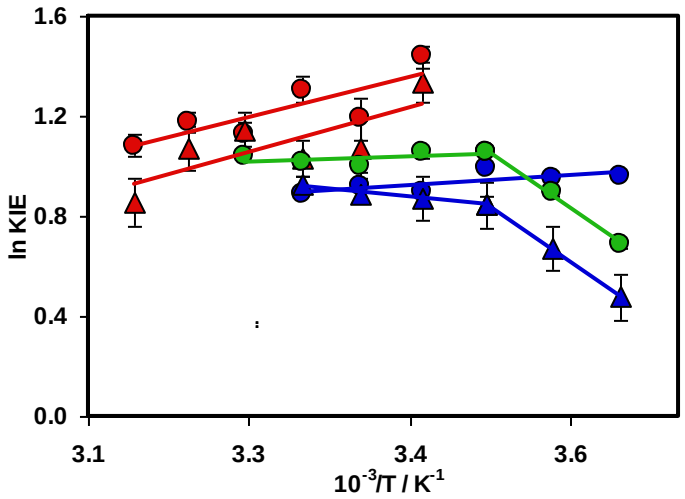

Figure 3.7: *KIEs measured under saturating conditions in H_2O (circle) and D_2O (triangle) plotted on a logarithmic scale against the inverse temperature for MpDHFR (blue) at pH 9, EcDHFR at pH 9.5[103] (green) and TmDHFR (red) at pH 7.*

As seen with EcDHFR, during catalysis by MpDHFR at elevated pH the chemical step is partially rate limiting and the KIE was temperature independent (on average 2.55 ± 0.11 in H_2O and 2.20 ±

0.11 in D_2O) within experimental errors (Figure 3.7 and Table 3.15). Under steady state conditions at pH 9.5, a breakpoint was noted for EcDHFR in the temperature dependence of the KIE in H_2O at temperatures below 15 ˚C. However, within the temperature range of 15 and 35 ˚C the KIEs remained constant within the experimental errors (Figure 3.7). This breakpoint was not seen for the MpDHFR catalysed reaction at elevated pH in H_2O, but seen when the reaction was carried out in D_2O. The difference in the temperature dependences of KIE for MpDHFR in H_2O and D_2O is most probably due to the D_2O buffer induced pK_a shift of the (*vide supra*). Recent data have shown no breakpoint either for in the temperature dependence of KIE for EcDHFR when performing the reaction at pH 9 under single turnover conditions.[47] The breakpoint for the DHFR catalysed reaction for both the mesophilic and the psychrophilic enzymes suggests contribution from kinetic complexity at the conditions used that caused a partial change in the rate limiting step at temperatures lower than 15 ˚C.

The activation energy for MpDHFR-catalyzed hydride transfer at pH 9 was found to be 15.6 ± 0.2 kJ mol^{-1}, compared to 17.1 ± 1.1 kJ mol^{-1} for deuteride transfer, leading to an activation energy difference (ΔE_a) of 1.5 ± 1.1 kJ mol^{-1} (Figure 3.7) and Arrhenius pre-exponential factor ratio (A_H/A_D) of 1.4 ± 0.5. This is similar to the activation energy difference and Arrhenius pre-exponential factor ratio observed for EcDHFR (Table 3.16).[103] The activation energy (and the activation enthalpy) for the hydride transfer reaction was most favorable for MpDHFR and least favorable for TmDHFR (Table 3.17) as seen previously under pre-steady state conditions.

Similar to the pre-steady state, all the three DHFRs show an inverse SKIE on the chemical step under steady state conditions. Proton inventories were linear (Figure 3.8) showing that the SKIE arises from a single protonation event,[104] consistent with the DHFR-catalyzed reaction. At 20 ˚C, while TmDHFR shows a higher SKIE (0.63 ± 0.18) than the value observed in the pre-steady state (0.42 ± 0.02), MpDHFR shows a slightly lower SKIE (0.48 ± 0.09) than that obtained under single turnover conditions (0.63 ± 0.04), but comparable to that obtained for EcDHFR under steady state (0.41 ± 0.05) and pre-steady state conditions (0.43 ± 0.18). For all the DHFRs, in the steady state the primary (1°) KIEs were independent of the isotopic composition of the solvent and the SKIEs were independent of the cofactor isotopic composition.

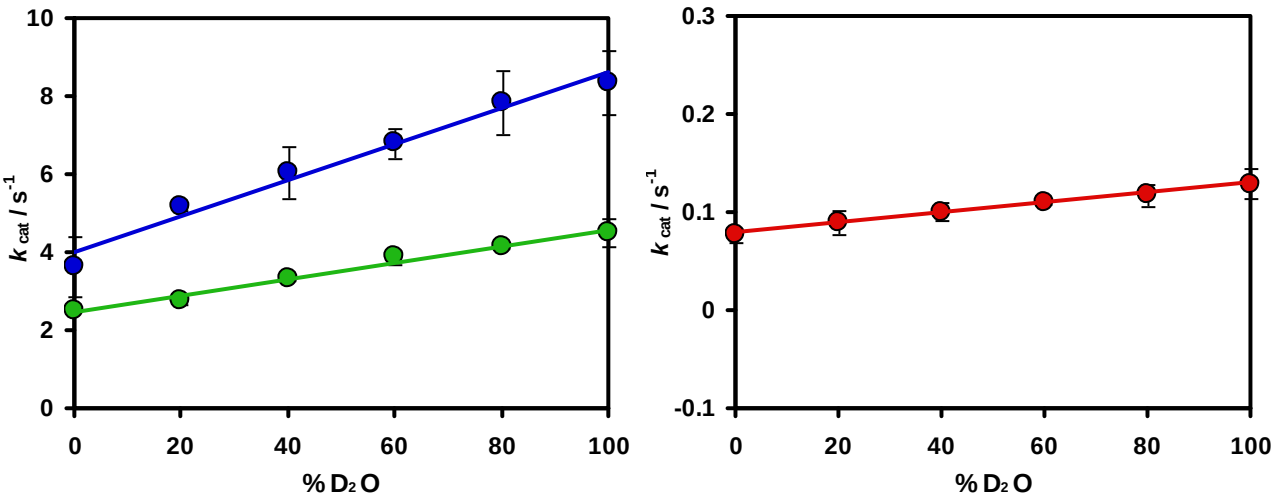

Figure 3.8: *Proton inventories for hydride transfer catalysed by MpDHFR (blue), EcDHFR (green) and TmDHFR (red) at pH 9, 9.5 and 7 respectively and 20 ˚C.*[98]

Table 3.12: *Temperature dependence of the steady state rate constants for hydride (k_{cat}^{H}) and deuteride (k_{cat}^{D}) transfer during catalysis by MpDHFR at pH 9.*

T (°C)	H_2O		D_2O	
	k_{cat}^{H} (s^{-1})	k_{cat}^{D} (s^{-1})	k_{cat}^{H} (s^{-1})	k_{cat}^{D} (s^{-1})
5	1.75 ± 0.14	0.67 ± 0.04	2.86 ± 0.27	1.35 ± 0.12
10	1.93 ± 0.08	0.75 ± 0.08	3.89 ± 0.52	1.88 ± 0.27
15	2.20 ± 0.16	0.81 ± 0.13	4.47 ± 0.74	2.00 ± 0.30
20	2.46 ± 0.19	1.00 ± 0.10	5.14 ± 0.65	2.17 ± 0.25
25	2.72 ± 0.21	1.09 ± 0.20	6.01 ± 0.82	2.65 ± 0.38
30	3.03 ± 0.15	1.25 ± 0.09	6.28 ± 0.93	2.97 ± 0.41

Table 3.13: *Temperature dependence and KIE of the steady state rate constants for hydride (k_{cat}^{H}) and deuteride (k_{cat}^{D}) transfer during catalysis by EcDHFR*[103] *at pH 9.5.*

T (^{o}C)	k_{cat}^{H} (s^{-1})	k_{cat}^{D} (s^{-1})	KIE[a]
5	0.349 ± 0.005	0.175 ± 0.003	2.99 ± 0.04
10	0.484 ± 0.004	0.197 ± 0.002	2.45 ± 0.03
15	0.600 ± 0.008	0.208 ± 0.001	2.88 ± 0.04
20	0.722 ± 0.009	0.252 ± 0.004	2.8 ± 0.06
25	0.927 ± 0.012	0.341 ± 0.008	2.72 ± 0.07
30	0.994 ± 0.005	0.359 ± 0.006	2.77 ± 0.05
35	1.090 ± 0.007	0.385 ± 0.006	2.83 ± 0.05

Data taken from reference[103]

Table 3.14: *Temperature dependence of the steady state rate constants for hydride (k_{cat}^{H}) and deuteride (k_{cat}^{D}) transfer during catalysis by TmDHFR at pH 7.*

T (^{o}C)	H_2O		D_2O	
	k_{cat}^{H} (s^{-1})	k_{cat}^{D} (s^{-1})	k_{cat}^{H} (s^{-1})	k_{cat}^{D} (s^{-1})
20	0.080 ± 0.013	0.019 ± 0.005	0.125 ± 0.033	0.033 ± 0.005
25	0.106 ± 0.023	0.032 ± 0.014	0.180 ± 0.044	0.062 ± 0.014
30	0.159 ± 0.043	0.043 ± 0.010	0.211 ± 0.030	0.075 ± 0.011
35	0.220 ± 0.025	0.071 ± 0.017	0.326 ± 0.049	0.104 ± 0.018
40	0.287 ± 0.043	0.089 ± 0.016	0.476 ± 0.100	0.162 ± 0.024
45	0.402 ± 0.056	0.136 ± 0.023	0.597 ± 0.106	0.253 ± 0.037

Table 3.15: *Temperature dependence of the steady-state KIE during catalysis by MpDHFR at pH 9.*

T (^{o}C)	H_2O	D_2O
5	2.61 ± 0.10	2.12 ± 0.13
10	2.58 ± 0.12	2.07 ± 0.20
15	2.71 ± 0.18	2.23 ± 0.23
20	2.46 ± 0.13	2.37 ± 0.17
25	2.51 ± 0.20	2.27 ± 0.20
30	2.42 ± 0.09	2.11 ± 0.20

Table 3.16: *Temperature dependence of the steady-state KIE during catalysis by TmDHFR at pH 7.*

T (^{o}C)	H_2O	D_2O
20	4.21 ± 0.32	3.80 ± 0.30
25	3.29 ± 0.47	2.91 ± 0.34
30	3.70 ± 0.35	2.81 ± 0.20
35	3.09 ± 0.27	3.13 ± 0.23
40	3.23 ± 0.23	2.93 ± 0.26
45	2.95 ± 0.22	2.35 ± 0.23

Table 3.17: *Steady state activation energies during catalysis by MpDHFR, EcDHFR and TmDHFR at pH 9, 9.5 and 7 respectively.*

Enzyme	E_a^H ($kJ.mol^{-1}$)	E_a^D ($kJ.mol^{-1}$)	ΔE_a ($kJ.mol^{-1}$)
MpDHFR	15.6 ± 0.2	17.1 ± 1.1	1.5 ± 1.1
EcDHFR[a]	22.4 ± 2.8	23.5 ± 4.0	1.1 ± 4.9
TmDHFR	50.5 ± 1.2	59.4 ± 2.6	8.9 ± 0.9

[a] taken from reference [103], above 15 ˚C

Table 3.18: *Steady state Arrhenius prefactors (A) during catalysis by MpDHFR, EcDHFR and TmDHFR at pH 9, 9.5 and 7 respectively.*

Enzyme	A_H (s^{-1})	A_D (s^{-1})	A_H/A_D
MpDHFR	$(1.5 \pm 0.7) \times 10^3$	$(1.1 \pm 0.1) \times 10^3$	1.4 ± 0.5
EcDHFR[a]	$(7.3 \pm 0.9) \times 10^3$	$(4.0 \pm 0.8) \times 10^3$	1.8 ± 0.42
TmDHFR	$(8.0 \pm 0.2) \times 10^7$	$(8.0 \pm 0.4) \times 10^8$	0.1 ± 0.006

[a] taken from reference [103], above 15 ˚C

Table 3.19: *Activation parameters for the MpDHFR, EcDHFR and TmDHFR catalyzed reaction at pH 9, 9.5 and 7 respectively.*

Parameter	MpDHFR	EcDHFR	TmDHFR
$\Delta H^{\ddagger}_H$ / kJ mol^{-1}	13.2 ± 0.2	20.0 ± 2.8 [b]	47.99 ± 1.23
$\Delta H^{\ddagger}_D$ / kJ mol^{-1}	14.7 ± 1.1	18.2 ± 2.0	56.93 ± 1.23
$\Delta S^{\ddagger}_H$ / J mol^{-1}	-192.2 ± 0.1	-179.3 ± 0.5 [b]	-102.10 ± 1.89
$\Delta S^{\ddagger}_D$ / J mol^{-1}	-194.8 ± 1.4	-193.7 ± 1.8	-82.97 ± 2.27
$\Delta G^{\ddagger}_H$ / kJ mol^{-1} [a]	70.5 ± 0.2	73.4 ± 2.8 [b]	78.43 ± 0.66
$\Delta G^{\ddagger}_D$ / kJ mol^{-1} [a]	72.8 ± 1.1	75.9 ± 2.0	81.67 ± 0.55

[a] At 25 °C; [b] Above 25 ºC.

3.4 Discussion

The role of protein motions in the chemical step during enzymatically catalysed reactions is one of the hot topics in modern enzymology. Several theories of enzyme catalysis have proposed that protein dynamics are coupled to tunnelling, leading to a variety of models for active promotion of tunnelling.[65,105-108] These models include rate-promoting vibrations,[38,48-49,109-110] vibrationally enhanced ground-state tunnelling[37,111] and environmentally coupled tunnelling.[26,30,34] Within these models, a discrimination was made between passive motions that help bring the substrates into reactive configurations (environmentally reorganization) and motions that actively modulate the tunnelling barrier (gating, or vibrational enhancement)[112-113] (Chapter 1). To study the contribution of

enzyme motion to catalysis, a determination of the temperature dependence of the primary kinetic isotope effects (KIEs) is often used.[43,107,114-115] Hydride transfer reactions in which contributions from quantum-mechanical tunnelling play a role and especially the hydride transfer reaction catalysed by dihydrofolate reductase (DHFR) was used for a long time as a model system to study such phenomena.

Studying enzyme homologues from different temperature environments allows a further understanding of DHFR catalysis. In this chapter, hydride transfer and kinetic isotope effects in the steady state and pre-steady state for the cold adapted enzyme MpDHFR were reported and compared to the data obtained with the mesophilic EcDHFR and the thermophilic TmDHFR. When measuring the chemical step, either in the pre-steady state or steady state, MpDHFR had the most favorable activation energy (and activation enthalpy) while TmDHFR had the least favorable variables. This is matched by MpDHFR having the least favourable Arrhenius prefactor (and activation entropy).

MpDHFR has higher rate constants for hydride transfer than the other two DHFRs. However, at the enzymes' typical operating temperatures the hydride transfer rate constant for MpDHFR is slightly lower than that of EcDHFR (255.0 ± 6.4, 317.3 ± 1.6 and 8.2 ± 0.1 s^{-1} for MpDHFR 2 ºC, EcDHFR at 37 ºC and TmDHFR at 90 ºC respectively). Similar to EcDHFR, MpDHFR shows inverse pre-exponential factor ratios (A_H/A_D) below the lower limit for the semi-classically calculated value of 0.71,[35,102] 0.13 and 0.12 for MpDHFR and EcDHFR respectively.

Within the environmentally coupled tunnelling model, when the KIEs are temperature dependent and the ratio of the pre-exponential factors is inverse, it was predicted that active dynamic motions are dominant and generate a temperature-dependent tunnelling distance. The experimentally observed inverse A_H/A_D and the temperature dependence of the KIEs reported here, suggest that DHFR actively modulates the tunnelling distance and hence the reaction rates under single turnover conditions at pH 7.0.[116] However, the KIE values seen for MpDHFR under pre-steady state conditions, which are smaller than those seen for EcDHFR and TmDHFR, suggest contributions from other different steps during the catalytic cycle causing kinetic complexity. Kinetic complexity has been shown previously to lead to the wrong estimated temperature dependence of the KIE.[99]

On the other hand, a temperature independent KIE is seen, according to the environmentally coupled tunnelling model, when the gating vibration does not modulate the tunnelling distance appreciably. Thus, the dominant environmental contribution becomes the environmental reorganization (passive

dynamics).[30] Such a case can be seen in TmDHFR at temperatures above 25 ˚C[64,97,101] and also when the chemical step was analysed for the two monomeric DHFRs in the steady state at elevated pH (*vide infra*).

When the chemical step for the MpDHFR catalysed reaction was determined at elevated pH under steady state conditions, the KIEs were in the same range as those obtained under pre-steady state conditions at pH 7, suggesting that the chemical step for MpDHFR is at least partially rate limiting in the steady state at pH 9, as seen previously with EcDHFR at pH 9.5.[103] MpDHFR has a temperature independent KIE at elevated pH similar to EcDHFR at temperatures higher than 15 ˚C and TmDHFR under pre-steady state conditions at pH 7.0. So, generally speaking, a temperature independent KIE was obtained for all of the three homologues, MpDHFR between 5 and 30 ˚C, EcDHFR between 15 and 35˚C, and TmDHFR between 25 and 65 ˚C.

A temperature dependent KIE was seen for TmDHFR at temperatures below 25 ˚C, increasing in value as the temperature fell, but at pH 7.0. The opposite is seen with EcDHFR at pH 9.5, with the KIE of EcDHFR falling as the temperature decreases below 15 ˚C suggesting kinetic complexity. Such behaviour was not observed for MpDHFR at the temperature range used, suggesting, perhaps that there is no re-organisation required for the MpDHFR active site at that temperature range. However, a previous study has shown a break point for the temperature dependence of the steady state KIE on the MpDHFR catalysed reaction at temperatures lower than 7.5 ˚C.[90]

As mentioned previously, at elevated pH the monomeric DHFRs homologues (MpDHFR and EcDHFR) display a temperature dependence of the KIE similar to that of the structurally more rigid and dimeric homologue TmDHFR at physiological pH.[101] This may suggest that all of the three enzymes rely on passive motions only to generate active site configurations conducive to hydrogen transfer. These observations were thought previously to suggest an evolutionary model in which catalysis progresses from a relatively rigid active site in the dimeric TmDHFR to a more flexible and kinetically more efficient structure in the monomeric homologues,[103] MpDHFR and EcDHFR, that actively promotes hydrogen transfer at physiological pH. However taking into consideration the rate constants of hydride transfer for the three homologues at their physiological temperatures (2 ºC for MpDHFR, at 37 ºC for EcDHFR and 90 ºC for TmDHFR) shows that MpDHFR is a slightly poorer catalyst than EcDHFR and is similar to TmDHFR in the steady state under the same conditions. Also, a recent study in our group has shown that the KIE on hydride transfer in EcDHFR is temperature dependent below pH 8 and temperature independent at or above this pH, indicating that

the temperature dependent KIEs observed at pH 7 must be physiologically relevant, in contrast to the temperature independent KIEs observed at elevated pH.[99] Thus it is inappropriate to compare the behaviour of the temperature dependence of KIE for the monomeric homologues at elevated pH with that of the dimeric enzyme at physiological pH.

Further findings during studies of the hydride transfer reaction catalysed by DHFR, in our group and different research groups as well, derived from investigating solvent effect on DHFR chemical step,[96,117] studying various DHFR variants[47] (as will be shown in later chapters of this thesis), in addition to computational studies,[46] have shown that the environmentally coupled tunnelling model is inadequate to explain catalysis by DHFR. Experimental data has indicated that protein dynamics are only important for the generation of the reaction ready conformation (RRC) on the free energy landscape and suggest no contribution for such motion to the chemical step during catalysis by DHFR.[47,96] Such annotations, in addition to accumulating evidence against current models that relate protein motions to chemical step, suggest that modulation of these models is essential to propose better understanding of the temperature dependence of the KIE for the hydride transfer reactions.

3.5 Conclusions

From the data presented here, it is clear that the rates of hydride transfer by MpDHFR, measured either in the steady state or the pre-steady state, are higher than those of EcDHFR and TmDHFR at all temperatures. However, at the typical operating temperatures of the three DHFRs (2 ˚C for MpDHFR,[92] 37 ˚C for EcDHFR and 90 ˚C for TmDHFR[61]) at pH 7, the hydride transfer rate constants were estimated to be 255.0 ± 6.4, 317.3 ± 1.6, and 8.2 ± 0.1 s^{-1}, respectively. Furthermore, it has been shown that the k_{cat} value for MpDHFR is very similar to TmDHFR (5.0 ± 1.5 and 4.5 ± 2.3 s^{-1} for MpDHFR and TmDHFR respectively) and very low compared to the mesophilic homologue EcDHFR (k_{cat} = 35.8 ± 2.6 s^{-1}) under the same conditions.[79,96] These observations suggest that MpDHFR is actually a slightly poorer catalyst than EcDHFR at their respective physiological temperatures under single turnover conditions and is equivalent to TmDHFR in the steady state. The activation energy (and enthalpy) for the hydride transfer reaction is most favourable for MpDHFR and least favourable for TmDHFR. This behaviour is comparable to that observed for the activation parameters for the steady-state reactions of MpDHFR and EcDHFR.[79] The temperature dependence of the KIE on hydride transfer is similar to that observed for EcDHFR,[103] and quite different to that of TmDHFR.[101] The lower value observed for the primary KIEs on hydride transfer in MpDHFR and the lower ΔE_a than EcDHFR suggest increased kinetic complexity on the measurements for

MpDHFR. Similar to EcDHFR, MpDHFR has shown a temperature independent KIE when the chemical step is isolated under steady state conditions, at elevated pH. Such behaviour was observed for the thermophilic and the dimeric homologue in the steady state at pH 7 where the chemical step is partially rate limiting, thus it is difficult to compare the behaviour of the steady state temperature dependence of the KIEs of the monomeric enzymes with that of the dimeric enzyme due to the different pH used. From the data obtained here, it seems reasonable to conclude that monomeric DHFRs (MpDHFR and EcDHFR) have similar kinetic behaviour for the hydride transfer step, exemplified by temperature dependent KIEs under physiological conditions, whereas dimeric DHFR (TmDHFR) has different kinetic behavior.

4

Role of the occluded conformation during catalysis by DHFR

4.1 Preface

During catalysis, DHFR from *Escherichia coli* (EcDHFR) cycles through five intermediates: E.NADPH, E.NADPH.DHF, E.NADP$^+$.THF, E.THF and E.NADPH.THF, with product (THF) release from the E.NADPH.THF mixed ternary complex being the rate limiting step at pH ≤7 under steady state conditions (Figure 4.1).[7]

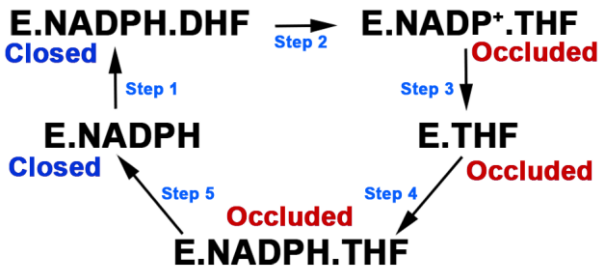

Figure 4.1: *Schematic representation of the catalytic pathway of EcDHFR. In E:NADPH and the Michaelis complex E:NADPH:DHF, the Met20 loop adopts the closed conformation. In the three product complexes, E:NADP$^+$, E:THF and E:NADPH:THF, the Met20 loop is in the occluded conformation.[59] In the steady state, product release from the E:NADPH:THF ternary complex (Step 5) is the rate limiting step, but hydride transfer becomes the rate limiting step at pH higher than 8.4.[7]*

The M20 loop (residues 9-24) of EcDHFR switches between two conformations during the catalytic cycle (Figure 4.2A). In the two reactant complexes (E.NADPH and E.NADPH.DHF), this loop adopts the 'closed' conformation, packing against NADPH and preventing solvent access to the active site. This conformation is stabilized by pairs of hydrogen bonds between residues in the M20 loop and the FG loop (residues 116 to 132 in EcDHFR), namely Gly15(O) to Asp122(HN) and Glu17(HN) to Asp122(Oδ2) (Figure 4.2B).[7,59] In the product binary and ternary complexes, on the other hand, this loop switches to the occluded conformation (Figure 4.2C). The two hydrogen bonds between the M20 loop and FG loop that stabilize the closed conformation are not formed and instead the occluded conformation is stabilized by two hydrogen bonds between Asn23 (O and HN) in the M20 loop and Ser148 (HN and γO2) in the GH loop (residues 142 to 149 in EcDHFR) (Figure 4.2C). The M20 loop prevents the nicotinamide group from entering the active site and it instead sticks out into solution. It has been proposed that movement between the closed and occluded conformations is important for both modifying ligand affinity and aiding progression through the catalytic cycle.[7,59]

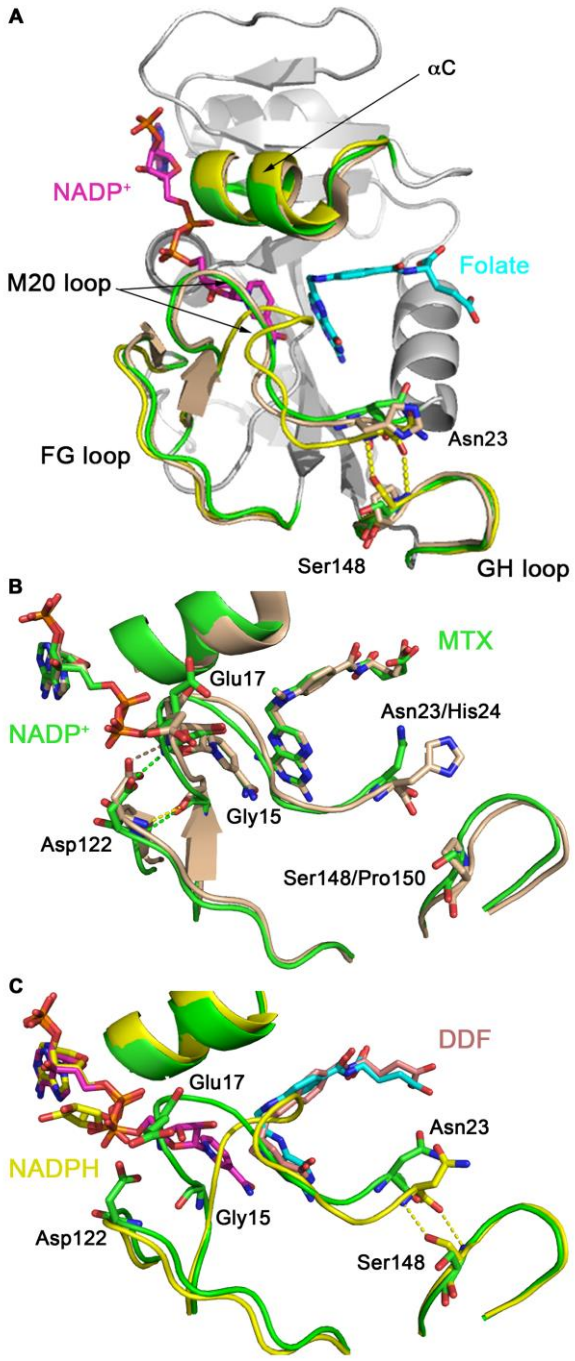

Figure 4.2: *(A) Cartoon representation of EcDHFR (gray, PDB 1RX2)[1] in the closed conformation, with the M20, FG and GH loops shown in green. The position of these loops in the occluded conformation in EcDHFR (yellow, PDB 1RX6)[1] and in the closed conformation for MpDHFR (wheat, PDB 3IA4)[4] are also shown. Ligands are shown as sticks, folate in cyan and NADP$^+$ in pink. (B) Alignment of the active site loops of EcDHFR (green, PDB 1DRE)[1] and MpDHFR (wheat, PDB 3IA4)[4] in complex with methotrexate (MTX) and NADPH (green for EcDHFR and wheat for MpDHFR) showing the residues participating in hydrogen bonds which stabilize the closed and occluded conformations in EcDHFR and corresponding residues in MpDHFR. Hydrogen bonds stabilizing the closed conformations are shown as dashed lines. (C) Alignment of the active site loops of EcDHFR in the closed conformation (green, PDB 1RX2)[1] with ligands as described in A, and in the occluded conformation (yellow, PDB 1RX6)[1] with 5,10-dideazatetrahydrofolate (DDF) in pale pink and NADPH in yellow, showing the residues participating in hydrogen bonds which stabilize the closed and occluded conformations. Hydrogen bonds stabilizing the occluded conformation are shown as dashed yellow lines.*

Although MpDHFR exhibits a very similar crystal structure to EcDHFR[91] and the two enzymes have 55% sequence identity,[92] Ser148 of EcDHFR is replaced with proline in MpDHFR, which cannot form either of the hydrogen bonds that stabilize the occluded conformation. In DHFR from *Lactobacillus casei* (LcDHFR)[112,118-119] Ser148 is replaced by alanine, which in principle can form the backbone hydrogen bond with Asn23 but not the side chain hydrogen bond (Figure 4.3). The

occluded conformation has not been observed in other DHFRs including LcDHFR,[119-120] which is known to have a very similar catalytic cycle to EcDHFR,[121] and the EcDHFR-S148A mutant is known to adopt the closed conformation in the product complex rather than an occluded conformation.[50] In addition to MpDHFR and LcDHFR, DHFRs from a number of other organisms have an alternative residue in place of Ser148 (Figure 4.4). It is therefore extremely unlikely that MpDHFR or other DHFRs with a proline residue replacing Ser148 are able to form the occluded conformation.

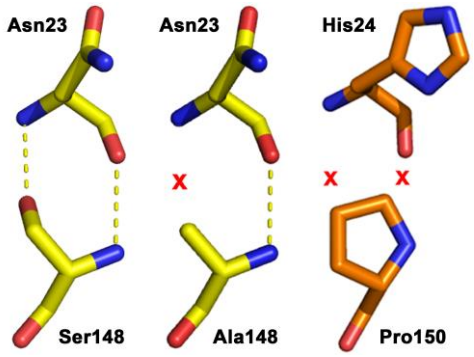

Figure 4.3: *Residues which stabilise the occluded conformation in EcDHFR (left), and the equivalent residues in the EcDHFR-S148A variant (middle) and in MpDHFR (right). In EcDHFR, two hydrogen bonds can form between Asn23 and. In EcDHFR-S148A, however, while Ala148 can theoretically form the backbone hydrogen bond with Asn23, the second hydrogen bond is eliminated and this variant was shown to adopt the closed conformation in the product complex[50] not the occluded conformation as the wild type EcDHFR.[59] In MpDHFR both hydrogen bonds which stabilize the occluded conformation in EcDHFR are lost (right) due to replacement of Ser148 by proline and it is therefore highly unlikely that the occluded conformation can form.*

To investigate the importance of the occluded conformation on catalysis by DHFR, two variants EcDHFR-S148P and MpDHFR-P150S were generated. The results presented in this chapter show that while MpDHFR-P150S follows a similar catalytic cycle to EcDHFR, with product release being the rate limiting step in the steady state at pH ≤7, kinetics and NMR studies support the idea that destabilizing the occluded conformation in EcDHFR-S148P prevents the fast release of $NADP^+$ from the active site after the chemical step, causing a change in the steady state rate limiting step without affecting the chemistry of the reaction (*vide infra*). However, despite lacking the key residue that stabilises the occluded conformation, MpDHFR follows the same catalytic cycle as EcDHFR at physiological pH, suggesting that different methodology is used in MpDHFR to facilitate product

release. Hence, this methodology seems to be inefficient at low pH, causing a different rate limiting step for MpDHFR.

Figure 4.4: *Alignment of the amino acid sequences of various DHFRs showing residues that participate in stabilizing the closed (blue) and the occluded (red) conformations in EcDHFR and the corresponding residues in DHFR from Moritella profunda (MpDHFR), Lactobacillus casei (LcDHFR), Moritella yayanosii (MyDHFR), Shewanella violacea (SvDHFR), Geobacillus stearothermophilus (BsDHFR), Streptococcus pneumoniae (SpDHFR), Bacillus anthracis (BaDHFR), Mycobacterium tuberculosis (MtDHFR), Mycobacterium avium (MaDHFR), Human (HsDHFR) and Mus musculus (mouse, MmDHFR).*

4.2 Structure and thermal stability for the EcDHFR-S148P and MpDHFR-P150S variants

Circular dichroism spectroscopy was used to demonstrate that EcDHFR-S148P and MpDHFR-P150S have similar secondary structure to their wild type counterparts (Figure 4.5). MpDHFR-P150S was found to melt at 55.4 ± 0.2 °C, similar to the melting temperature of wild type EcDHFR (51.6 ± 0.7 °C)[122] or wild type MpDHFR in the presence of methotrexate (53.7 ± 0.6 °C) and considerably higher than that of apo-MpDHFR (37.5 ± 0.8 °C).[79] The melting point of EcDHFR-S148P was 59.6 ± 0.2 °C. This suggests that while the S148P mutation did not decrease the thermal stability for EcDHFR, MpDHFR is more tolerant of high temperature after replacing Pro150 with serine.

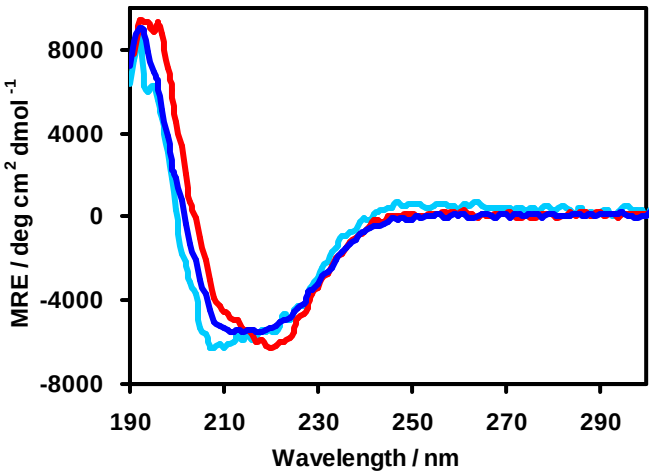

Figure 4.5: *CD spectra for MpDHFR (blue), MpDHFR-P150S (cyan) and EcDHFR-S148P (red) at 20 ℃.*

4.3 Temperature dependence of k_H and KIE for the two variants (EcDHFR-S148P and MpDHFR-P150S)

The pH dependence of the hydride transfer rate constant was measured under single turnover conditions in MTEN buffer (Figure 4.6) at 5 °C for MpDHFR[96] and MpDHFR-P150S (Table 4.1) and at 25 °C for EcDHFR[99] and EcDHFR-S148P (Table 4.1). The two mutants were found to have similar pH dependences with pK_a values around 6.5 with comparable hydride transfer rates to their wild type counterparts (Table 4.2).

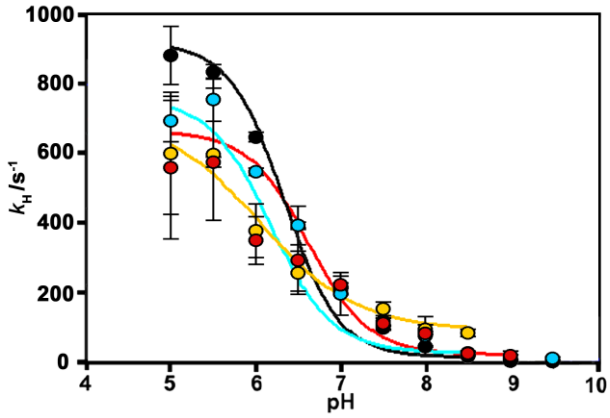

Figure 4.6: *pH dependence of the rate constant for hydride transfer (k_H) for MpDHFR (cyan) and MpDHFR-P150S (orange) at 5 ℃ and EcDHFR[99] (black) and EcDHFR-S148P (red) at 25 ℃.*

Table 4.1: *pH dependence of the rate constants for hydride transfer (k_H) for the MpDHFR, MpDHFR-P150S EcDHFR and EcDHFR-S148P catalyzed reaction in MTEN buffer at 5 ºC.*

pH	MpDHFR	MpDHFR-P150S	EcDHFR[a]	EcDHFR-S148P
5	690.9 ± 59.1	598.2 ± 175.4	878.68 ± 83.00	693 ± 136.5
5.5	752.2 ± 61.6	595.6 ± 189.2	832.36 ± 20.87	584.2 ± 72.3
6	545.3 ± 10.2	375.9 ± 76.8	645.17 ± 13.68	587.5 ± 100.7
6.5	391.8 ± 55.2	255.8 ± 61.4	392.56 ± 8.78	nd
7	195.4 ± 61.6	219.5 ± 27.1	203.70 ± 7.40	170.1 ± 7.9
7.5	115.3 ± 10.2	152.2 ± 19.9	97.26 ± 5.47	nd
8	75.5 ± 55.2	93.4 ± 13.1	44.68 ± 1.83	43.0 ± 1.7
8.5	25.4 ± 5.86	83.5 ± 10.0	16.89 ± 0.37	nd
9	14.2 ± 6.0	nd	2.52 ± 0.02	7.7 ± 1.2
9.5	10.2 ± 3.5	nd	nd	nd

nd: not determined, [a] taken from ref [99]

Table 4.2: *pK_a for the MpDHFR and MpDHFR-P150S catalyzed reaction at 5 ºC and for EcDHFR and EcDHFR-S148P at 25 ºC.*

Enzyme	pK_a
MpDHFR	6.50 ± 0.10
MpDHFR-P150S	6.04 ± 0.31
EcDHFR	6.61 ± 0.20
EcDHFR-S148P	6.40 ± 0.03

The kinetic isotope effect (KIE) on hydride transfer for MpDHFR-P150S, EcDHFR-S148A and EcDHFR-S148P was found to depend on temperature in a fashion similar to their wild type counterparts (Figure 4.7 and Tables 4.3-4.7), indicating that destabilizing the occluded conformation in MpDHFR and EcDHFR-S148P does not affect hydride transfer. Since both EcDHFR-S148A and wild type MpDHFR are known to be able to form the closed conformation,[50,62] this suggests that all DHFRs stu55

died here are able to form the closed conformation in which hydride transfer occurs, and therefore shows that conformational changes between the closed and the occluded conformation do not affect the actual chemistry of the reaction. This is in agreement with recent studies, which also showed that conformational dynamics between the closed and occluded states do not affect the chemical step.[46-47]

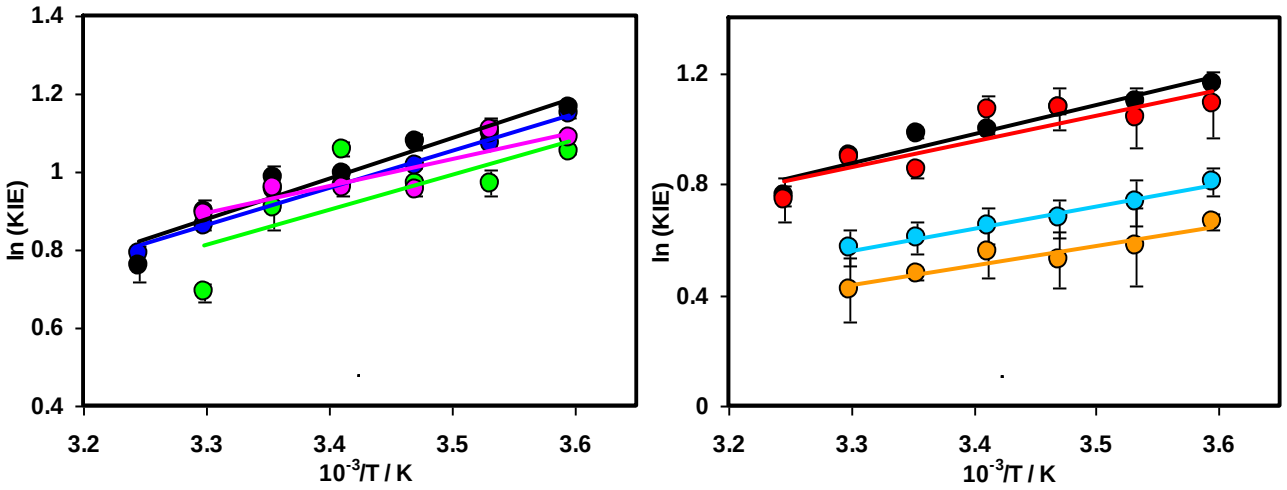

Figure 4.7: *Kinetic isotope effect on hydride transfer at pH 7 by EcDHFR[47] (black), EcDHFR-N23PP (green), EcDHFR-S148A (pink), EcDHFR-N23PP/S148A[47] (blue), EcDHFR-S148P (red), MpDHFR[96] (cyan) and MpDHFR-P150S (orange), plotted on a logarithmic abscissa as a function of the inverse temperature.*

Table 4.3: *Temperature dependence of the pre-steady-state rate constants for hydride (k_H) and deuteride (k_D) transfer during catalysis by EcDHFR and MpDHFR at pH 7.*

T (^{o}C)	EcDHFR[a]		MpDHFR	
	k_H (s^{-1})	k_D (s^{-1})	k_H (s^{-1})	k_D (s^{-1})
5	81.9 ± 1.7	26.9 ± 1.9	267.6 ± 14.4	118.9 ± 14.5
10	106.3 ± 3.1	34.1± 3.4	327.2 ± 14.4	157.2 ± 25.6
15	135.3 ± 5.6	44.6± 3.7	420.3 ± 21.3	213.9 ± 25.1
20	159.8 ± 7.9	60.2 ± 4.1	484.4 ± 28.0	253.0 ± 30.4
25	203.7 ± 7.4	75.1 ± 5.4	526.8 ± 23.2	288.0 ± 24.8
30	235.4 ± 13.8	98.5 ± 2.8	570.5 ± 44.1	323.5 ± 26.9
35	287.9 ± 12.0	125.9 ± 3.5	nd	nd

nd: not determined, [a] data measured by Dr Joel Loveridge[47]

Table 4.4: *Temperature dependence of the pre-steady-state rate constants for hydride (k_H) and deuteride (k_D) transfer during catalysis by EcDHFR-S148P and MpDHFR-P150S at pH 7.*

T (^{o}C)	EcDHFR-S148P		MpDHFR-P150S	
	k_H (s^{-1})	k_D (s^{-1})	k_H (s^{-1})	k_D (s^{-1})
5	87.2 ± 8.2	29.4 ± 20.1	268.0 ± 2.2	138.3 ± 10.9
10	111.9 ± 10.4	39.5 ± 24.3	285.4 ± 33.5	160.5 ± 53.3
15	134.6 ± 21.0	46.1 ± 18.6	351.9 ± 0.3	207.5 ± 50.5
20	158.7 ± 23.0	54.6 ± 13.6	420.4 ± 87.7	241.3 ± 19.8
25	180.8 ± 0.8	77.3 ± 6.2	337.1 ± 8.4	210.0 ± 7.3
30	235.9 ± 10.7	96.4 ± 2.8	348.7 ± 9.1	229.4 ± 56.7
35	265.4 ± 42.8	126.3 ± 3.9	nd	nd

nd: not determined

Table 4.5: *Temperature dependence of the pre-steady-state rate constants for hydride (k_H) and deuteride (k_D) transfer during catalysis by EcDHFR-N23PP and EcDHFR-S148A at pH 7.*

T (^{o}C)	EcDHFR-N23PP		EcDHFR-S148A	
	k_H (s^{-1})	k_D (s^{-1})	k_H (s^{-1})	k_D (s^{-1})
5	11.85 ± 0.21	4.15 ± 0.07	89.00 ± 1.41	30.00 ± 0.71
10	15.70 ± 0.42	5.95 ± 0.07	122.00 ± 5.66	40.35 ± 4.74
15	19.10 ± 0.14	7.25 ± 0.07	121.70 ± 0.99	47.00 ± 2.83
20	27.10 ± 0.14	9.40 ± 0.14	157.50 ± 0.71	60.50 ± 0.71
25	36.50 ± 0.71	14.75 ± 1.06	213.00 ± 2.83	81.50 ± 0.71
30	46.00 ± 1.41	23.05 ± 0.07	252.00 ± 1.41	103.50 ± 0.71

Table 4.6: *Temperature dependence of the pre-steady-state rate constants for hydride (k_H) and deuteride (k_D) transfer during catalysis by N23PP/S148A at pH 7.*[a]

T (^{o}C)	k_H (s^{-1})	k_D (s^{-1})
5	12.9 ± 0.2	4.1 ± 0.2
10	15.2 ± 0.1	5.2 ± 0.3
15	18.2 ± 0.4	6.6 ± 0.1
20	21 ± 0.4	8.0 ± 0.5
25	25.9 ± 0.3	10.0 ± 0.3
30	32.6 ± 0.4	13.8 ± 0.6
35	37.1 ± 1.3	16.8 ± 0.4

[a] Data measured by Dr Joel Loveridge[47]

Table 4.7: *Temperature dependence of the pre-steady-state KIE during catalysis by EcDHFR, MpDHFR,* EcDHFR-S148P *and* MpDHFR-P150S *at pH 7.*

T (^{o}C)	EcDHFR[a]	MpDHFR	EcDHFR-S148P	MpDHFR-P150S
5	3.04 ± 0.22	2.25 ± 0.13	2.97 ± 0.35	1.94 ± 0.10
10	3.12 ± 0.32	2.08 ± 0.17	2.83 ± 0.31	1.78 ± 0.25
15	3.03 ± 0.28	1.96 ± 0.13	2.92 ± 0.22	1.70 ± 0.17
20	2.65 ± 0.22	1.91 ± 0.13	2.91 ± 0.15	1.74 ± 0.16
25	2.71 ± 0.22	1.83 ± 0.10	2.34 ± 0.10	1.61 ± 0.03
30	2.39 ± 0.16	1.76 ± 0.11	2.45 ± 0.33	1.52 ± 0.18
35	2.29 ± 0.11	nd	2.10 ± 0.16	nd

nd: not determined, [a] data measured by Dr Joel Loveridge[47]

Table 4.8: *Temperature dependence of the pre-steady-state kinetic isotope effect during catalysis by EcDHFR-N23PP, -S148A and N23PP/S148A at pH 7.*

T (^{o}C)	EcDHFR-N23PP	EcDHFR-S148A	EcDHFR-N23PP/S148A[a]
5	2.86 ± 0.01	2.74 ± 0.01	3.15 ± 0.03
10	2.64 ± 0.02	3.02 ± 0.06	2.92 ± 0.03
15	2.63 ± 0.01	2.59 ± 0.03	2.76 ± 0.01
20	2.88 ± 0.01	2.60 ± 0.01	2.63 ± 0.03
25	2.47 ± 0.04	2.61 ± 0.01	2.59 ± 0.02
30	2.00 ± 0.02	2.43 ± 0.01	2.36 ± 0.02
35	nd	nd	2.21 ± 0.04

[a]Rate constants measured by Dr Joel Loveridge

Table 4.9: *Pre steady state activation energies during catalysis by MpDHFR, MpDHFR-P150S, EcDHFR and EcDHFR-S148P, -N23PP, -S148A and -N23PP/S148A at pH 7.*

Enzyme	E_a^H ($kJ.mol^{-1}$)	E_a^D ($kJ.mol^{-1}$)	ΔE_a ($kJ.mol^{-1}$)
MpDHFR	21.6 ± 2.2	28.1 ± 2.6	6.6 ± 3.4
MpDHFR-P150S	21.1 ± 3.2	26.1 ± 2.1	5.0 ± 3.8
EcDHFR[a]	29.9 ± 0.6	37.8 ± 0.6	7.9 ± 0.9
EcDHFR-S148P	26.1 ± 1.5	33.6 ± 2.4	7.5 ± 2.9
EcDHFR-N23PP	38.7 ± 1.5	46.1 ± 3.8	7.5 ± 4.1
EcDHFR-S148A	28.5 ± 2.9	34.2 ± 1.5	5.7 ± 3.2
EcDHFR-N23PP/S148A[a]	25.7 ± 0.9	33.4 ± 1.2	7.7 ± 1.5

[a] Rate constants measured by Dr Joel Loveridge[47]

Table 4.10: *Pre steady state Arrhenius prefactors (A) during catalysis by MpDHFR, MpDHFR-P150S, EcDHFR and EcDHFR-S148P, -N23PP, -S148A and -N23PP/S148A at pH 7.*

Enzyme	A_H (s^{-1})	A_D (s^{-1})	A_H/A_D
MpDHFR	$(3.2 \pm 0.2) \times 10^6$	$(2.4 \pm 0.2) \times 10^7$	0.13 ± 0.09
MpDHFR-P150S	$(2.4 \pm 0.2) \times 10^6$	$(1.1 \pm 0.1) \times 10^7$	0.22 ± 0.1
EcDHFR[a]	$(2.82 \pm 0.1) \times 10^7$	$(2.34 \pm 0.03) \times 10^8$	0.12 ± 0.002
EcDHFR-S148P	$(7.2 \pm 0.2) \times 10^6$	$(5.9 \pm 0.2) \times 10^7$	0.12 ± 0.04
EcDHFR-N23PP	$(2.1 \pm 0.1) \times 10^8$	$(1.8 \pm 0.1) \times 10^9$	0.12 ± 0.08
EcDHFR-S148A	$(2.0 \pm 0.1) \times 10^7$	$(8.0 \pm 0.3) \times 10^7$	0.25 ± 0.08
EcDHFR-N23PP/S148A[a]	$(8.2 \pm 0.2) \times 10^5$	$(7.4 \pm 0.2) \times 10^6$	0.11 ± 0.04

[a] Rate constants measured by Dr Joel Loveridge[47]

4.4 Steady-state kinetics

4.4.1 Steady state pH dependences

The pH dependences of the steady state rate constants (k_{cat}) were measured for MpDHFR, EcDHFR and their variants. For the MpDHFR catalyzed reaction, the pH dependance is bell shaped with a maximal rate at pH ~7 and apparent pK_a values of 8.1 and 5.7 at 20 ºC (Figure 4.8).[79] On the other hand, the reaction catalyzed by EcDHFR is characterized by a sigmoidal pH dependence,[123] with a pH independent k_{cat} of 9.0 ± 1.7 s^{-1} at low pH and 20 ºC (Figure 4.8). The decrease in k_{cat} for MpDHFR at low pH has been shown previously not to be due to protonation of His24 (the only ionic residue close to the active site) (Table 4.13). It was shown as well that the reduction in k_{cat} at low pH is not due to enzyme inactivation, as the half life of MpDHFR is around 40 min at pH 5.[79]

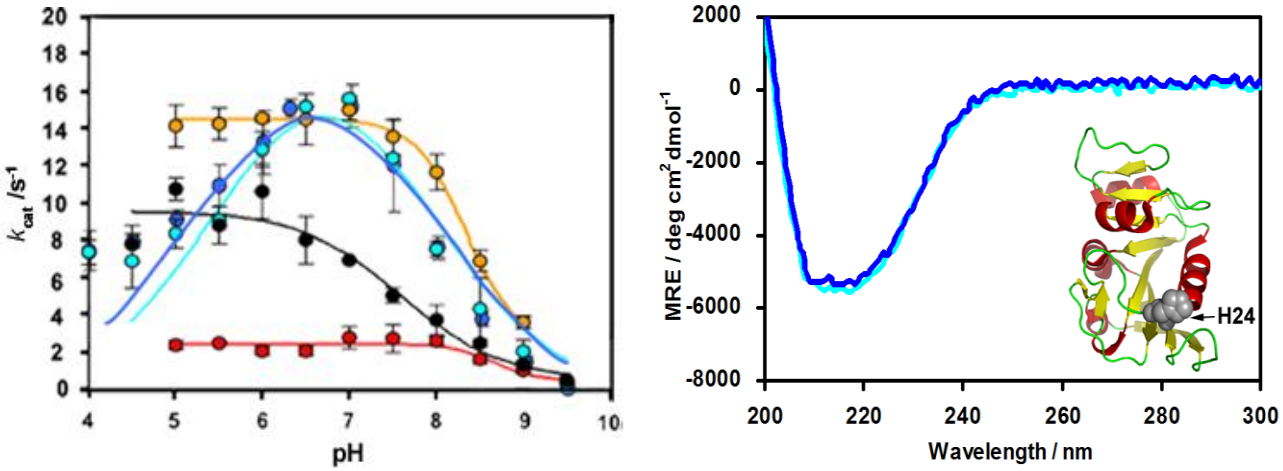

Figure 4.8: *pH dependence of k_{cat} (left) for MpDHFR (cyan), MpDHFR-H24N (blue), MpDHFR-P150S (orange), EcDHFR (black) and EcDHFR-S148P (red) and CD spectra (right) of wild-type MpDHFR (cyan) and MpDHFR-H24N (blue) at 20 °C. The inset is a cartoon representation of the MpDHFR structure showing the position of H24.*

Interestingly, the pH dependence of k_{cat} for MpDHFR-P150S was found to be sigmoidal like that of EcDHFR, with a pH independent k_{cat} of 14.5 ± 0.3 s^{-1}, very similar to k_{cat} for wild type MpDHFR at pH 7 and 20 ºC (15.6 ± 0.2 s^{-1})[6] (Table 4.11). On the other hand, a five-fold decrease in the value of k_{cat} was observed for EcDHFR-S148P (2.1 ± 0.2 s^{-1}) compared to wild type EcDHFR (10.6 ± 1.5 s^{-1}) at pH 6 and 20 ºC (Table 4.11). Similar to their wild type counterparts,[79,122] the two variants have a KIE of unity at pH 7 under steady state conditions (Table 4.12).

Table 4.11: *pH dependence of the steady state rate constant (k_{cat}) for the MpDHFR, MpDHFR-P150S, MpDHFR-H24N, EcDHFR and EcDHFR-S148P catalyzed reaction in MTEN buffer at 20 ºC.*

pH	k_{cat} / s^{-1}				
	MpDHFR	MpDHFR-P150S	MpDHFR-H24N	EcDHFR	EcDHFR-S148P
4	7.4 ± 0.7	nd	7.55 ± 1.51	nd	nd
4.5	6.9 ± 1.4	nd	8.05 ± 0.53	nd	nd
5	8.3 ± 0.7	14.1± 1.1	9.18 ± 0.80	10.7 ± 0.6	2.4 ± 0.2
5.5	9.1± 2.1	14.2 ± 0.9	11.01 ± 1.50	8.8 ± 1.0	2.5 ± 0.1
6	12.4 ± 0.9	14.5 ± 0.2	13.32 ± 2.42	10.6 ± 1.5	2.1 ± 0.2
6.5	15.2 ± 1.9	14.5 ± 1.4	15.11 ± 0.90	8.0 ± 1.3	2.0 ± 0.3
7	15.6 ± 1.7	15.0 ± 0.6	15.24 ± 1.65	6.9 ± 0.1	2.8 ± 0.4
7.5	12.4 ± 0.9	13.59 ± 0.9	12.05 ± 3.52	5.0 ± 0.4	2.7 ± 0.5
8	7.5 ± 0.7	11.69 ± 1.0	7.70 ± 0.86	3.7 ± 0.8	2.6 ± 0.2
8.5	4.3 ± 0.5	6.9 ± 0.6	3.88 ± 0.55	2.5 ± 0.2	1.6 ± 0.2
9	2.0 ± 0.2	3.6 ± 0.3	1.61 ± 0.41	1.3 ± 0.2	1.0 ± 0.2
9.5	0.3 ± 0.6	nd	0.20 ± 0.05	0.5 ± 0.1	0.5 ± 0.1

nd: not determined, [a] taken from ref [99]

Table 4.12: *pH dependence of the KIE during catalysis by MpDHFR, MpDHFR-P150S and S148P-EcDHFR in MTEN buffer at 20 ºC.*

pH	MpDHFR[a]	MpDHFR-P150S	EcDHFR-S148P
5	1.0 ± 0.1	1.0 ± 0.2	1.2 ± 0.1
5.5	nd	0.9 ± 0.1	1.1 ± 0.1
6	1.0 ± 0.1	1.0 ± 0.1	1.0 ± 0.2
6.5	nd	1.2 ± 0.2	1.1 ± 0.2
7	1.0 ± 0.1	1.3 ± 0.1	1.1 ± 0.1
7.5	1.3 ± .01	1.7 ± 0.2	1.2 ± 0.1
8	1.7 ± 0.1	1.7 ± 0.1	1.2 ± 0.1
8.5	1.8 ± 0.1	1.9 ± 0.1	2.0 ± 0.2
9	2.7 ± 0.1	2.0 ± 0.2	2.7 ± 0.2

[a] taken from ref [79]

4.4.2 Effect of pH on K_M for EcDHFR-S148P and MpDHFR-P150S

K_M for NADPH and DHF were measured for EcDHFR-S148P and MpDHFR-P150S at pH 7 and pH 5 at 20 ºC (Table 4.13). Both have similar K_M values as their wild type counterparts for both DHF and NADPH at pH 7, although K_M for DHF with EcDHFR-S148P at pH 5 is 10 times higher than that of the wild type.

Table 4.13: *K_M for NADPH and DHF with EcDHFR, EcDHFR-S148P, MpDHFR and MpDHFR-P150S at 20 ºC.*

Enzyme	pH	K_M^{DHF} (µM)	K_M^{NADPH} (µM)
EcDHFR[a]	7	0.7 ± 0.2	4.8 ± 1.0
	5	0.7 ± 0.5	Nd
EcDHFR-S148P	7	0.7 ± 0.1	4.7 ± 0.7
	5	6.8 ± 0.5	5.5 ± 0.4
MpDHFR[b]	7.5	2.4 ± 0.2	5.7 ± 0.2
	5	0.4 ± 0.1[c]	10.8 ± 3.1
MpDHFR- P150S	7	2.2 ± 0.2	10.7 ± 0.6
	5	3.2 ± 0.5	15.2 ± 0.9

nd: not determined, [a]: taken from reference [79], [b]: taken from reference [7], c: at pH 5.5.

This type of bell-shaped steady-state pH dependence has been seen previously when residues in helix αC (Figure 4.2A) in EcDHFR were replaced by those of helix αC of LcDHFR, which lacks Ser148 (EcDHFR numbers) and most likely cannot form the occluded conformation.[124] A similar pH dependence was also obtained when the three residues Glu-Lys-Asn were inserted in the αC helix of EcDHFR.[125] While these two EcDHFR αC mutants have about the same k_H and k_{cat} as the wild type EcDHFR at pH 7, k_{cat} is reduced by 50% at lower pH,[124-125] similar to MpDHFR.[79] In the case of the EKN insertion,[125] the decrease in k_{cat} at low pH was demonstrated to be due to impaired dissociation of THF from the E.NADPH.THF mixed ternary complex,[125] which is the rate limiting step in EcDHFR under steady state conditions.[7]

4.5 Steady state rate limiting step for MpDHFR, EcDHFR-S148P and MpDHFR-P150S

Dissociation rate constants

The dissociation rate constants (k_{off}) of THF from different complexes were measured at pH 6 and 25 ºC for MpDHFR and the two variants to explore the rate limiting step (Table 4.17). The results show that k_{cat} for MpDHFR-P150S at low pH is limited by the dissociation of THF from the mixed E.NADPH.THF ternary complex, as seen for wild type EcDHFR.[7] For MpDHFR, the rate constant for THF release from the mixed ternary complex E.NADPH.THF at pH 6 (k_{off} = 19.1 s^{-1}) is in the same order of magnitude as k_{cat} at pH 7 (15.6 s^{-1}) (Table 4.14). In turn, at pH 5, the k_{off} value is 15.7 ± 1.0 s^{-1}, while k_{cat} drops significantly to 8.3 ± 0.8 s^{-1}. This implies that in the MpDHFR reaction the magnitude of k_{off} is essentially unaffected by the decrease of pH while the rate-determining step has shifted from the dissociation of E.NADPH.THF to an alternative chemical step. For EcDHFR-S148P, k_{cat} is limited by the dissociation of THF from the product ternary complex E.$NADP^+$.THF, not from the mixed ternary complex E.NADPH.THF as in the wild type EcDHFR and the MpDHFR-P150S reaction. The k_{off} values for EcDHFR-S148P and MpDHFR-P150S are similar to that of the wild type MpDHFR, suggesting that the mutation did not affect dissociation of THF.

Table 4.14: *Dissociation rate constants k_{off} for THF from the various DHFRs, measured using the competition method with methotrexate as the trapping ligand, at 25 ℃ in MTEN buffer, pH 6.*

Complex	k_{off} (s^{-1})				
	EcDHFR[a]	MpDHFR	EcDHFR-S148P	MpDHFR-P150S	LcDHFR[b]
E.THF	0.97 ± 0.1	0.55 ± 0.1	0.5 ± 0.1	0.9 ± 0.2	0.5 ± 0.1
E.NADPH.THF	12.0 ± 1.0	19.1 ± 2.0	18.4 ± 0.8	17.3 ± 2.0	40.0 ± 8.0
E.$NADP^+$.THF	2.4 ± 0.3	3.8 ± 1.0	2.6 ± 0.1	2.5 ± 1.0	1.7 ± 0.2
k_{cat} (s^{-1})[c]	9.5 ± 1.4	15.4 ± 0.3	2.4 ± 0.3	14.5 ± 0.4	31.0 ± 2.0

[a]: taken from reference [7], [b]: taken from reference [68] (pH 6.5), [c]: pH independent value

4.6 NMR investigation

HSQC spectroscopy was employed to investigate how the occluded conformation modifies the enzyme's affinity to $NADP^+$. When $NADP^+$ is bound by DHFR, the amide functionality of the ligand experiences a substantial change in chemical environment due to an ordered network of hydrogen bonds inside the active site.[59] When the nicotinamide ring is inside the active site, the nicotinamide amide protons should have very different chemical shifts to those in solution, partly due to the hydrophobic environment of the active site and partly due to the hydrogen bonds, which form between this group and the backbone carbonyls of Ala7 and Ile14 in the protein. When the nicotinamide group is not held within the active site, the amide chemical shifts should resemble those in free solution. When the amide group of $NADP^+$ is labeled with a ^{15}N isotope, the change in chemical environment can be seen by ^1H-^{15}N HSQC measurement. Data obtained from this experiment should then reveal insights into how $NADP^+$ binds to different DHFRs, including EcDHFR, EcDHFR-S148P, MpDHFR and MpDHFR-P150S.

The measurements were obtained for DHFRs in two complexes: the Michaelis complex (DHFR.$NADP^+$.folate) and the product complex (DHFR.NADPH.THF). In the latter complex, no difference was observed for the four DHFRs used in this study and the spectra obtained were very similar to that of the free ligand in absence of the enzyme, indicating that the $NADP^+$ protons are free in solution (Figure 4.9). However, in the Michaelis complex (DHFR.$NADP^+$.folate), a very remarkable difference was observed (Figure 4.10).

The ^1H-^{15}N HSQC spectrum of the free ligand mixture, ^{15}N-labeled $NADP^+$ and folate, at pH 7 and 20 °C shows a pair of signals at δ_N 109.9 ppm and δ_H 7.7 and 8.5 ppm, which correspond to the labelled nitrogen atom and its attached protons, respectively (Figure 4.10). When EcDHFR was added to the mixture, the resulting ^1H-^{15}N HSQC NMR spectrum displays a pair of signals with chemical shifts that are similar to the ones of the free ligand (Figure 4.10), thus indicating the nicotinamide moieiety of $NADP^+$ is outside the active site. In contrast, when the wild type enzyme was replaced by the S148P variant, an extra pair of $^{15}N/^1H$ signals at δ_N 107.2 ppm and δ_H 8.4 and 10.2 ppm was observed (Figure 4.10). This, therefore, suggests that a noticeable population of $NADP^+$ is bound to the active site of EcDHFR-S148P. Since substitution of Ser148 with a proline residue would destabilize the occluded conformation, the NMR data might suggest that the mutant has a stronger binding affinity to the oxidized cofactor $NADP^+$ because of its inability to adapt to the occluded conformer. This can be confirmed by performing further binding studies for DHFR with various ligands.

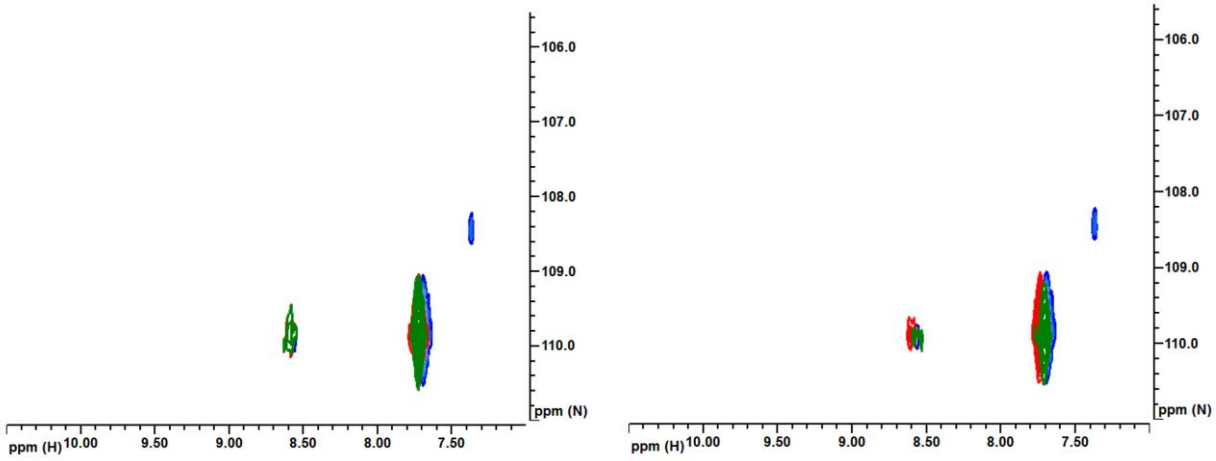

Figure 4.9: *Left: ^{1}H-^{15}N HSQC spectra for ^{15}N-labeled NADP^{+} in free solution with THF (blue), and in complex with THF and MpDHFR (green) or MpDHFR-P150S (red). Right: ^{1}H-^{15}N HSQC spectra for ^{15}N-labeled NADP^{+} in free solution with THF (blue) and in complex with THF plus EcDHFR-S148P (green) or wild type EcDHFR (red), right, at pH 7 and 20 ℃.*

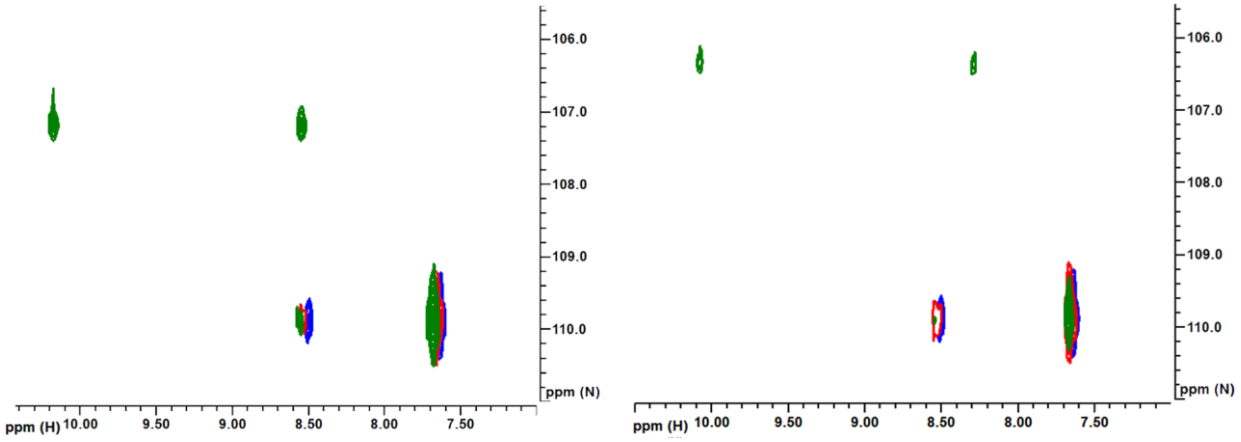

Figure 4.10: *Left: ^{1}H-^{15}N HSQC spectra for ^{15}N-labeled NADP^{+} in free solution with folate (blue) and in complex with folate plus EcDHFR (red) or EcDHFR-S148P (green) at pH 7 and 20 ℃, Right: ^{1}H-^{15}N HSQC spectra for ^{15}N-labeled NADP^{+} in free solution with folate (blue) and in complex with folate plus MpDHFR (green) or MpDHFR-P150S (red) at pH 7 and 20 ℃.*

Interestingly, replacement of Pro150 with a serine residue in MpDHFR generated an opposite effect on the binding with NADP^{+}. A significant amount of ^{15}N-labeled NADP^{+} binds to the wild type MpDFHR, as the ^{15}N/^{1}H signals of the bound ligand can be seen in the ^{1}H-^{15}N HSQC spectrum (free ligand at δ_N 109.9 ppm and δ_H 7.7 and 8.5 ppm *vs*. bound ligand at δ_N 106.3 ppm and δ_H 8.3 and 10.2 ppm, Figure 4.10). On the other hand, MpDHFR-P150S, similar to EcDHFR, as its corresponding NMR spectrum only shows the ^{15}N/^{1}H signals of the free ligand (δ_N 109.9 ppm and δ_H 7.7 and 8.5

ppm, Figure 4.10). Eventually, this leads us to propose that the serine replacement in MpDHFR likely introduces hydrogen bond(s) that can promote the occluded conformation, which in turn decreases the enzyme affinity for $NADP^+$.

In an attempt to study the effect of pH on the binding of $NADP^+$, the same set of NMR experiments were carried out in buffer at pH 5.5 in the Michaelis complex (DHFR.$NADP^+$.folate) (Figures 4.11 to 4-13). While the change in the pH does not affect the binding of $NADP^+$ to the EcDHFR-S148P variant (Figure 4.11), two additional peaks representing bound $NADP^+$ were observed for EcDHFR at the same pH (Figure 4.11). Unfortunately, both wild type MpDHFR and the P150S variant precipitated at high concentration at this pH, thus prohibiting proper NMR data collection. For MpDHFR at pH 6.6, while some precipitation can be observed, the two peaks of the bound $NADP^+$ can be seen clearly (Figures 4.13).

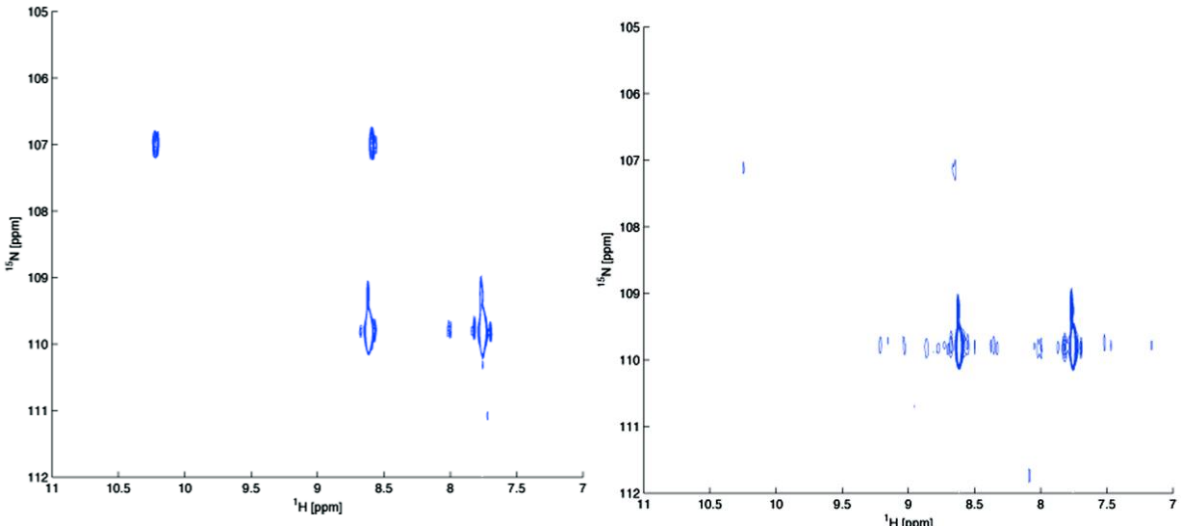

Figure 4.11: *(^{1}H-^{15}N) HSQCs for ^{15}N(AM)-$NADP^+$ with EcDHFR-S148P (left) and EcDHFR (right) at 20 ℃ in the ternary complex E.$NADP^+$.folate at pH 5.5.*

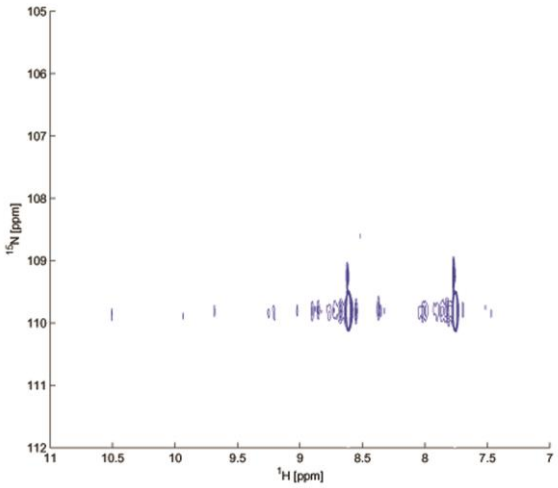

Figure 4.12: *(^{1}H-^{15}N) HSQCs for ^{15}N(AM)-NADP^{+} with MpDHFR-P150S at pH 5.5 and 20 ℃ in the ternary complex E.NADP^{+}.folate. Enzyme precipitation at high concentration and low pH prevented proper NMR measurements.*

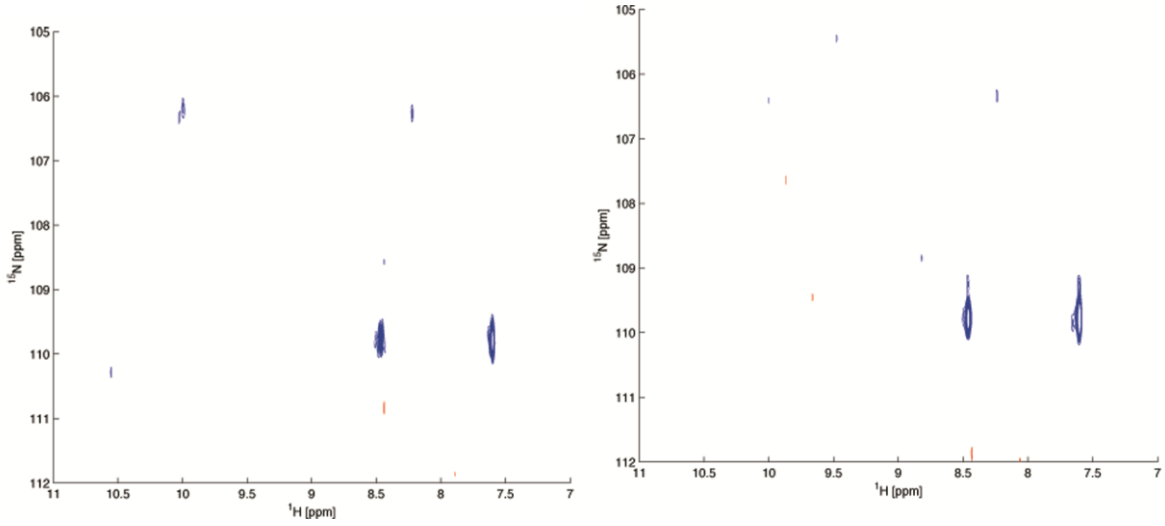

Figure 4.13: *(^{1}H-^{15}N) HSQCs for ^{15}N(AM)-NADP^{+} with MpDHFR at 20 ℃ in the ternary complex E.NADP^{+}.folate at pH 6.6 (left) and 5.5 (right). The enzyme precipitated at low pH due to the high protein concentration used for the measurements.*

Taking all the data together is suggesting that EcDHFR-S148P binds tighter to NADP^{+} than its wild type counterpart, which most probably causes the change in the rate limiting step to the release of THF from the ternary complex E.NADP^{+}.THF instead of the mixed ternary complex E.NADPH.THF. Therefore the amount of NADP^{+} binding to MpDHFR is expected to increase at low pH to cause the change in the rate limiting step. The NMR data for MpDHFR could not support this due to enzyme precipitation at low pH, but EcDHFR shows a very weak binding to NADP^{+} at pH

5.5, suggesting that at low pH the affinity of EcDHFR to $NADP^+$ has increased. This in turn can lead us to thinking that probably the same happens with MpDHFR at low pH causing the change in the rate limiting step.

4.7 Role of the occluded conformation

EcDHFR is often used as a model to study the relationship between protein dynamics and the chemical step of enzyme catalysis. This enzyme has been demonstrated to proceed through a cycle of ordered physical steps with THF release from the mixed ternary complex, E.NADPH.THF, being rate-determining at physiological pH.[7] Moreover, the enzyme was shown to oscillate between the closed and the occluded conformations, which have been proposed to help progression through the catalytic cycle.[73,126-128] On the other hand, DHFR from another bacterial species, *Moritella profunda*, is unlikely to adopt the occluded conformation, because it lacks the key residue (Ser148 in EcDHFR) to stabilize this conformer. Hence, it is of great interest to investigate the importance of the occluded conformation in DHFR catalysis.

In this part of the thesis, we show that the role of the occluded conformation in EcDHFR catalysis is to modify the enzyme's affinity to NADPH/$NADP^+$. The first line of evidence is provided by our kinetic characterization of the EcDHFR-S148P reaction, which shows a sharp decrease of k_{cat} while the rate constants for hydride transfer (k_H) and THF dissociation (k_{off}), and the Michaelis constants (K_M), remain essentially unaffected. Also, this mutant has a stronger affinity for the oxidized cofactor $NADP^+$, as shown in the (^1H-^{15}N) HSQC studies. Taking all these data together, we conclude that the occluded conformation does not affect the step of hydride transfer but assists $NADP^+$ release from active site instead (Figure 4.14).

It is well established that $NADP^+$ is first released from the product complex, followed by NADPH entry and THF release in the EcDHFR catalytic cycle.[7] Previously, it was proposed that THF release from the mixed ternary complex, E.NADPH.THF, is promoted by the repulsive interactions between the pyrophosphate moiety of NADPH and the *p*-aminobenzoyl-L-glutamate (pABG) moiety of THF.[59] Yet, it remains unclear how the enzyme manages to differentiate between NADPH and $NADP^+$, as both compounds are structurally similar. The decrease of $NADP^+$ binding affinity in the occluded conformer could help to guide EcDHFR through the physical steps in a sequential manner. Also, it has been suggested that fidelity to the order of the physical steps is of great importance to the function of EcDHFR, to prevent product inhibition as bacterial cells contain equal amounts of NADPH and $NADP^+$, in contrast to eukaryotic cells in which $NADP^+$ represents only 1% of the

NADPH concentration.[59] This idea is further supported by the remarkably different k_{off} and k_{cat} values that were measured with EcDHFR-S148 (Table 2). Because the rate constant for THF release from the mixed ternary complex is significantly higher than the steady-state reaction rate constant, it implies that the EcDHFR-S148P reaction is not exclusively limited by THF release.

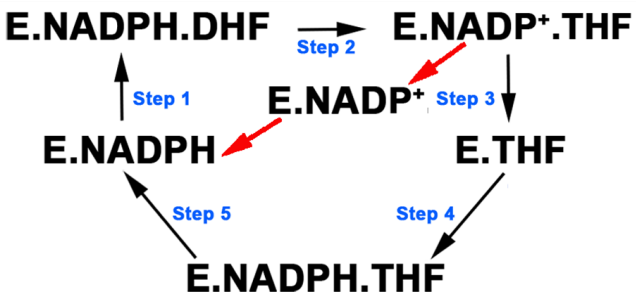

Figure 4.14: *Schematic representation of the catalytic pathway of DHFR in the presence of the occluded conformation (steps from 1 to 5). The red arraws is showing the divertion of the catalytic cycle pathway that can happen in the absence of the occluded confomation.*

Our investigations provide a better understanding of the MpDHFR catalytic cycle as well. As suggested by the results of our binding studies, the product THF does not release from MpDHFR until $NADP^+$ is replaced by NADPH in the ternary complex. Thus, MpDHFR likely follows a well-ordered catalytic cycle, which is similar to that of EcDHFR. Nevertheless, certain aspects of MpDHFR catalysis are dramatically different. This enzyme could not adopt the occluded conformation as the key serine residue in the GH loop is replaced by a rigid proline residue, which lacks both groups (OH and NH) responsible for formation of the hydrogen bonds important to the occluded conformation. The ^1H-^{15}N HSQC studies point out that MpDHFR has a stronger affinity to $NADP^+$ than the *E. coli* counterpart, due to the lack of the occluded conformation. It is unclear how MpDHFR could faithfully follow the physical steps in a consecutive manner. Possibly, MpDHFR has evolved to possess a stronger affinity for THF, thereby ensuring that $NADP^+$ first exits from the active site after the step of hydride transfer. This is evident by the slightly higher (~1.6x) k_{off} value measured for THF in the MpDHFR.NADPH.THF complex. Alternatively, MpDHFR might bind more weakly to $NADP^+$ than the *E. coli* variant. However, additional work is needed to quantify the extent of $NADP^+$ binding. Moreover, the pH rate profile of the MpDHFR reaction shows a bell-shaped curve, instead of the sigmoidal curve that was observed with the EcDFHR reaction and k_{off} for THF from the MpDHFR.$NADP^+$.THF complex at pH values below 6 is faster than k_{cat}. This can be due to the existence of two parallel kinetic pathways. Whereas one pathway employs the 'regular' EcDHFR catalytic pathway, the parallel pathway might have an alternative rate-determining step,

which could be the release of $NADP^+$ or the generation of apoenzyme. As a matter of fact, similar hypotheses have been suggested for DHFRs from Human (HsDHFR)[129-130] and *Mycobacterium tuberculosis* (MtDHFR).[70] In particular, the occluded conformers of these enzymes have never been observed, and the amino acid sequence seem to lack the key serine residue for stabilizing this conformer.[70,129-130]

Perhaps more interestingly, the descending limb at low pH was removed when the occluded conformation is enabled in the MpDHFR catalysis *via* a Pro150Ser site-directed mutation. This indicates that the occluded conformation rescues the enzyme from poor steady-state activity at low pH. A probable explanation is that product binding is weakened at low pH due to a change in-protonation state(s) in product(s) and/or the enzyme; this might disturb the order of physical steps, consequently slowing the reaction rate. In contrast, when the occluded conformation is enabled in the MpDHFR-P150S reaction, the order of product release is strictly controlled and consequently the rate of reaction is retained. It is somewhat unfortunate that high concentration of MpDHFR leads to protein aggregation in acidic condition, precluding us from obtaining additional NMR data and insights into the habits of product binding. Currently, our group continues the investigation using other experimental methods, including solvent isotope effect measurement and/or binding isotope effect measurements of isotopically labeled products.

4.8 Conclusions

In this chapter, the role of the occluded conformation was investigated by a combination of techniques, including site-directed mutagenesis, steady and pre-steady-state kinetics, binding measurement and NMR studies. It was clearly revealed that the occluded conformation does not affect the step of hydride transfer. Yet, it is of great importance for EcDHFR catalysis, because it controls the enzyme's affinity for $NADP^+$ and guides the enzyme through the physical steps in a strictly ordered manner. Inability to form the occluded conformation had a strong impact on EcDHFR, resulting in a change in the steady state rate limiting step and a great decrease in the value of k_{cat}. MpDHFR seems to follow a similar catalytic cycle, but it functions efficiently without the involvement of an occluded conformation. This enzyme might have evolved to hold a stronger affinity to THF or a weaker affinity to $NADP^+$, either of which ensures the sequential order of product release at pH 7. However, this character of MpDHFR is hampered in acidic condition, decreasing the steady-state reaction rate constant and contributing to the bell-shaped curve in the pH rate profile, diverting the reaction into two parallel kinetic pathways as has been described previously for MtDHFR.[70] This impairment, interestingly, could be rescued by enabling the occluded

conformation in the MpDHFR catalytic cycle. Since many DHFRs lack a hydrogen bond donor in the position corresponding to Ser148, and since the occluded conformation has been observed only in EcDHFR, the occluded conformation is unlikely to be universal and the *E. coli* enzyme may not always be the best choice for the study of general aspects of catalysis by dihydrofolate reductase.

5

Loop dynamics during catalysis by dihydrofolate reductase

5.1 Preface

Studying protein variants is a very important tool to understand the relation between enzyme structure, dynamic and catalysis. Although many protein variants have properties similar to their corresponding wild-type structures, the replacement of a single amino acid often produces dramatic changes in enzymes structures, stabilities, and function.[131-133] Many proteins exist simultaneously in multiple conformations and previous studies have provided evidence of the importance of enzyme motion during catalysis by DHFR.[7,77,127,134-135] Various X-ray crystallographic structures for DHFR from *Escherichia coli* (EcDHFR) indicate that the enzyme assumes different conformations along the reaction pathway as discussed in detail in Chapters 1 and 4.[7,59,74,136-137]

Often the effect of a single mutation is distributed over many protein properties. Enzyme mutation can have various effects on the protein structure; such as affecting ligand binding, resulting in an altered affinity for a substrate, product, and inhibitor. In addition, it can increase or decrease enzymatic activity;[138-140] and can cause changes in protein stability,[141] or disturb the protein conformations[142] and the rates of conformational change.[143] In this chapter, different MpDHFR and EcDHFR variants were designed, produced using site-directed mutagenesis and studied alongside the wild type enzymes to elucidate the role of individual amino acids or areas of the proteins in terms of structure and function.

5.2 Choosing MpDHFR and EcDHFR variants

Dihydrofolate reductase contains three mobile loops: the M20 loop (residues 9-24), FG loop (residues 116 to 132 in EcDHFR), and GH loop (residues 142 to 149 in EcDHFR). The movements of these three loops were thought to be essential for catalysis.[7,59,127]

In particular, depending on the nature of the bound ligand, two different conformations have been observed for the M20 loop (residues 9-24) of EcDHFR: closed and occluded.[7] The M20 loop adopts the closed conformation when the substrate (DHF) and the coenzyme (NADPH) are bound to EcDHFR. This conformation is stabilized by hydrogen bonding interactions between the M20 loop and the FG loop.[7,59] The M20 loop switches to the occluded conformation in the product binary and ternary complexes and two new hydrogen bonds are formed between the M20 loop and the GH loop.[7,59]

Mutations in the GH loop in position 150 (MpDHFR number) were discussed in chapter 4 in detail. In this chapter, the effect of site directed mutagenesis in the M20 loop and FG loop on DHFR catalysis will be studied.

5.3 Mutation in the M20 loop

Alignment of the amino acid sequences for the two DHFR homologues, EcDHFR and MpDHFR shows three major differences in the M20 loop (Figure 5.1).

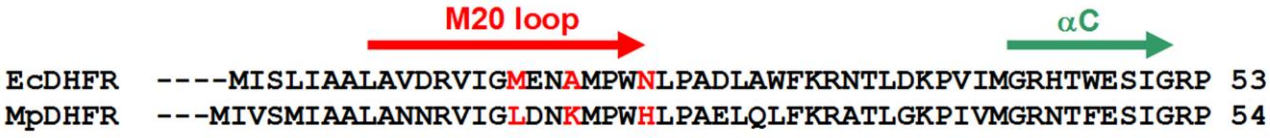

Figure 5.1: *Alignment of the amino acid sequences of EcDHFR and MpDHFR showing the main different residues in the M20 loop in red.*

These residues are methionine 16 (replaced by leucine in MpDHFR), alanine 19 (replaced by lysine in MpDHFR) and asparagine 23 (replaced by histidine in MpDHFR). The backbone of asparagine 23 in EcDHFR was found to form two hydrogen bonds with serine 148 in the GH loop in the product complex to stabilize the occluded conformation. Since MpDHFR is most probably not capable of forming the occluded conformation due to the absence of serine 148 (replaced with proline in MpDHFR, see chapter 4 for further details), the replacement of asparagine 23 in EcDHFR with histidine in MpDHFR should not have any effect on the hydride transfer step. Furthermore, the MpDHFR-H23N variant (EcDHFR numbers) has a similar pH dependence in the steady state to the wild type MpDHFR with similar k_{cat} values, suggesting that the mutation did not affect the steady state rate limiting step. In addition, this variant has a similar CD spectrum to wild type MpDHFR, indicating no change in the secondary structure for this variant compared to wild type MpDHFR (see chapter 4).

The mutations in the M20 loop were created mainly in two positions (positions 16 and 19) in both EcDHFR and MpDHFR (Figure 5.2), to investigate the role of these active site residues in catalysis by dihydrofolate reductase. The differences in these positions are the most dramatic changes to the M20 loop between the two enzymes.

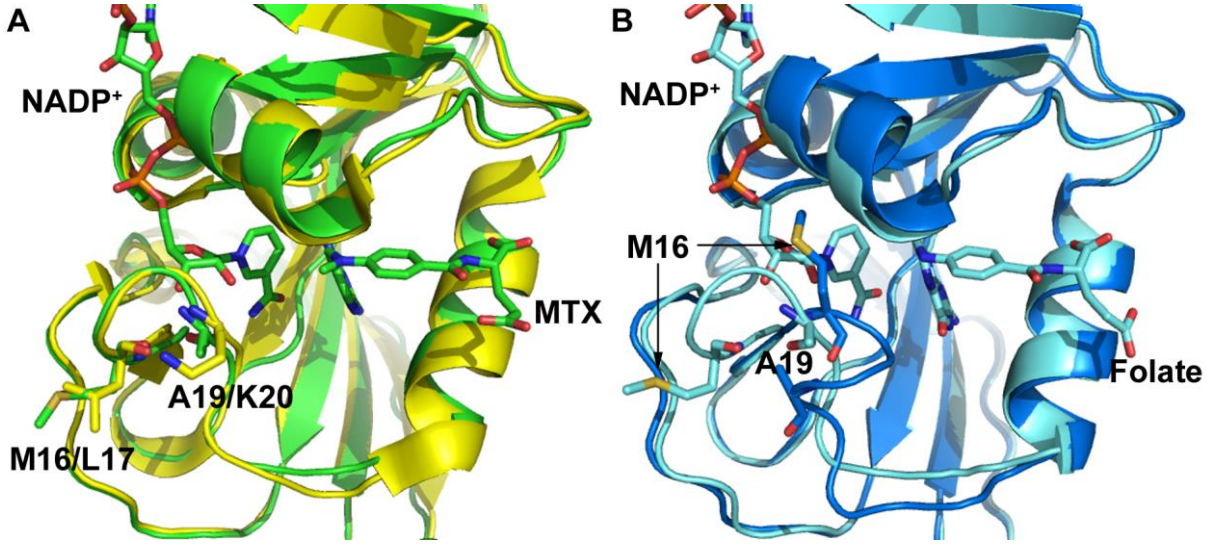

Figure 5.2: *(A) Alignment of the active site loops of EcDHFR (green, PDB 1DRE)[1] and MpDHFR (yellow, PDB 3IA4)[4] in complex with methotrexate (MTX) and $NADP^+$ (green) showing the position of M16 and A19 in EcDHFR and the corresponding residues in MpDHFR (L17 and K20). (B) Alignment of EcDHFR (cyan, PDB 1RX2)[1] in the closed conformation, in complex with $NADP^+$ and folate and EcDHFR (blue, PDB 1RX6)[1] in the occluded conformation showing the difference of the position of M16 and A19 in the closed and the occluded conformation.*

5.3.1 EcDHFR variants at positions 16 and 19

The temperature dependence of hydride/deuteride transfer and the kinetic isotope effect (KIE) were measured, under single turnover conditions, for the variants EcDHFR-M16L, EcDHFR-A19K (Figure 5.3 and Table 5.1), EcDHFR-M16L/A19K, EcDHFR-M16L/S148P (Figure 5.4 and Table 5.2), EcDHFR-A19K/S148P and EcDHFR-M16L/A19K/S148P (Figure 5.5 and Table 5.4). The data obtained were compared to the temperature dependence of the rate constants and kinetic isotope effect for wild type EcDHFR (Figure 5.6).

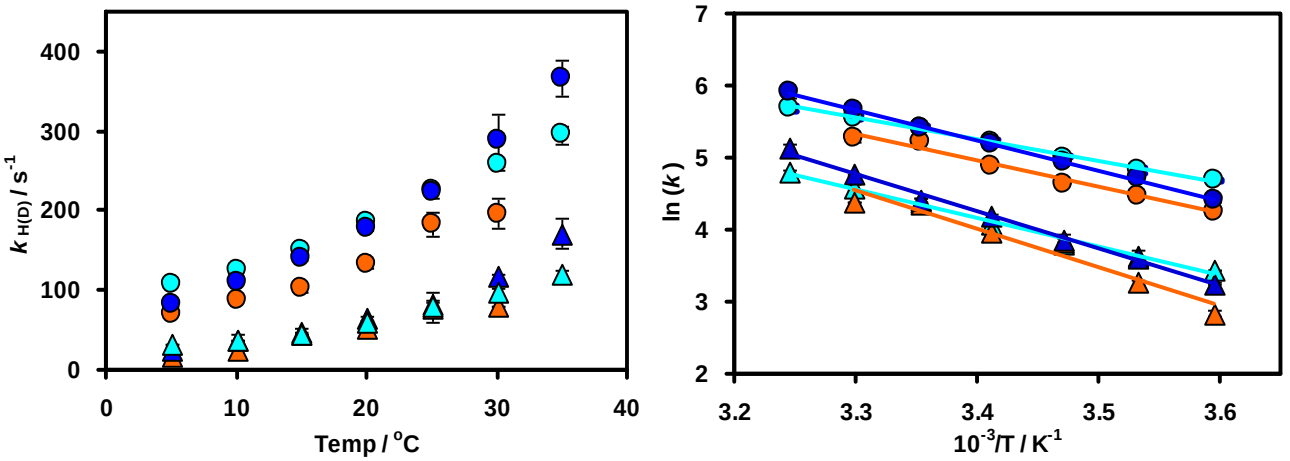

Figure 5.3: *Temperature dependence (right) and Arrhenius plots (left) of the pre-steady-state rate constants for hydride (k_H, circles) and deuteride (k_D, triangles) transfer during catalysis by wild type EcDHFR (blue), EcDHFR-M16L (cyan) and EcDHFR-A19K (orange) at pH 7.*

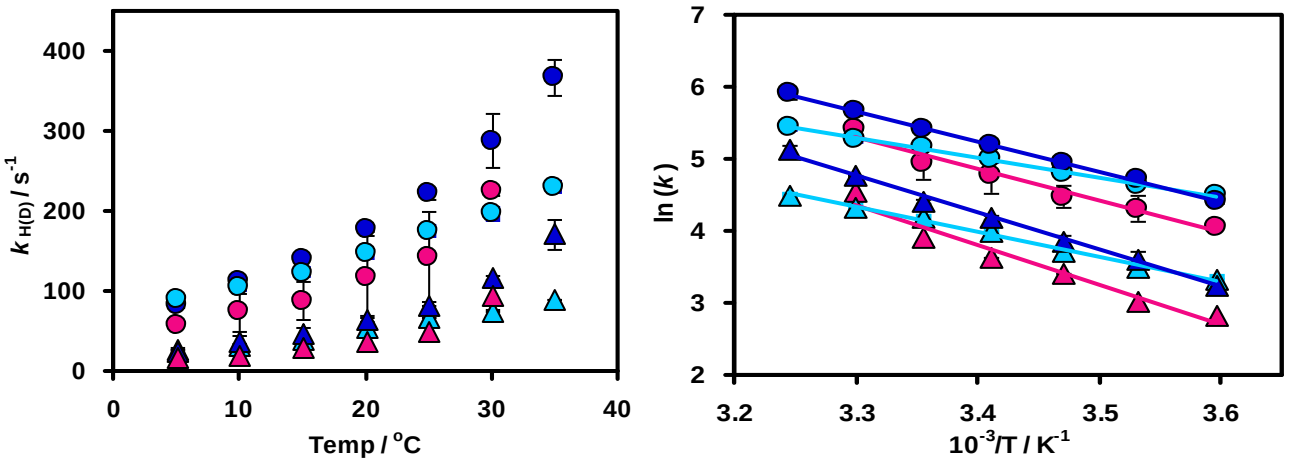

Figure 5.4: *Temperature dependence (right) and Arrhenius plots (left) of the pre-steady-state rate constants for hydride (k_H, circles) and deuteride (k_D, triangles) transfer during catalysis by wild type EcDHFR (blue), EcDHFR-M16L/S148P (light blue) and EcDHFR-A19K/S148P (pink) at pH 7.*

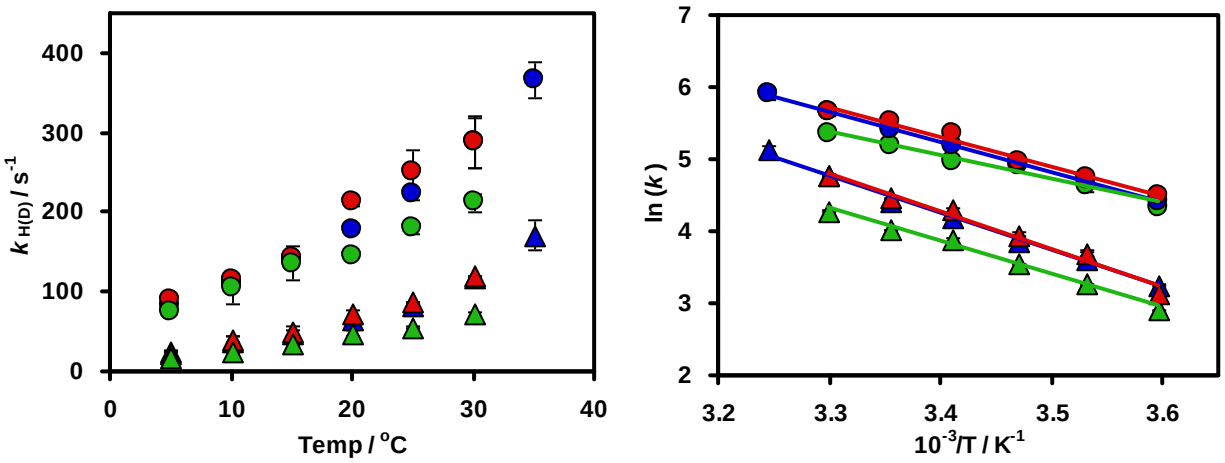

Figure 5.5: *Temperature dependence (right) and Arrhenius plots (left) of the pre-steady-state rate constants for hydride (k_H, circles) and deuteride (k_D, triangles) transfer during catalysis by wild type EcDHFR (blue), EcDHFR-M16L/A19K (red) and EcDHFR-M16L/A19K/S148P (green) at pH 7.*

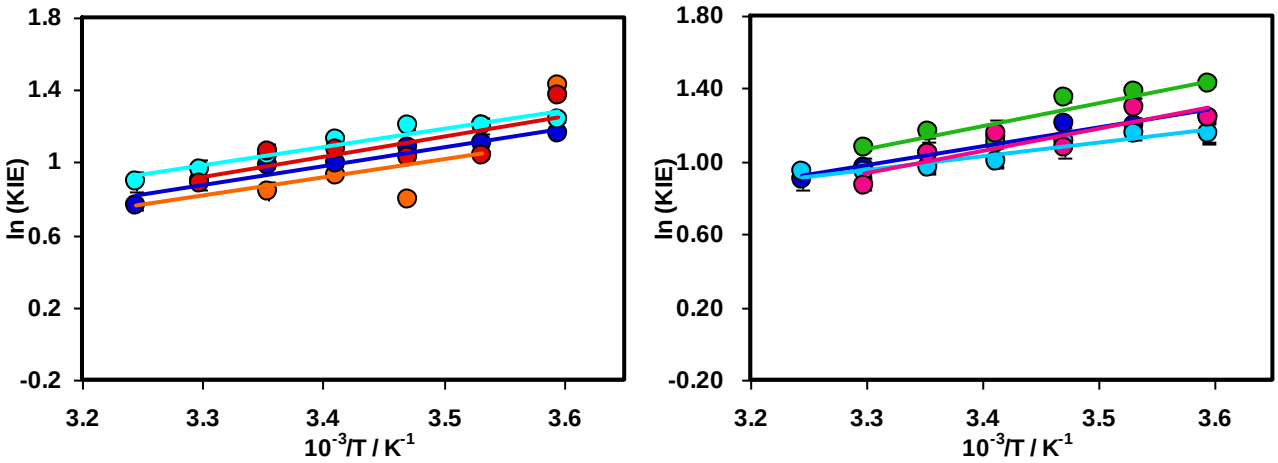

Figure 5.6: *The temperature dependence of KIEs plotted on a logarithmic scale against the inverse temperature during catalysis by wild type EcDHFR (blue), EcDHFR-M16L (cyan), EcDHFR-A19K (orange) and EcDHFR-M16L/A19K (red) left, and by wild type EcDHFR (blue), EcDHFR-M16L/S148P (light blue), EcDHFR-A19K/S148P (pink) and EcDHFR-M16L/A19K/S148P (green), right, under single turnover conditions at pH 7.*

The six variants EcDHFR-M16L, -A19K, -M16L/S148P, -A19K/S148P, -M16L/A19K and -M16L/A19K/S148P have similar hydride transfer rate constants to the wild type EcDHFR (Figures 5.3 to 5.5) and similar temperature dependence of the KIE (Figure 5.6), indicating that the mutation did not affect the chemical step. However, while the mutation did not affect hydride transfer, a dramatic decrease in the steady state rate constant (k_{cat}) was obtained for all the variants (Table 5.6). The steady state rate constant of EcDHFR represents the rate of the product (THF) release from the

ternary complex E.NADPH.THF[7] (k_{cat} = 6.9 ± 0.1 s^{-1} at pH 7 and 20 ˚C). The EcDHFR-M16L variant has shown very similar K_M values to wild type EcDHFR for both NADPH and DHF (Table 5.15), however the smallest k_{cat} of the six variants was obtained for this variant and the EcDHFR-M16L/S148P variant as well, followed by EcDHFR-M16L/A19K/S148P (k_{cat} = 0.66 ± 0.12 s^{-1}) and EcDHFR-M16L/A19K (k_{cat} = 1.67 ± 0.12 s^{-1}). The EcDHFR-A19K and EcDHFR-A19K/S148P variants show the highest k_{cat} in all the EcDHFR variants studied here with a value comparable to that obtained for the EcDHFR-S148P variant as was shown in Chapter 4 (k_{cat} = 2.15 ± 0.25, 2.2 ± 0.40 and 2.8 ± 0.4 s^{-1} for EcDHFR-A19K, EcDHFR-A19K/S148P and EcDHFR-S148P respectively).

Table 5.1: *Temperature dependence of the pre-steady-state rate constants for hydride (k_H) and deuteride (k_D) transfer during catalysis by EcDHFR-M16L and A19K at pH 7.*

	EcDHFR-M16L[a]		EcDHFR-A19K	
T (^{o}C)	k_H (s^{-1})	k_D (s^{-1})	k_H (s^{-1})	k_D (s^{-1})
5	108.91 ± 1.24	31.49 ± 0.06	70.87 ± 0.32	17.15 ± 2.05
10	124.65 ± 5.66	37.57 ± 0.09	87.60 ± 0.71	26.35 ± 5.95
15	150.36 ± 1.74	45.20 ± 0.61	102.38 ± 3.85	46.33 ± 1.87
20	185.57 ± 3.18	59.93 ± 0.73	133.28 ± 5.96	52.68 ± 4.56
25	226.00 ± 2.97	79.91 ± 5.00	183.54 ±15.26	79.18 ± 19.34
30	258.36 ± 7.52	98.72 ± 4.48	197.05 ± 19.73	80.75 ± 0.78
35	296.01 ± 11.85	121.14 ± 4.34	nd	nd

nd: not determined, [a] rate constants measured by Jiannan Guo

Table 5.2: *Temperature dependence of the pre-steady-state rate constants for hydride (k_H) and deuteride (k_D) transfer during catalysis by EcDHFR-M16L/S148P and A19K/S148P at pH 7.*

	EcDHFR- M16L/S148P[a]		EcDHFR-A19K/S148P	
T (^{o}C)	k_H (s^{-1})	k_D (s^{-1})	k_H (s^{-1})	k_D (s^{-1})
5	89.2 ± 4.2	28.2 ± 0.7	85.2 ± 0.8	16.9 ± 1.9
10	104.6 ± 2.1	33.0 ± 0.8	74.7± 23.4	20.4 ± 4.2
15	123.3± 3.3	40.8 ± 0.4	88.4± 24.2	30.3 ± 0.2
20	146.9± 3.3	54.2 ± 0.8	118.6 ± 50.2	37.7 ± 0.2
25	175.0 ± 5.8	66.6 ± 0.3	141.6 ± 58.7	49.9 ± 5.8
30	196.3 ± 7.0	76.0 ± 1.8	225.3 ± 5.0	94.5 ± 11.5

35	230.9 ± 4.9	90.3 ± 0.5	nd	nd

[a] data measured by Jiannan Guo, nd: not determined

Table 5.3: *Temperature dependence of the pre-steady-state kinetic isotope effect during catalysis by EcDHFR-M16L, A19K, M16L/S148P and A19K/ S148P at pH 7.*

T (^{o}C)	EcDHFR-M16L[a]	EcDHFR-A19K	EcDHFR-M16L/S148P[a]	EcDHFR-A19K/S148P
5	3.46 ± 0.04	4.13 ± 0.06	3.16 ± 0.17	3.45 ± 0.06
10	3.32 ± 0.15	3.33 ± 0.11	3.17 ± 0.10	3.65 ± 0.21
15	3.33 ± 0.06	2.21 ± 0.03	3.02 ± 0.08	2.92 ± 0.16
20	3.10 ± 0.07	2.53 ± 0.05	2.71 ± 0.07	3.15 ± 0.24
25	2.83 ± 0.18	2.32 ± 0.13	2.63 ± 0.09	2.84 ± 0.25
30	2.62 ± 0.14	2.44 ± 0.06	2.58 ± 0.11	2.38 ± 0.06
35	2.44 ± 0.13	nd	2.56 ± 0.06	nd

nd: not determined, [a] rate constants measured by Jiannan Guo, nd: not determined

Table 5.4: *Temperature dependence of the pre-steady-state rate constants for hydride (k_H) and deuteride (k_D) transfer during catalysis by EcDHFR-A19K/M16L and A19K/M16L/S148P at pH 7.*

	EcDHFR- M16L/A19K		EcDHFR- M16L/A19K/S148P	
T (^{o}C)	k_H (s^{-1})	k_D (s^{-1})	k_H (s^{-1})	k_D (s^{-1})
5	89.35 ± 3.75	22.80 ± 1.70	76.00 ± 2.26	18.30 ± 0.42
10	114.85 ± 1.63	40.50 ± 3.54	104.60 ± 19.23	26.35 ± 0.49
15	142.50 ± 0.71	51.00 ± 5.66	136.25 ± 21.14	35.25 ± 0.35
20	214.00 ± 4.24	73.50 ± 4.95	145.50 ± 0.71	48.50 ± 3.54
25	252.00 ± 28.28	87.00 ± 1.41	181.00 ± 8.49	56.50 ± 0.71

30	288.50 ± 31.82	119.50 ± 2.12	213.00 ± 11.31	73.00 ± 1.41

Table 5.5: *Temperature dependence of the pre-steady-state kinetic isotope effect during catalysis by EcDHFR-M16L/A19K and M16L/A19K/ S148P at pH 7.*

T (^{o}C)	EcDHFR-M16L/A19K	EcDHFR-M16L/A19K/S148P
5	3.92 ± 0.04	4.15 ± 0.02
10	2.84 ± 0.04	3.97 ± 0.11
15	2.79 ± 0.06	3.87 ± 0.09
20	2.91 ± 0.04	3.00 ± 0.04
25	2.90 ± 0.07	3.20 ± 0.03
30	2.41 ± 0.06	2.92 ± 0.03

Table 5.6: *Steady-state turnover number (k_{cat}) measured at pH 7 and 20 ^{o}C during catalysis by different EcDHFR variants.*

Enzyme	k_{cat} (s^{-1})
WT-EcDHFR	6.9 ± 0.10
EcDHFR-M16L	0.47 ± 0.01
EcDHFR-A19K	2.15 ± 0.25
EcDHFR-M16L/S148P[a]	0.42 ± 0.01
EcDHFR-A19K/S148P	2.2 ± 0.40
EcDHFR-M16L/A19K	1.67 ± 0.12
EcDHFR-A19K/M16L/S148P	0.66 ± 0.12

[a] measured by Jiannan Guo

5.3.2 MpDHFR variants at position 16 and 19 (EcDHFR numbering)

The temperature dependence of hydride/deuteride transfer and the kinetic isotope effect (KIE) were measured, under single turnover conditions, for the variants MpDHFR-M16L, MpDHFR-A19K (Tables 5.7 and 5.9), MpDHFR-M16L/P150S, MpDHFR-A19K/P150S (Tables 5.8 and 5.9), MpDHFR-M16L/A19K and MpDHFR-M16L/A19K/P150S (Tables 5.10 and 5.11). The data obtained were compared to the temperature dependence of the rate constants and kinetic isotope effect for wild type MpDHFR (Figures 5.7 to 5.10).

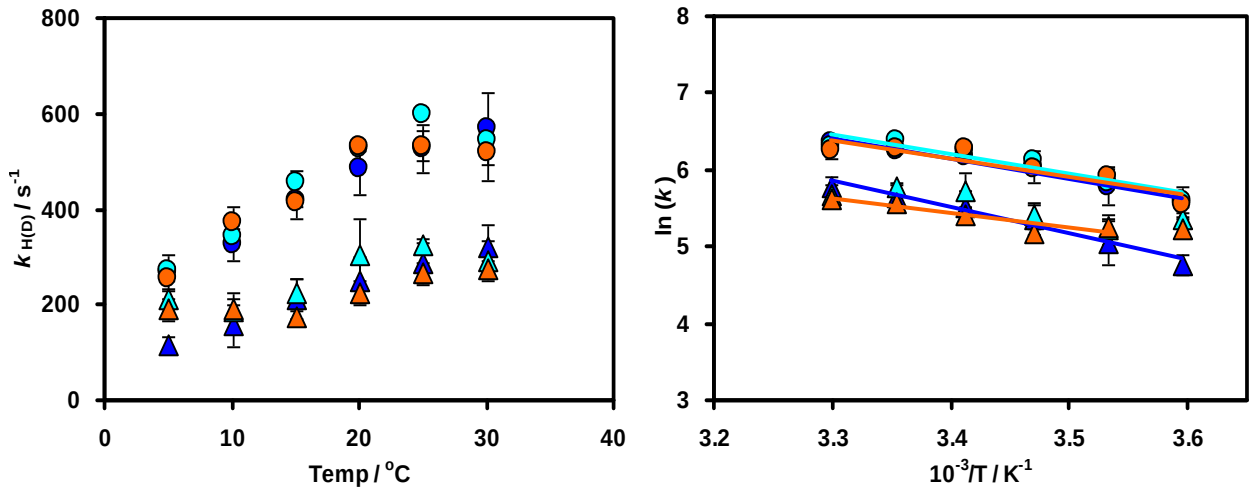

Figure 5.7: *Temperature dependence (left) and Arrhenius plots (right) of the pre-steady-state rate constants for hydride (k_H, circles) and deuteride (k_D, triangles) transfer during catalysis by wild type MpDHFR (blue), MpDHFR-L16M (cyan) and MpDHFR-K19A (orange) at pH 7.*

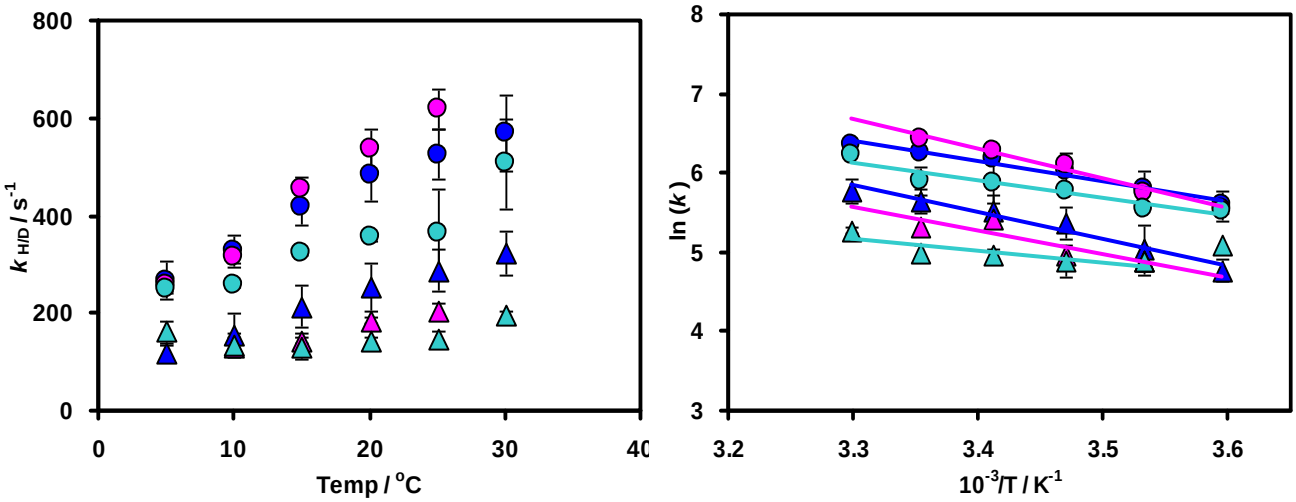

Figure 5.8: *Temperature dependence (left) and Arrhenius plots (right) of the pre-steady-state rate constants for hydride (k_H, circles) and deuteride (k_D, triangles) transfer during catalysis by wild type MpDHFR (blue), MpDHFR-L16M/P150S (light blue) and MpDHFR-K19A/P150S (pink) at pH 7.*

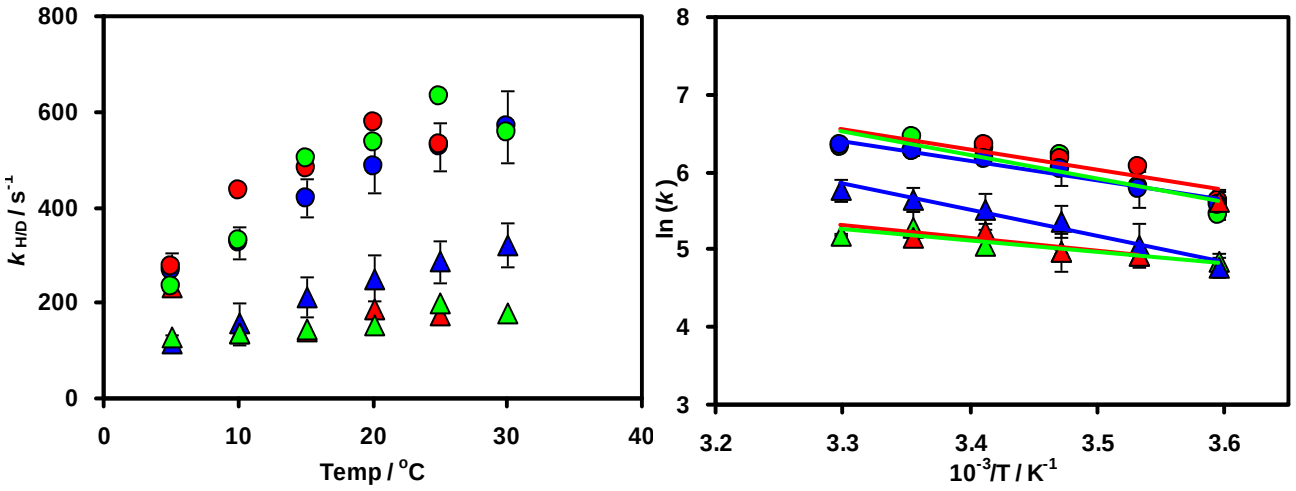

Figure 5.9: *Temperature dependence (left) and Arrhenius plots (right) of the pre-steady-state rate constants for hydride (k_H, circles) and deuteride (k_D, triangles) transfer during catalysis by wild type MpDHFR (blue), MpDHFR-L16M/K19A (red) and MpDHFR-L16M/K19A/P150S (green) at pH 7.*

The rate constants and the KIE for all the single MpDHFR variants were similar to wild type MpDHFR at most temperatures (Figure 5.7). However, the rate of deuteride transfer for the single mutants were similar to the rate of hydride transfer at 5 ˚C, unlike their wild type counterpart (Figure 5.7), resulting in a KIE of 1.27 ± 0.12 and 1.34 ± 0.15 for MpDHFR-L16M and MpDHFR-K19A respectively, indicating that hydride transfer becomes less rate limiting at such conditions for these two variants (Figure 5.10, right). A similar effect was obtained for the double variant MpDHFR-L16M/K19A but with higher KIEs compared to the wild type counterpart and the single variants at temperatures ≥ 10 ˚C (Figure 5.10, left).

For the double variant MpDHFR-L16M/K19A and the triple variant MpDHFR-L16M/K19A/P150S, not much difference was observed for the rate constants of hydride transfer; however the rate constants for deuteride transfer were less temperature dependent than those obtained for the wild type MpDHFR (Figure 5.9). For the triple variant in addition to the two variants MpDHFR-L16M/P150S and MpDHFR-K19A/P150S, the temperature dependences of the KIEs showed two phases with a breakpoint at 10 or 15 ˚C (Figure 5.10, right). Similar behavior was reported previously for EcDHFR at pH 9.5. Interestingly, the values of the KIEs obtained for the triple variant and all the double variants above the breakpoint were higher than those observed for their wild type counterpart at the same temperatures, and comparable to that observed for EcDHFR (Figure 5.9).

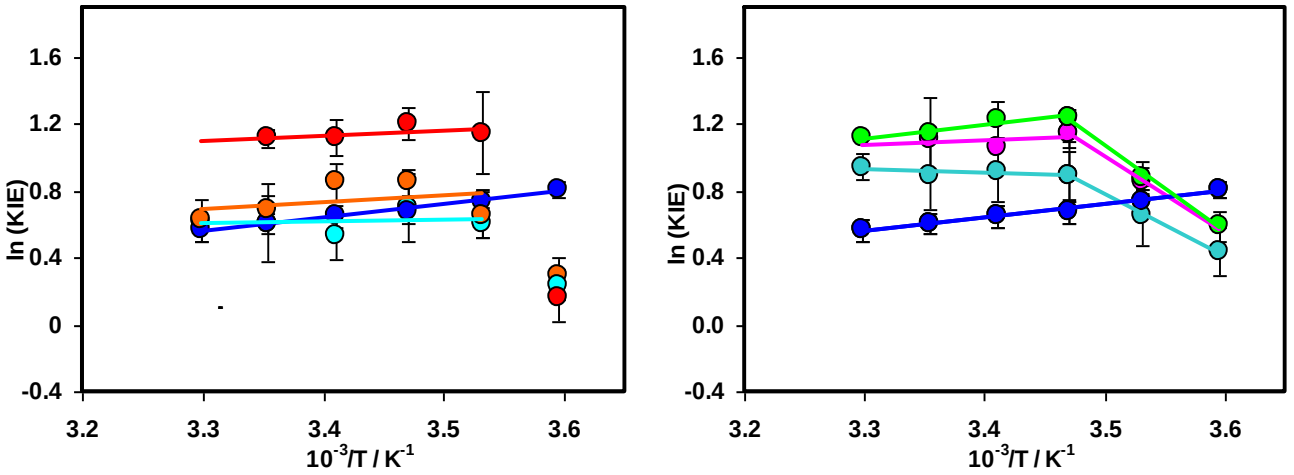

Figure 5.10: *Temperature dependence of the kinetic isotope effect (KIE) plotted on a logarithmic scale against the inverse temperature for wild type MpDHFR (blue), MpDHFR-L16M (cyan), MpDHFR-K19A (orange) and MpDHFR-L16M/K19A (red) (left), and wild type MpDHFR (blue), MpDHFR-L16M/P150S (light blue), MpDHFR-K19A/P150S (pink) and MpDHFR-L16M/K19A/P150S (green) (right), measured under single turnover conditions at pH 7.*

The steady state rate constants (k_{cat}) were measured as well for all the MpDHFR variants in phosphate buffer at pH 7 and 20 ^{o}C (Table 5.12). In contrast to the corresponding EcDHFR variants, the values of k_{cat} observed for the MpDHFR variants were in the same order of magnitude compared to the wild type MpDHFR. Furthermore, the values of k_{cat} were elevated in the single variants with k_{cat} values of 21.56 ± 1.56 for MpDHFR-L16M and 18.08 ± 0.73 for MpDHFR-K19A compared to 14.78 ± 0.79 for wild type MpDHFR under the same conditions.[79] However, k_{cat} values for all of the double and the triple variants were decreased slightly compared to wild type MpDHFR (Table 5.12).

Table 5.7: *Temperature dependence of the pre-steady-state rate constants for hydride (k_H) and deuteride (k_D) transfer during catalysis by MpDHFR-L16M and K19A at pH 7.*

	MpDHFR-L16M		MpDHFR-K19A	
T (^{o}C)	k_H (s^{-1})	k_D (s^{-1})	k_H (s^{-1})	k_D (s^{-1})
5	271.77 ± 4.81	214.00 ± 19.61	255.20 ± 5.21	191.00 ± 21.71
10	344.80 ± 4.24	187.25 ± 37.66	372.10 ± 33.69	192.50 ± 19.77
15	457 ± 23.76	226.10 ± 30.69	416.25 ± 8.77	177.00 ± 12.83
20	525.73 ± 3.54	307.83 ± 72.83	533.50 ± 7.78	227.00 ± 25.15
25	600.32 ±0.14	325.60 ± 13.44	533.00 ± 30.54	268.00 ± 19.24
30	543.23 ± 13.86	292.55 ± 41.01	520.50 ± 58.45	277.25 ± 15.90

Table 5.8: *Temperature dependence of the pre-steady-state rate constants for hydride (k_H) and deuteride (k_D) transfer during catalysis by MpDHFR-L16M/P150S and MpDHFR-K19A/P150S at pH 7.*

	MpDHFR-L16M/P150S		MpDHFR-K19A/P150S	
T (^{o}C)	k_H (s^{-1})	k_D (s^{-1})	k_H (s^{-1})	k_D (s^{-1})
5	250.65 ± 8.27	162.10 ± 23.05	259.15 ± 14.35	nd
10	257.75 ± 3.89	133.95 ± 24.11	314.00 ± 8.49	132.50 ± 17.68
15	324.85 ± 3.04	132.60 ± 26.94	453.50 ± 26.16	145.00 ± 7.07
20	357.50 ± 7.07	142.90 ± 10.54	536.50 ± 42.43	185.00 ± 6.36
25	428.70 ± 19.80	148.88 ± 13.88	619.00 ± 40.00	205.00 ± 15.56
30	507.33 ± 91.05	196.87 ± 7.94	nd	nd

nd: not determined

Table 5.9*: Temperature dependence of the pre-steady-state kinetic isotope effects during catalysis by MpDHFR-L16M, K19A, L16M/P150S and MpDHFR-K19A/P150S at pH 7.*

T (^{o}C)	MpDHFR-L16M	MpDHFR-K19A	MpDHFR-L16M/P150S	MpDHFR-K19A/P150S
5	1.27 ± 0.12	1.34 ± 0.15	1.55 ± 0.23	nd
10	1.84 ± 0.37	1.93 ± 0.26	1.92 ± 0.35	2.37 ± 0.32
15	2.02 ± 0.29	2.35 ± 0.18	2.45 ± 0.50	3.13 ± 0.24
20	1.71 ± 0.40	2.35 ± 0.26	2.50 ± 0.19	2.90 ± 0.20
25	1.84 ± 0.08	1.99 ± 0.18	2.88 ± 0.30	3.02 ± 0.30
30	1.86 ± 0.26	1.88 ± 0.24	2.58 ± 0.47	nd

nd: not determined

Table 5.10: *Temperature dependence of the pre-steady-state rate constants for hydride (k_H) and*

deuteride (k_D) transfer during catalysis by MpDHFR-L16M/K19A and L16M/K19A/P150S at pH 7.				
	MpDHFR-L16M/K19A		MpDHFR-L16M/K19A/P150S	
T (^{o}C)	k_H (s^{-1})	k_D (s^{-1})	k_H (s^{-1})	k_D (s^{-1})
5	278.00 ± 37.07	235.50 ± 11.21	233.50 ± 3.82	129.00 ± 11.31
10	433.52 ± 28.61	137.25 ± 32.17	330.50 ± 3.54	137.50 ± 13.44
15	479.83 ± 43.60	144.28 ± 144.28	504.50 ± 19.09	145.00 ± 4.24
20	576.05 ± 42.46	188.00 ± 15.56	537.50 ± 48.79	156.50 ± 9.19
25	531.33 ± 25.42	174.15 ± 5.87	632.00 ± 48.08	201.50 ± 40.31
30	nd	nd	556.50 ± 4.95	181.85 ± 1.63
nd: not determined				

Table 5.11: *Temperature dependence of the pre-steady-state kinetic isotope effect during catalysis by MpDHFR-L16M/K19A and L16M/K19A/P150S at pH 7.*

T (^{o}C)	MpDHFR-L16M/K19A	MpDHFR-L16M/K19A/P150S
5	1.18 ± 0.17	1.81 ± 0.16
10	3.16 ± 0.77	2.40 ± 0.24
15	3.33 ± 0.32	3.48 ± 0.17
20	3.06 ±0.34	3.43 ± 0.37
25	3.05 ± 0.18	3.14 ± 0.67
30	nd	3.06 ± 0.04
nd: not determined		

Table 5.12: *Steady-state turnover number (k_{cat}) measured at pH 7 and 20 ^{o}C during catalysis by different MpDHFR*

variants.	
Enzyme	k_{cat} (s^{-1})
WT-MpDHFR	14.78 ± 0.79
MpDHFR-M16L	21.56 ± 1.56
MpDHFR-A19K	18.08 ± 0.73
MpDHFR-M16L/P150S[a]	10.04 ± 0.77
MpDHFR-A19K/P150S	9.75 ± 1.02
MpDHFR-M16L/A19K	9.75 ± 1.02
MpDHFR-A19K/M16L/P150S	12.74 ± 2.04

5.4 Mutation in the FG loop – variants at positions 124 and 123 (MpDHFR numbering)

X-ray crystallographic data reported by Sawaya and Kraut proposed that the M20 loop of DHFR modulates ligand specificity by adopting either of two conformations (closed and occluded),[59] as described previously. Hydrogen bonds between the M20 loop and neighboring loops are the key stabilizing contacts for these conformations. The closed M20 conformation occurring in substrate complexes (E.NADPH and E.NADPH.DHF) relies on interactions with the FG loop, whereas the occluded conformation occurring in product complexes involves interactions with the GH loop (see chapter 3 for further details). Hydrogen bonds act as support for stabilisation of the M20 loop, maintaining its various conformations throughout the catalytic cycle[59] (see Chapter 1) and different variants indicated the importance of hydrogen bonding between the FG and M20 loops to catalysis.[71] MpDHFR and EcDHFR have a conserved aspartate residue at position 124 (D122 in EcDHFR numbering) and glycine residue at position 123 (G121 in EcDHFR numbering) (Figure 5.11). Aspartic acid 122 of EcDHFR has been extensively studied by Benkovic and coworkers,[126] with substitution to asparagine, serine or alanine. Such variants of EcDHFR disrupt the hydrogen bonding potential between the highly mobile M20 loop and the FG loop. In this part of the thesis, we targeted the hydrogen bond between the side chain of Asp124 in the FG loop in MpDHFR and the amide backbone of Glu18 in the Met20 loop for mutagenesis to weaken the strength of this bond.

Glycine 121 (EcDHFR numbers) has also seen much investigation by many research groups both in terms of effect on enzyme stability through equilibrium unfolding and CD spectroscopy experiments and catalytic efficiency through kinetic experiments.[71,122,144-146] For further investigation of the effect of mutation in the FG loop on catalysis by MpDHFR, hydride transfer by the variant MpDHFR-G123V, where the mutation in the FG loop is 19 Å away from the active site, was studied as well.

Replacing G123 with a bulky hydrophobic valine residue most probably will affect the loop flexibility. Our study will spot the influence of this mutation on hydride transfer by MpDHFR and make it comparable with previous data reported for the same variant in EcDHFR.

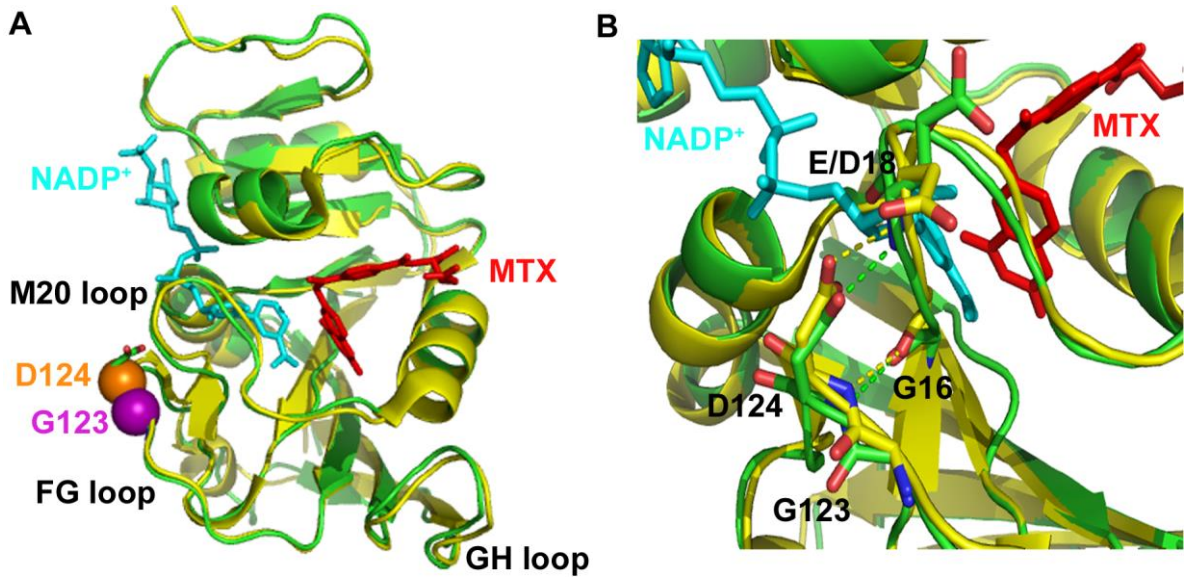

Figure 5.11: *Cartoon representation showing the positioning of residue G123 (violet sphere) and D124 (orange sphere) in EcDHFR (PDP 1DRE, green) and MpDHFR (PDP 3IA4, yellow) (A) and hydrogen bonding between D124 (EcDHFR numbers) in the FG loop and residues E/D18 and G16 in the M20 loop (MpDHFR numbering), (B). $NADP^+$, MTX and residues G16, E/D18, G123 and D124 are shown in stick representation.*

5.4.1 Temperature dependence of k_H and KIE for the FG loop variants

The temperature dependence of the hydride/deuteride transfer rate constant by the two variants, MpDHFR-G123V and -D124N were measured with both NADPH and NADPD (Table 5.13), and the temperature dependence of the kinetic isotope effect for each variant was obtained by dividing the rate of hydride transfer by the rate of deuteride transfer (Table 5.14).

For the MpDHFR-D124N variant, the mutation did not affect either the rate of hydride/deuteride transfer or the kinetic isotope effect (Figures 5.12 and 5.13). The enzyme showed very similar behavior to the wild type MpDHFR under pre-steady state conditions. The only difference obtained was in the steady state rate that showed a ~35 fold decrease in the MpDHFR-D124N variant (k_{cat} = 0.41 ± 0.08) compared to wild type MpDHFR.

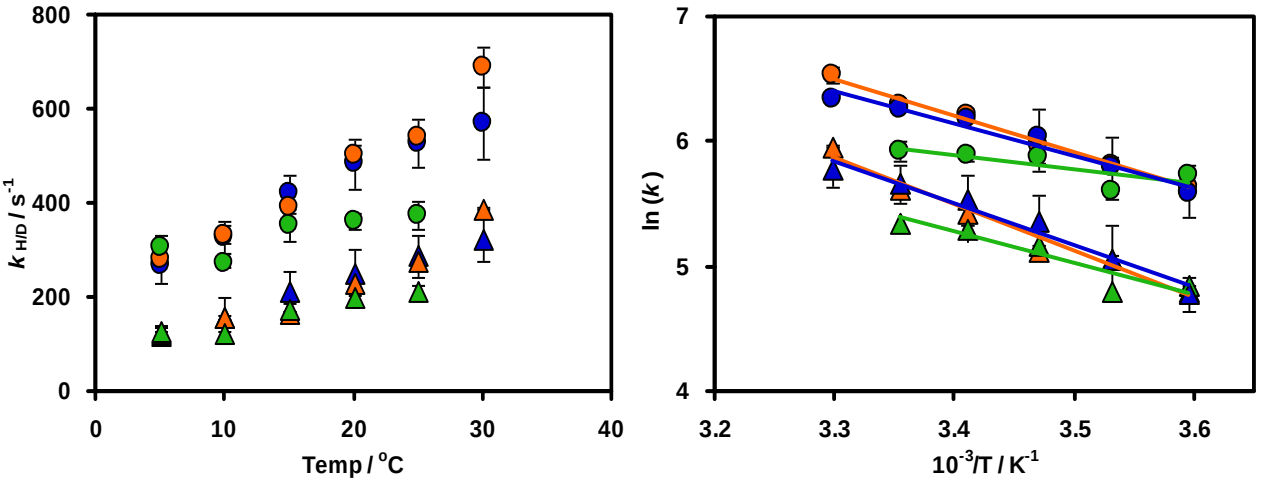

Figure 5.12: *The temperature dependence of the pre-steady-state rate constant (left) and corresponding Arrhenius plot (right) with NADPH (circles) and NADPD (triangles) for wild type MpDHFR (blue), MpDHFR-D124N (orange), and MpDHFR-G123V (green) catalysis, measured under single turnover conditions at pH 7.*

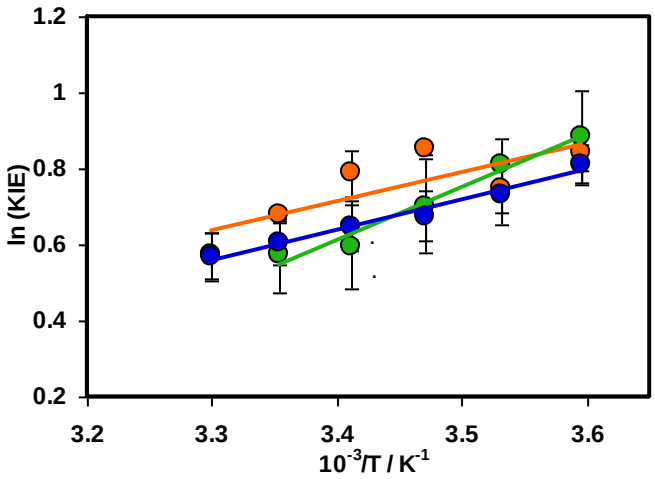

Figure 5.13: *Temperature dependence of the kinetic isotope effect (KIE) plotted on a logarithmic scale against the inverse temperature for wild type MpDHFR (blue), MpDHFR-D124N (orange), and MpDHFR-G123V (green) catalysis, measured under single turnover conditions at pH 7.*

However, the temperature dependence of the KIE for the MpDHFR-G123V variant was similar to its wild type counterpart within experimental errors (Figure 5.13). This enzyme has shown a remarkable decrease in hydride transfer rates at temperatures ≥ 20 ˚C. The decrease in hydride transfer rate constants at higher temperatures might suggest a decrease in the thermostability of this variant. This variant has shown very similar K_M values for both NADPH and DHF to the wild type MpDHFR[90] and a k_{cat} value of 0.47 ± 0.04 s^{-1} similar to the MpDHFR-D124N, suggesting that these two mutations are having similar effect on the steady state kinetics.

The results for both variants are very different compared to the data reported previously for the same variants with EcDHFR. Replacing D124 in EcDHFR (D122 in EcDHFR numbering) with asparagine causes a 25 fold decrease in the rate of hydride transfer and the enzyme shows a kinetic isotope effect of 1.6 ± 0.2 under steady state conditions, suggesting contribution from the chemical step. In addition, the affinity for the reduced cofactor decreases 3-4 fold, whereas binding of the oxidized cofactor was not affected. In case of the MpDHFR-D124N, the only difference was obtained is the decrease in the value of k_{cat} compared to the wild type enzyme. A similar effect was reported previously for the EcDHFR variant suggesting change in the catalytic cycle for these two variants.

Table 5.13: *Temperature dependence of the pre-steady-state rate constants for hydride (k_H) and deuteride (k_D) transfer during catalysis by MpDHFR-D124N and -G123V at pH 7.*

	MpDHFR-D124N		MpDHFR-G123V	
T (^{o}C)	k_H (s^{-1})	k_D (s^{-1})	k_H (s^{-1})	k_D (s^{-1})
5	282.50 ± 0.71	122.00 ± 5.66	307.50 ± 24.75	127.00 ± 11.46
10	334.00 ± 19.80	158.00 ± 4.24	273.50 ± 7.78	121.50 ± 7.78
15	393.50 ± 4.95	168.00 ± 1.41	355.00 ± 35.36	176.00 ± 12.73
20	503.00 ± 18.38	229.00 ± 11.31	360.50 ± 16.26	199.00 ± 20.01
25	540.00 ± 9.90	274.50 ± 2.12	373.95 ± 28.35	211.00 ± 12.73
30	689.50 ± 41.72	389.00 ± 1.41	nd	nd

Table 5.14: *Temperature dependence of the pre-steady-state kinetic isotope effects during catalysis by MpDHFR-D124N and -G123V at pH 7.*

T (^{o}C)	MpDHFR-D124N	MpDHFR-G123V
5	2.32 ± 0.11	2.42 ± 0.29
10	2.11 ± 0.14	2.25 ± 0.16
15	2.34 ± 0.04	2.02 ± 0.25
20	2.20 ± 0.13	1.81 ± 0.20
25	1.97 ± 0.04	1.77 ± 0.17
30	1.77 ± 0.11	nd

Table 5.15: *K_M for NADPH and DHF for different EcDHFR and MpDHFR variants at pH 7 and 20 ℃.*

Enzyme	K_M^{DHF} (μM)	K_M^{NADPH} (μM)
EcDHFR[a]	0.7 ± 0.2	4.8 ± 1.0
EcDHFR-S148P	0.7 ± 0.1	4.7 ± 0.7
EcDHFR-A19K	0.9 ± 0.2	nd
EcDHFR-A19K/S148P	0.7 ± 0.1	nd
EcDHFR-M16L[b]	0.7 ± 0.1	6.2 ± 0.3
MpDHFR[c]	2.4 ± 0.2	5.7 ± 0.2
MpDHFR-P150S	2.2 ± 0.2	10.7 ± 0.6
MpDHFR-K19A	nd	8.2 ± 0.1
MpDHFR-L16M/K19A	nd	10.5 ± 0.1
MpDHFR-L16M/K19A/P150S	nd	20.9 ± 0.1
MpDHFR-G123V[d]	1.1 ± 0.1	8.7 ± 0.1

nd: not determined, [a]: taken from reference [79], [b]: measured by Jiannan Guo, [c]: taken from reference [7] at pH 7.5, [d]: measured by Dr Rhiannon Evans.

5.5 Discussion

Enzymes are known to switch between conformations; even so, understanding the contribution of enzyme motions to catalysis is difficult. The static window into the DHFR catalytic cycle provided by X-ray crystallographic data indicates two conformations for the M20 loop (closed and occluded) exist in liganded complexes.[7,59] The contributions of these studies emphasize the importance of the motion of the mobile loops (M20 loop, FG loop and GH loop) during catalysis by EcDHFR. The work presented in this thesis has focused on catalysis by DHFR from the cold adapted enzyme *Moritela profunda* (MpDHFR) and spotting the differences between this enzyme and the mesosphilic homologue from *Escherichia coli* which has been studied extensively. In this chapter we demonstrated the effect of mutation in the M20 loop and FG loop on catalysis by both enzymes. Compared to the widely studied EcDHFR, the psychrophilic MpDHFR shows extensive conservation of catalytically important residues.[62] Our study targeted residues in the highly mobile M20 loop, in

particular positions L16 and K19 (EcDHFR numbers) in MpDHFR and compared to the opposite residues in the mesophilic homologue, EcDHFR (M16 and A19).

All the EcDHFR variants studied here have shown rate constants and temperature dependence of the KIE comparable to their wild type counterpart in the pre-steady state, indicating that the mutations did not affect the chemical step. However, a decrease was observed in the turnover numbers for all the EcDHFR variants. Taking the position of M16 and A19 in consideration is highly suggestive that the mutation in these two positions has affected the motion of the M20 loop (Figure 5.2). The effect of the mutations is comparable to that seen in chapter four when the interactions between the M20 and GH loops were perturbed in the EcDHFR-S148P variant. On the other hand, the opposite mutations in the MpDHFR variants did not cause a big difference in the steady state rate constant. These observations support the suggestion that MpDHFR does not depend on large scale motions of the loop regions during catalysis.[96]

Although the temperature dependence of the rate constants and the KIEs for the single variants MpDHFR-L16M and K19A were very similar to the wild type MpDHFR, except at 5 ˚C, the double and the triple variants (MpDHFR-L16M/K19A and -L16M/K19A/P150S) showed a breakpoint at 15 ˚C with similar temperature dependence of the KIE at temperatures higher than 15 ˚C. However, the KIE values were higher compared to those obtained for wild type MpDHFR at the same temperatures. The higher KIE values for the double and the triple MpDHFR variants were most probably due to the change in the electrostatic forces at the active site compared to the wild type. Psychrophilic enzymes have been suggested to improve the electrostatic fields at the active site of as a part of adaptation to catalysis at low temperatures.[147] Electrostatic interactions were found to be stabilised at lower temperatures and modification of the electrostatic potential of key residues central to ligand binding and catalysis was suggested be a strategy for cold adaptation.[148] While the basic side chain of Lys19 was initially thought to interact with the oppositely charged folate during the reaction causing the high k_{cat} values for MpDHFR,[60] the crystal structure of MpDHFR subsequently showed that the side chain of K19 is projecting out in solution (Figure 5.2A),[62] thus interaction between the side chain of K19 and folate is most probably unlikely to occur. Thus, replacing M16 and A19 in EcDHFR with leucine and lysine, respectively, in MpDHFR might instead be a kind of structure adaptation for the psychrophilic DHFR.

In this chapter we also studied the effect of weakening the bond strength between the M20 loop and the FG loop by replacing Asp124 in MpDHFR with an asparagine residue. The side chain of this

residue was thought to form a hydrogen bond with the amide backbone of Glu17 in the M20 loop, as proposed from the X-ray data reported by Sawaya and Kraut in 1997.[59] This loop interaction between the FG loop and the M20 loop was thought to be essential for stabilizing the closed conformation in EcDHFR.[59,126,134] Disturbing the hydrogen bonding between the M20 loop and the FG loop in EcDHFR has significantly affected the chemical step, causing around 25 to 55 fold reduction in the rate constants of hydride transfer and causing the chemical step to contribute to the steady state turnover as shown from the increase in the kinetic isotope effect under saturating conditions.[126]

The G121V variant has been extensively studied in EcDHFR as well in different research groups using molecular dynamics, CD, NMR and fluorescence in addition to kinetic studies.[71,122,134] Substitution of Gly121 by valine (or other bulky side chains) has a dramatic effect on the kinetics of EcDHFR, decreasing the hydride transfer rate constant by up to 1000 fold and resulting in an additional kinetic step in the reaction mechanism.[71] However, various molecular dynamics, CD, and fluorescence studies of apo-EcDHFR have suggested that the G121V mutation causes structural perturbation by destabilising the contacts between the Met20 and the FG loops.[122] It has been suggested that the G121V mutation as well as the D122 variants in EcDHFR, at a position distant from the active site, interferes with coupled loop movements and appears to impair catalysis by destabilizing the closed Michaelis complex.[126,134]

Interestingly, in contrast to EcDHFR, neither substitution of D122 (124 in MpDHFR) with asparagine nor the substitution of G121 (123 in MpDHFR) with valine in MpDHFR seems to significantly affect the chemical step of this enzyme as shown from the data presented in this part of the thesis. However, these two substitutions affected the steady state rate dramatically in MpDHFR, causing around a 35 fold decrease in k_{cat} value at pH 7 and 20 ˚C.

In EcDHFR, substitutions of Asp122 were found to perturb all ligand complexes, changing the catalytic pathway preferred by wild-type DHFR under saturating conditions of substrate and cofactor.[126] Most probably this is the case for the FG loop variants in MpDHFR, changing the steady state rate limiting step and causing a big decrease in $k_{cat.}$ Weaker hydrogen bonding between the M20 and FG loops was thought to facilitate the binding and release of THF.[126] The steady state rate constants for the MpDHFR FG loop variants are similar to the dissociation rate constant of THF from the E.THF binary complex. This might suggest that disturbing the interactions between the M20 loop and the FG loop in MpDHFR diverts the catalytic cycle to the release of THF from the E.THF binary complex instead of the product ternary complex E.NADPH.THF. This might be the

case as well for the EcDHFR-M16L variant, which has a similar steady state rate constant. In all of the three variants, most probably due to the weak interactions between the M20 and the FG loops, the steady state rate constant was decreased dramatically without any significant change in the chemical step. However these observations cannot be confirmed in the absence of kinetic binding measurements of the dissociation rate constants for these variants.

Previous quantum mechanical and molecular mechanical simulation studies suggested that the G121V mutation in EcDHFR leads to an altered transition state structure, with a concomitant increase in the activation free energy barrier,[144,149] and also perturbs the critical hydrogen-bonding interactions between the M20 and FG loops.[150] Venkitakrishnan *et al*. have shown that the G121V variant adopts the occluded conformation in the E:folate:NADPH and E:folate:$NADP^+$ complexes in contrast to what was observed for the wild-type DHFR, which occupies the closed conformation in the same complexes. [134] This striking difference between the G121V variant and wild type EcDHFR was thought to be the reason for the decrease in the hydride transfer rate constant for the G121V variant by destabilizing of the closed state shifting the equilibrium towards the occluded conformation. As shown previously (Chapter 4), MpDHFR lacks the key residue that stabilizes the occluded conformation. Therefore, destabilization of the closed conformation in MpDHFR most probably will lead to formation of a destabilized closed conformation rather than favouring the occluded conformation, which in the absence of its stabilizing bonds will presumably never form.

Interestingly, a recent NMR study has shown that the EcDHFR-G121V.NADPH.MTX complex, which most resembles the transition state, forms a closed complex. That study showed that in the G121V transition state analog complex, the FG and M20 loops suffer excursions away from this accurate alignment causing changes in active site geometry[151]. These results suggest that EcDHFR-G121V can form the closed conformation but conformational fluctuation is different to the wild type enzyme. This was suggested as well when replacing M42 (≈20 Å away from the active site) with tryptophan in EcDHFR.[152] Such variant was found to affect the hydrogen transfer rate constant dramatically.[150,153] Thus, it might be interesting to study the effect of similar mutation (M42W) on the hydride transfer rate of MpDHFR as previous studies in our group have shown that this kind of mutation in MpDHFR decreases the steady state rate constant significantly.[90]

We have suggested previously that the electrostatic preorganization within the active site during DHFR reaction is determined by the conformational state of the enzyme at the point of reaction.[47] MpDHFR cannot form the occluded conformation and mutations in the FG loop in positions 121 and

122 did not affect the chemical step, but only the physical steps as shown from the change in the steady state rate constant. In light of these findings the decrease in the rate of the chemical step for the FG variants in EcDHFR most probably is not due to impairing loop dynamics. Thus, the dynamic properties of DHFR and its mutants clearly affect the conformational motions that are important for the turnover of substrate to product, but no correlation between these conformational motions and the chemical motions that chemical step. The G121V mutation in EcDHFR most likely affected the active site preorganization which in turn manifests in alterations to the chemical step. This effect was not seen in the same variant in MpDHFR suggesting that MpDHFR does not use loop dynamics to modulate the active site conformation. This is unlikely to be a kind of adaptation of the psychrophilic enzyme as we have shown previously in Chapter 4 that many other DHFRs from various organisms, including DHFR from the mesophilic bacterium *Lactobacillus casei* (LcDHFR) and DHFR from the thermophilic species *Geobacillus stearothermophilus* (BsDHFR), lack the key residues that stabilize the occluded conformation.

5.6 Conclusions

Recently, studying the EcDHFR-N23PP/S148A variant has shown that conformational fluctuations are not directly involved in the chemical step of the reaction for EcDHFR.[47] In Chapter 4 we demonstrated that the occluded conformation does not affect the chemical step of the DHFR reaction and only modifies the affinity of the enzyme to ligands. In addition, many DHFRs are actually lacking the key residues which stabilize the occluded conformation, including MpDHFR, suggesting that the occluded conformation might be a specific case for EcDHFR rather than a general phenomenon for all DHFRs. In this part of the thesis we provide evidence that the dynamic nature of the mesophilic enzyme from *Escherichia coli* is not observed for the psychrophilic homologue from *Moritella profunda*.

The first line of evidence was derived from mutation in the M20 loop, which most probably disturbed the dynamic of that highly mobile loop in EcDHFR, causing a sharp decrease in the turnover numbers for all the EcDHFR variants studied here. This reflects the physical steps of the catalytic cycle, without perturbing the nature of the chemistry of the hydride transfer reaction. On the contrary, none of the MpDHFR variants has shown a large difference in the turnover number, suggesting that such M20 loop dynamics observed in EcDHFR do not control the catalytic cycle in MpDHFR.

The second line of evidence was derived from the mutation in the FG loop. In contrast to the reported data from similar mutations for EcDHFR, mutation in positions 121 and 122 in MpDHFR did not affect the chemical step of the reaction as shown from the similar temperature dependences of the KIE compared to the wild type MpDHFR. Instead the two variants have shown a sharp decrease in the steady state rate.

The data presented here in addition to the data presented in chapter four provide evidence that MpDHFR is using a different mechanism in modulating the enzyme's ability to form different ligand complexes compared to the mesophilic enzyme EcDHFR. However, the two enzymes use the same catalytic cycle and the nature of the chemistry in both enzymes is similar.

6

Effect of salt and denaturants on catalysis by dihydrofolate reductase

6.1 Preface

Since buffer conditions (salt and pH) can have dramatic effects on the stability of proteins, the description of a protein's stability is incomplete without a consideration of the role of solvent in protein folding and function. In the presence of cosolvents/cosolutes, a protein can fluctuate among vast numbers of folded and unfolded conformations, and this can occur via many different pathways, and leading to enzymes stabilizition or destabilization.[154] Explaining how different salts stabilize or denature a protein is still a subject of debate.[155] However, some general features are clear. Cosolutes that stabilize proteins cause preferential hydration, where the cosolute is expelled from the protein surface. Such salt cosolutes have the effect of salting-out hydrophobic moieties (*i.e.*, they cause weak interactions between protein and water and promote protein-protein hydrophobic interactions) and their efficiency is consistent with the idea that these salts affect the water structure.[156] Alternatively, cosolutes such as I_2, $(SCN)_2$, or guanidinium HCl, that destabilize proteins, salt-in the peptide group (*i.e.*, promote solvent/solute interactions), and may act by breaking protein hydrogen bonds and interact preferentially with the protein surface which in turn leads to denaturation of the macromolecule.[157-158]

Previous studies showed the effect of salt and different denaturants on the stability, structure and dynamic of proteins.[157,159-162] To understand the contribution of different electrostatic effects and denaturants on the stabilization, related to the associated structural changes and enzyme activity, in this chapter we are going to monitor enzyme activity as a function of salt concentration, or denaturant concentration, and examine their effect on the dihydrofolate reductase (DHFR) chemical step

6.2 Effect of denaturants on catalysis by dihydrofolate reductase

The mechanism of protein denaturation by urea and guanidinium hydrochloride in aqueous solutions is still an unsolved and important problem in protein chemistry, in spite of the presence of many experimental and theoretical studies on denaturation of proteins by these molecules.[163-167] It is still unclear whether these molecules act directly by binding to peptide groups, thereby weakening internal hydrogen bonds, or indirectly by causing a change in the structure of water's hydrogen bond network around hydrophobic groups in proteins, thereby increasing their solubility and weakening the hydrophobic effect. It is also possible that both mechanisms are operating.[163-167]

To investigate the effect of denaturants on catalysis by DHFR, different concentrations of urea and guanidinium hydrochloride were added to potassium phosphate buffers, pH 7 and used for kinetic experiments.

6.2.1 Effect of urea on catalysis by MpDHFR

The effect of urea on catalysis by dihydrofolate reductase, hydride transfer (k_H) rate constants and steady state rate constants (k_{cat}) were measured for MpDHFR in potassium phosphate buffers, pH 7, containing 0-7 M urea (Figure 6.1).

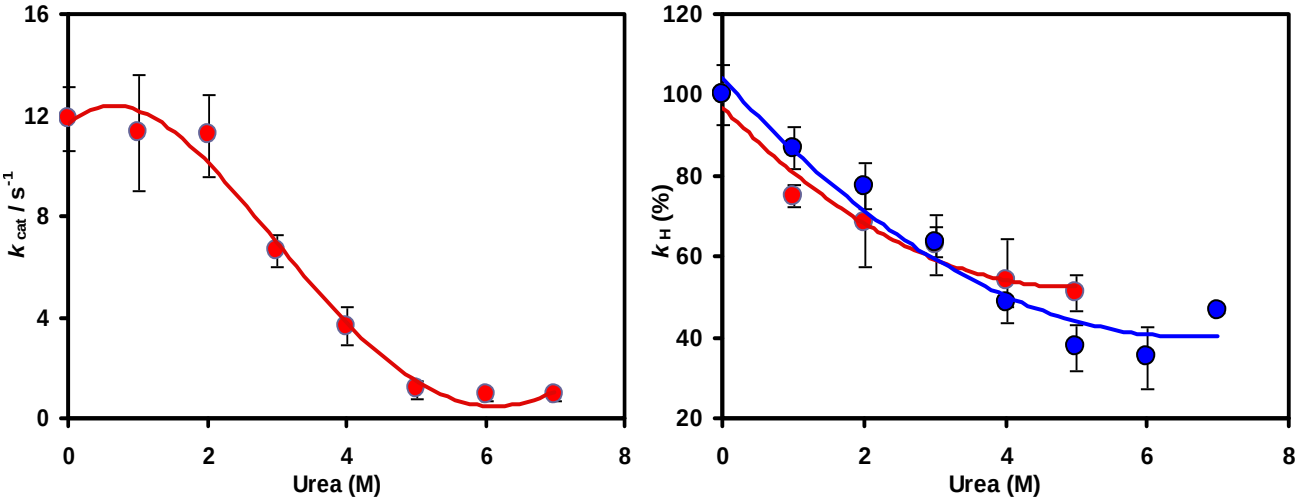

Figure 6.1: *Left, effect of urea denaturation on the steady state rate constant (k_{cat}) for MpDHFR. Right, effect of different concentrations of urea on the rate constant of hydride transfer (k_H) during catalysis by MpDHFR (red) and EcDHFR (blue) at pH 7 and 20 ℃.*

Previous work reported by Xu *et al.*, has shown that the concentration of urea required for half denaturation of the MpDHFR enzyme is 1.6 M.[60] This value shows that the conformational stability for MpDHFR in urea is lower than the mesophilic (EcDHFR) and the thermophilic (TmDHFR) homologues which need 3.1[168] and 5.5[169] M urea, respectively, to reach the mid denaturation point.

Measurements of the turnover number for MpDHFR at various concentrations of urea show that, within experimental errors, the steady state rate constant is not affected when using 2 M urea in the experimental buffer (Figure 6.1, left). However, at about 3.2 M of urea, a 50% decrease in the steady state rate constant was observed and more than 90% of the activity was reduced at 5-7 M urea (Table 6.1). During measuring the steady state kinetics in this thesis, DHFR was incubated in the urea

containing buffer for 1 min. before the measurements were made. This explains why MpDHFR lost 50% of its activity in the steady state at 3.2 M urea, while it was found that 1.6 M urea has a 50% denaturation (i.e., when the enzyme was allowed to fully equilibrate), as reported previously.[60]

The rate constants of hydride transfer were also measured at different concentrations of urea (Table 6.2). The data presented here shows that different concentrations of urea are affecting the pre-steady state rates for both enzymes, MpDHFR and EcDHFR, in a similar manner (Figure 6.1, right). Both of the mesophilic and the psychrophilic enzyme lose half of their activity when using around 4 M of urea in the reaction buffer. This perhaps might give indication that the chemical step is less affected by the structure denaturation than the other physical steps involved in the DHFR catalytic cycle.

In contrast to what was observed for MpDHFR and EcDHFR, urea was found to activate the dimeric and thermophilic DHFR from *Thermotoga maritima*.[94] In addition, enzyme activity for DHFR from Chinese hamster increased to about twice that of the native enzyme at 1.5 M urea, and then fell with increased urea concentration until complete inactivation occurred at 4 M.[170] Apart from TmDHFR, which has similar properties to both eukaryotic and prokaryotic DHFRs,[94,171] this property has only been observed only for vertebrate DHFRs, most probably due to loosening up of the protein structure near the active site.[161,172]

***Table 6.1**: Steady-state rate constants (k_{cat}) during catalysis by MpDHFR in different concentrations of urea at pH 7 and 20* °C.

Urea (M)	k_{cat} /s^{-1}
0	11.89 ± 1.29
1	11.31 ± 2.31
2	11.22 ± 1.60
3	6.66 ± 0.63
4	3.65 ± 0.75
5	1.18 ± 0.35
6	0.94 ± 0.20
7	0.92 ± 0.19

Table 6.2: *Pre-steady state hydride transfer rate constant (k_H) during catalysis by MpDHFR and EcDHFR in different concentrations of urea at pH 7 and 20* °C.

Urea (M)	MpDHFR	EcDHFR
	k_H /s^{-1}	k_H /s^{-1}
0	341.15 ± 25.37	194.99 ± 0.84
1	196.40 ± 16.65	177.13 ± 9.93
2	241.66 ± 30.18	143.57 ± 11.13
3	182.36 ± 50.52	119.53 ± 7.19
4	185.17 ± 35.05	96.61 ± 1.97
5	222.08 ± 42.91	81.38 ± 11.07
6	nd	79.16 ± 14.84
7	nd	90.58 ± 1.54

6.2.2 Effect of guanidinium hydrochloride (Gdn-HCl) on catalysis by MpDHFR

For further investigation of the effect of enzyme denaturants on DHFR catalysis, the effect of guanidinium hydrochloride (Gdn-HCl) on hydride transfer rate constants (k_H) and steady state rate constants (k_{cat}) was measured for EcDHFR, MpDHFR and TmDHFR in potassium phosphate buffers, pH 7, containing 0-1 M Gdn-HCl (Figure 6.2).

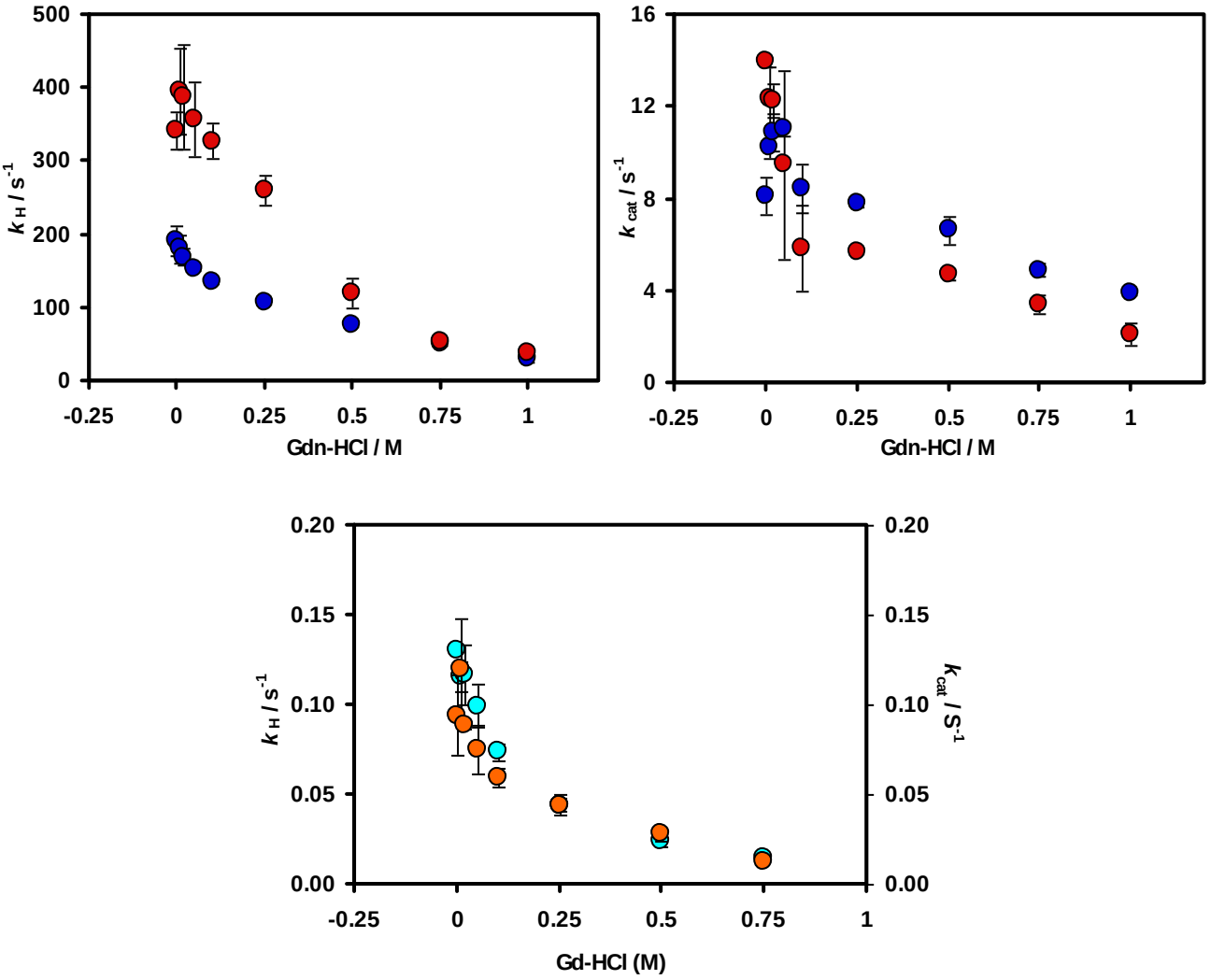

Figure 6.2: *Effect of different concentrations of Gdn-HCl on catalysis by MpDHFR (red), EcDHFR (blue) and TmDHFR (k_H in cyan and k_{cat} in orange), at pH 7 and 20 ℃.*

The activity of the three enzymes was decreased by increasing the concentration of Gdn-HCl (Figure 6.2). TmDHFR, despite being activated in the presence of urea,[94] is the most sensitive of the three enzymes to Gdn-HCl and lost 50% of its activity at 100 mM Gdn-HCl, which is about the same value that Glansdorff *et al*. have reported previously.[94] MpDHFR seems to be the most stable of the three enzymes to Gdn-HCl (Table 6.3). This enzyme lost 50% of its activity in the pre-steady state at about

400 mM Gdn-HCl, while EcDHFR lost half of its activity at 250 mM Gdn-HCl. On the other hand, activation of EcDHFR was seen at very low concentrations of Gdn-HCl in the steady state where the rate-limiting step is the product release step (Table 6.4).[7]

Table 6.3: *Pre-steady-state hydride rate constants (k_H) during catalysis by MpDHFR, EcDHFR and TmDHFR in different concentrations of Gdn-HCl at pH 7 and 20* °C.

Gdn-HCl (M)	k_H (s^{-1})		
	MpDHFR	EcDHFR	TmDHFR
0	341.15 ± 25.37	192.22 ± 20.30	0.13 ±0.010
0.01	395.57 ± 59.23	179.93 ± 18.98	0.12 ±0.008
0.02	388.12 ± 71.48	169.50 ± 11.41	0.12 ±0.017
0.05	356.90 ± 51.98	153.92 ± 3.65	0.10 ±0.012
0.1	327.19 ± 24.33	135.10 ± 2.08	0.07 ±0.004
0.25	259.34 ± 20.53	106.63 ± 2.74	0.04 ±0.004
0.5	119.44 ± 19.90	77.22 ± 4.13	0.02 ±0.004
0.75	52.82 ± 4.49	51.18 ± 2.91	0.01 ±0.003
1	37.35 ± 6.39	30.91 ± 4.68	nd

nd: not determined

Table 6.4: *Steady-state rate constants (k_{cat}) during catalysis by MpDHFR, EcDHFR and TmDHFR in different concentrations of Gdn-HCl at pH 7 and 20* °C.

Gdn-HCl (M)	k_{cat} / s^{-1}		
	MpDHFR	EcDHFR	TmDHFR
0	13.94 ± 0.20	8.12 ± 0.83	0.09 ± 0.023
0.01	12.36 ± 1.33	10.21 ± 0.46	0.12 ± 0.028
0.02	12.28 ± 0.72	10.88 ± 0.84	0.09 ± 0.003
0.05	9.48 ± 4.08	11.02 ± 0.27	0.08 ± 0.014
0.1	5.87 ± 1.86	8.45 ± 1.05	0.06 ± 0.005
0.25	5.72 ± 0.15	7.80 ± 0.20	0.04 ± 0.006
0.5	4.72 ± 0.25	6.64 ± 0.60	0.03 ± 0.004
0.75	3.42 ± 0.42	4.91 ± 0.29	0.01 ± 0.004
1	2.11 ± 0.48	3.91 ± 0.07	nd

nd: not determined

6.3 Salt effect on catalysis by MpDHFR

Previous work was done in our group to explore the effect of various salts on the steady state rate constant of MpDHFR.[90] For further investigation, the pre-steady state rate constant of hydride transfer and the kinetic isotope effect for MpDHFR were measured at pH 7 and 20 °C with NADPH and NADPD using 100 mM potassium phosphate buffer containing various concentrations of NaCl, KF and KCl.

The rate constant for hydride transfer is not affected by different salt concentration (Figure 6.3). However, with NADPD the rate constant decreased with increasing salt concentration. The deuteride transfer rate constant is salt independent above 0.5 M of NaCl and KCl, but not with KF. MpDHFR has shown a salt dependent KIE at concentrations lower than 0.5 M of NaCl and KCl. However, there was no further salt dependence of the KIE at concentrations higher than 0.5 M. In contrast to MpDHFR, recent work in our group done by Dr Joel Loveridge has shown that the rate constants during the EcDHFR reaction and the kinetic isotope effect are salt independent.

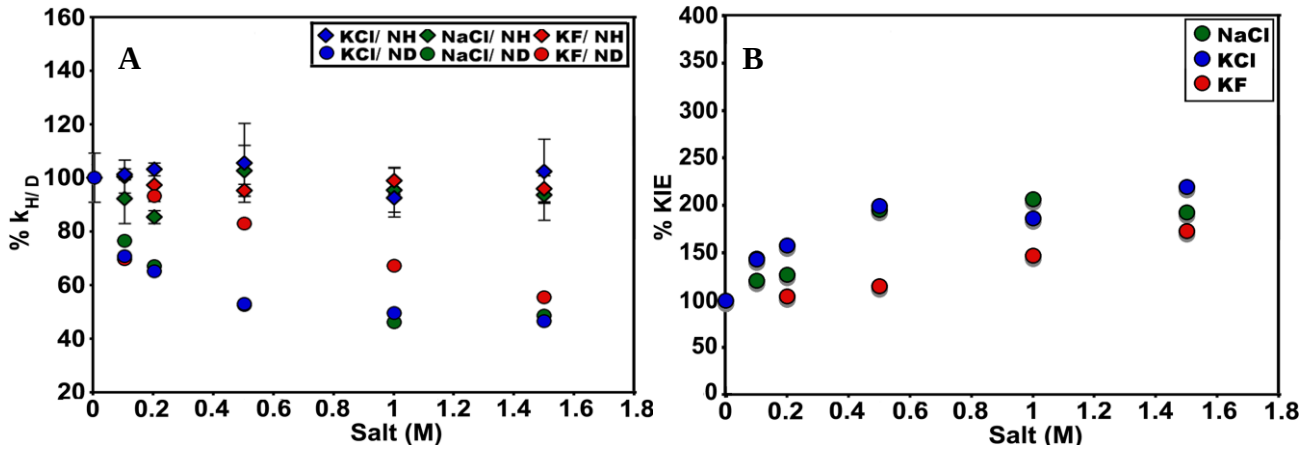

Figure 6.3: *A. Rate constants for hydride (diamonds) and deuteride (circles) transfer catalysed by MpDHFR in the presence of varying concentrations of salts at 20 ℃. B. Pre-steady state KIE for MpDHFR with different salts at 20 ℃.*

Previously, the effect of various salts (NaCl, KCl, and KF) and their concentration on the steady state rate constant of TmDHFR[173] and MpDHFR[90] has been investigated. For TmDHFR, a significant decrease in the specific activity of the enzyme was noted when the ionic strength of KF was raised above 0.1 M. The specific activity of TmDHFR was increased somewhat with NaCl across the

concentration range studied with ~8% increase in activity compared to ~0 M NaCl. KCl slightly increased the steady state rate of TmDHFR up to ~250 mM, but at concentrations above 0.5 M the rate decreased to ~80% of the initial activity at low ionic strength. Increasing the ionic strength of the solution in which the enzyme was incubated was found also to increase the thermal melting temperature of TmDHFR.[173]

The steady-state reaction catalysed by MpDHFR in the presence of various salts (NaCl, KCl, and KF) shows a similar effect to that seen with TmDHFR, except the specific activity was decreased below that at ~0 M with NaCl and KCl at concentrations above 0.5 M. In addition, the effect of KF on the specific activity was different to that seen in TmDHFR as the rate of MpDHFR was not reduced to below that at ~0 M until concentrations above 0.75 M, with about 10% average increase. An activating effect on the steady state reaction for MpDHFR was seen at concentrations lower than 0.5 M of NaCl and KCl, with an average increase in the rate constant of ~20% for NaCl and ~12% for KCl.[90] Similar to the salt effect seen in TmDHFR, and the effect of bound ligands on the thermal stability of MpDHFR, the presence of salt also increased the thermal melting point of the psychrophilic enzyme. This was seen with each salt used, suggesting the anion is no more responsible for the stabilising effect than the cation.

DHFR from the halophilic bacterium *Haloferax volcani*i (HvDHFR) is activated as well at high salt concentrations. This finding was attributed to the effect of salt on substrate affinity.[157] However, while salts were found to stabilize both enzymes, EcDHFR and HvDHFR, by a common mechanism,[157] the mesophilic DHFR showed loss of steady state activity with increasing salt concentrations. This reduction in the turnover number for EcDHFR is not accompanied by any significant change in structure or substrate binding affinities. It was suggested that the loss of catalytic ability for EcDHFR in the presence of salt may arise from an reduced flexibility of the enzyme as it becomes more stable in the presence of salt.[157] EcDHFR is known to have mobile and flexible loops which undergo conformational changes during the catalytic cycle (see Chapter 1).[71,75,174] However, this hypothesis cannot be confirmed in the absence of NMR data for EcDHFR at different salt concentrations to assess the effect of salt on enzyme flexibility.

Generally speaking, in the steady state the behaviour of the mesophilic enzyme is similar to the psychrophilic DHFR at salt concentration $\geq$ 0.5M. Both enzymes suffer from a decrease in turnover numbers and show structure stability. Under pre-steady state conditions both enzymes show salt independent kinetic isotope effect under the same conditions (EcDHFR at all salt concentrations and

MpDHFR at salt concentration ≥ 0.5M). These observations show the similarity between the two enzymes and suggest adaptation from MpDHFR to the environment of its original organism, *Moritella profunda*, which needs NaCl for growth and is classified as a moderately halophilic bacterium.[175] The loss of activity with increasing concentrations of chloride salts for EcDHFR may be due to impaired loop dynamics causing changes to the rate-determining step at high salt concentrations.[157] But taking into consideration our previous findings that MpDHFR does not depend on loop dynamics during progress through the catalytic cycle (see Chapters 4 and 5) and the increased thermal stability for both enzymes at high salt concentrations, it may instead be that reduction in the weak interactions such as electrostatic interactions cause the decrease in the steady state rate constant at high salt concentrations rather than affecting the enzyme flexibility.

Table 6.5: *Pre-steady-state rate constant with NADPH (k_H) during catalysis by MpDHFR in different concentrations of NaCl, KCl and KF at pH 7*

[Salt] (M)	NaCl	KCl	KF
0	327.61 ± 30.06	327.61 ± 21.26	327.61 ± 30.10
0.1	301.94 ± 30.53	331.62 ± 4.69	328.92 ± 20.22
0.2	279.53 ± 7.78	337.69 ± 5.47	318.68 ± 20.37
0.5	335.95 ± 30.79	35.63 ± 47.90	312.10 ± 7.22
0.1	312.21 ± 26.83	302.93 ± 16.44	323.80 ± 16.22
1.5	306.66 ± 30.86	335.18 ± 27.72	313.91 ± 15.86
2	266.21 ± 14.58	368.39 ± 6.31	419.25 ± 22.53

Table 6.6: *Pre-steady-state rate constant with NADPD (k_D) during catalysis by MpDHFR in different concentrations of NaCl, KCl and KF at pH 7*

[Salt] (M)	NaCl	KCl	KF
0	257.98 ± 24.75	257.98 ± 24.75	257.98 ± 24.75
0.1	196.36 ± 12.86	171.76 ± 15.15	161.14 ± 26.39
0.2	173.01 ± 14.11	158.14 ± 14.14	188.87 ± 72.82
0.5	135.40 ± 13.29	131.07 ± 7.60	172.72 ± 58.26
0.1	119.40 ± 4.35	132.67 ± 6.74	142.32 ± 43.55
1.5	125.57 ± 3.33	129.02 ±1 2.65	142.87 ± 0.01
2	118.61 ± 9.51	160.48 ± 39.77	153.91 ± 13.00

Table 6.7: *Pre-steady-state kinetic isotope effect during catalysis by MpDHFR in different concentrations of NaCl, KCl and KF at pH 7*			
[Salt] (M)	NaCl	KCl	KF
0	1.27 ± 0.13	1.27 ± 0.12	1.27 ± 0.13
0.1	1.54 ± 0.12	1.39 ± 0.09	2.04 ± 0.17
0.2	1.62 ± 0.09	2.14 ± 0.09	1.69 ± 0.39
0.5	2.48 ± 0.13	2.64 ± 0.15	1.81 ± 0.34
0.1	2.61 ± 0.09	2.28 ± 0.07	2.28 ± 0.31
1.5	2.44 ± 0.10	2.60 ± 0.13	2.20 ± 0.05
2	2.24 ± 0.10	2.30 ± 0.25	2.73 ± 0.10

Table 6.8: *Effect of salts on the steady state rate constants for the MpDHFR reaction at pH 7*			
[Salt] (M)	NaCl	KCl	KF
0	11.41± 0.82	11.41± 0.82	11.41± 0.82
0.1	14.78 ± 0.79	14.89 ± 0.79	13.45 ± 0.66
0.2	15.41 ± 0.76	12.98 ± 0.47	13.28 ± 0.78
0.5	12.22 ± 0.68	11.17 ± 0.58	12.72 ± 0.48
0.75	10.65 ± 0.57	9.03 ± 0.42	11.24 ± 0.53
1.0	7.95 ± 0.26	6.59 ± 0.34	9.80 ± 0.35
Data measured by Dr Rhiannon Evans[90]			

6.4 Temperature dependence of the pre-steady state hydride transfer rate constant and KIEs for MpDHFR and EcDHFR at 0.5 M NaCl.

To investigate the effect of salt on the temperature dependence of the KIE for DHFR the pre-steady state rate constant for hydride/deuteride transfer (k_H/k_D) during MpDHFR and EcDHFR catalysis was measured at pH 7.0 as a function of temperature between 5 and 30 °C using 100 mM potassium phosphate buffer, 10 mM βME and 0.5 M NaCl.

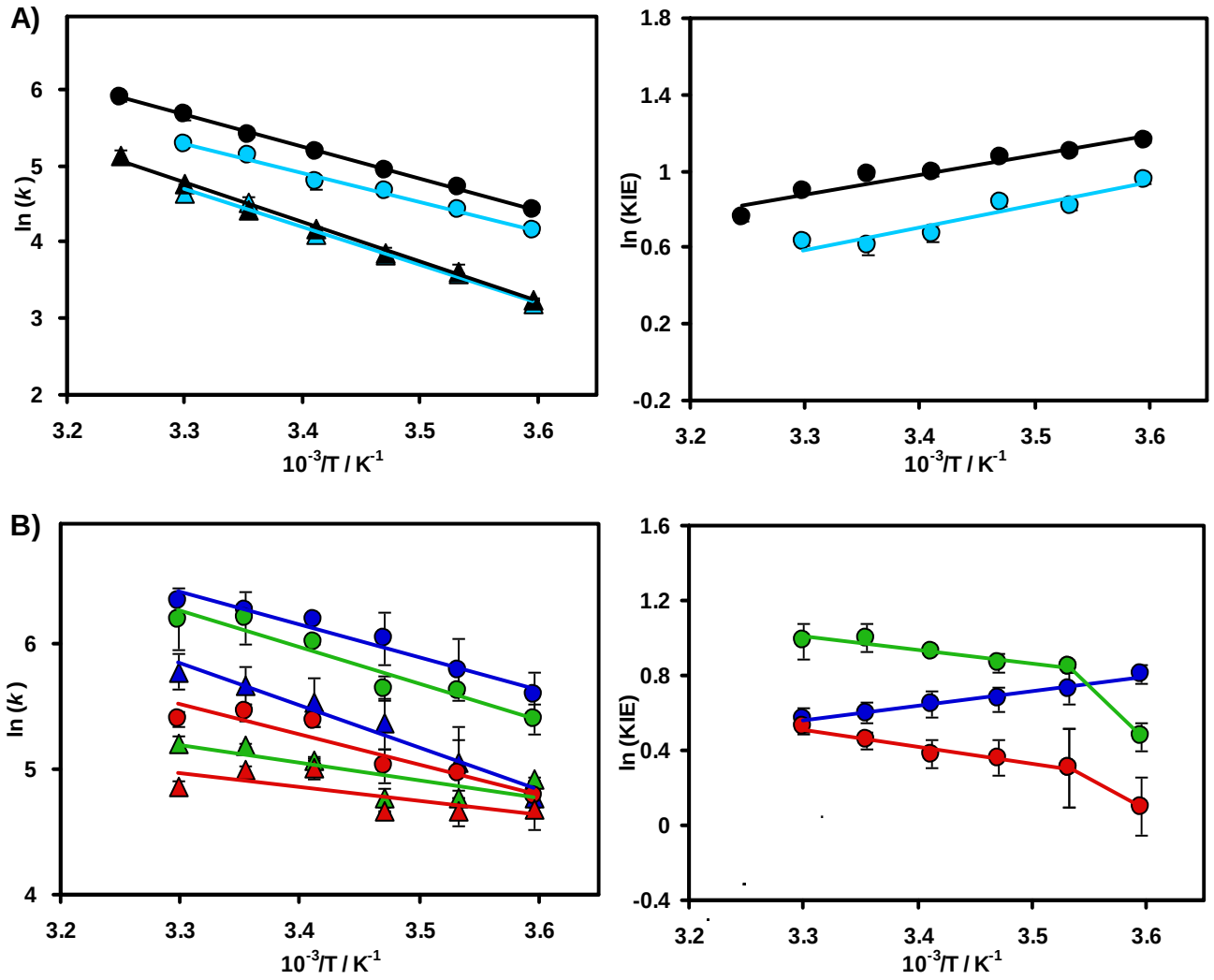

Figure 6.4: *Arrhenius plots for hydride (circle)/deuterium (triangle) transfer and the corresponding KIEs for the reaction catalysed by EcDHFR (A) using 0.1 M (black) and 0.5 M (cyan) NaCl, and MpDHFR (B) using 0.1 M (blue), 0.5 M (green) and 0.5 M NaCl with 33% glycerol (red).*

For EcDHFR, using 0.5 M NaCl affected the rate constants of hydride transfer but not deuteride transfer rate constants, which caused the decrease in the KIE values. The KIE was decreased by increasing temperature either at low or high salt concentration (Figure 6.4A). On the other hand, the

KIE for MpDHFR in 0.5 M NaCl and 0.5 M NaCl with 33% glycerol increases with temperature (Figure 6.4B), suggesting the chemical step is masked by kinetic complexity at low temperatures (*i.e.*, the chemical step becomes less rate limiting). To explore if the effect of salt on the kinetic isotope effect during catalysis by MpDHFR is due to effects on enzyme flexibility and not electrostatic interactions, the temperature dependence of the KIE was measured in 0.5 M salt and 33% glycerol. The data obtained was very similar to that in absence of glycerol, indicating that the change in the temperature dependence of the KIE is due to changing active site electrostatic forces rather than enzyme dynamics.

Table 6.9: *Temperature dependence of the pre-steady-state rate constants for hydride (k_H) and deuteride (k_D) transfer during catalysis by EcDHFR and MpDHFR at 0.5 M NaCl and pH 7.*

	EcDHFR		MpDHFR	
T (^{o}C)	k_H (s^{-1})	k_D (s^{-1})	k_H (s^{-1})	k_D (s^{-1})
5	63.83 ± 1.08	24.51 ± 1.24	233.98 ± 7.35	137.46 ± 2.94
10	83.01 ± 3.53	36.59 ± 0.16	277.80 ± 4.35	122.21 ± 8.19
15	107.20 ± 3.53	46.20 ± 1.81	278.42 ± 22.56	122.21 ± 4.39
20	119.85 ± 9.95	60.98 ± 2.06	404.36 ± 3.13	162.72 ± 3.24
25	168.10 ± 5.01	91.11 ± 6.79	437.73 ± 6.82	17.77 ± 7.63
30	196.32 ± 0.61	104.71 ± 2.01	488.80 ± 119.64	182.45 ± 10.49

Table 6.10: *Temperature dependence of the pre-steady-state rate kinetic isotope effect during catalysis by EcDHFR and MpDHFR at 0.5 M NaCl and pH 7.*

T (^{o}C)	EcDHFR	MpDHFR
5	2.60 ± 0.05	1.70 ± 0.04
10	2.27 ± 0.04	2.27 ± 0.07
15	2.32 ± 0.05	2.28 ± 0.09
20	1.97 ± 0.09	2.49 ± 0.02
25	1.84 ± 0.08	2.48 ± 0.05
30	1.87 ± 0.02	2.68 ± 0.25

Table 6.11: *Temperature dependence of the pre-steady-state rate constants for hydride (k_H) and deuteride (k_D) transfer and kinetic isotope effect (KIE) during catalysis by EcDHFR and MpDHFR at 0.5 M NaCl, pH 7 and 33% glycerol.*			
T (^{o}C)	k_H (s^{-1})	k_D (s^{-1})	KIE
5	119.45 ± 9.69	107.63 ± 16.50	1.11 ± 0.17
10	144.37 ± 37.95	106.08 ± 11.34	1.36 ± 0.28
15	152.31 ± 20.49	106.08 ± 1.12	1.44 ± 0.13
20	219.60 ± 12.70	149.88 ± 13.93	1.47 ± 0.11
25	233.41 ± 15.20	148.01 ± 3.95	1.58 ± 0.07
30	221.38 ± 14.04	130.38 ± 4.30	1.70 ± 0.07

The salt effect on the pre-steady state rate constants and temperature dependence of the KIEs was examined as well for the EcDHFR-S148P and EcDHFR-A19K/S148P variants (Figure 6.5) to test the hypothesis that impairing loop dynamics in MpDHFR is probably the reason for the striking differences in the salt effect on the temperature dependence of KIE in the mesophilic and the psychrophilic enzyme.

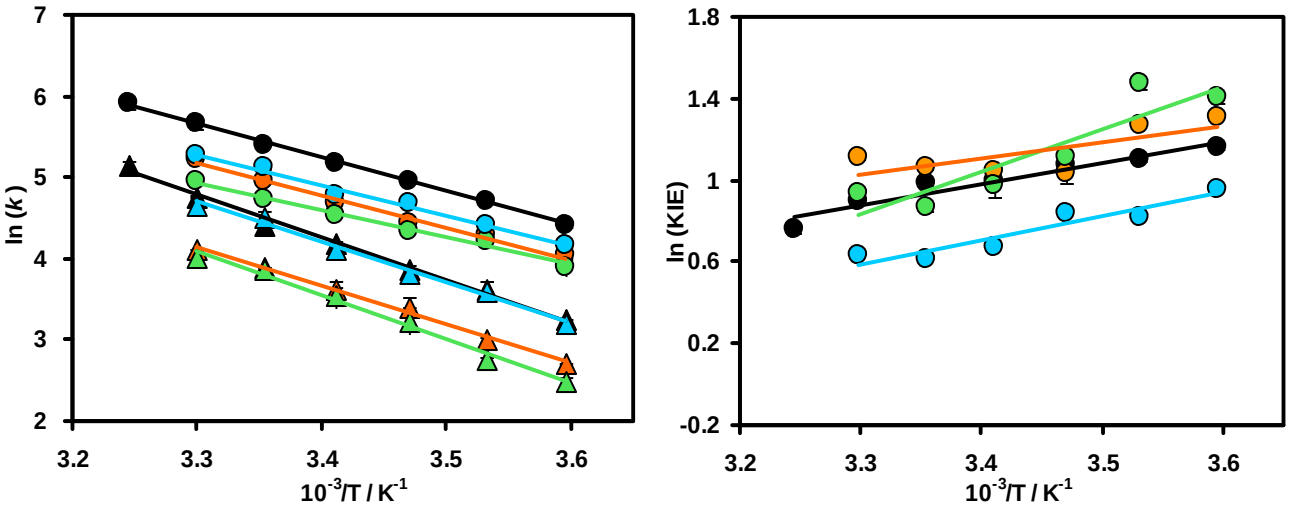

Figure 6.5: *Arrhenius plots (right) and temperature dependence of KIE (left) of the pre-steady-state rate constants for hydride (k_H, circles) and deuteride (k_D, triangles) transfer at pH 7 during catalysis by wild type EcDHFR at 0.1 M salt (black) and 0.5 M salt (cyan) and for the two variants EcDHFR-S148P (green) and EcDHFR-A19K/S148P (orange) at 0.5 M salt.*

The two variants at 0.5 M NaCl show very similar rate constants and temperature dependence of the KIE to the wild type EcDHFR (Tables 6.12 and 6.13). These data indicate that impairing loop dynamics in MpDHFR is not the reason for the salt effect observed here for this enzyme.

Table 6.12: *Temperature dependence of the pre-steady-state rate constants for hydride (k_H) and deuteride (k_D) transfer during catalysis by EcDHFR and MpDHFR at 0.5 M NaCl and pH 7.*

	EcDHFR-S148P		EcDHFR-A19K/S148P	
T (^{o}C)	k_H (s^{-1})	k_D (s^{-1})	k_H (s^{-1})	k_D (s^{-1})
5	56.56 ± 0.37	15.22 ± 0.01	49.15 ± 5.51	12.02 ± 0.80
10	72.70 ± 1.15	20.34 ± 0.21	68.55 ± 6.83	15.72 ± 0.45
15	83.78 ± 1.15	29.89 ± 3.80	77.00 ± 6.83	25.30 ± 4.38
20	107.55 ± 6.15	37.82 ± 0.82	92.69 ± 2.70	34.75 ± 6.01
25	142.00 ± 1.41	49.10 ± 0.42	113.58 ± 3.29	47.64 ± 1.05
30	185.50 ± 0.71	61.00 ± 0.71	142.00 ± 1.41	55.42 ± 2.39

Table 6.13: *Temperature dependence of the pre-steady-state rate kinetic isotope effect during catalysis by EcDHFR and MpDHFR at 0.5 M NaCl and pH 7.*

T (^{o}C)	EcDHFR-S148P	EcDHFR-A19K/S148P
5	3.72 ± 0.01	4.09 ± 0.13
10	3.57 ± 0.02	4.36 ± 0.10
15	2.80 ± 0.13	3.04 ± 0.19
20	2.84 ± 0.06	2.67 ± 0.18
25	2.89 ± 0.01	2.38 ± 0.04
30	3.04 ± 0.01	2.56 ± 0.04

6.5 Conclusions

Studying the origins of the stability of proteins is essential to understand their structure and function. Protein stability is the result of a delicate balance of strong attractive and repulsive forces, yielding the free energy of stabilization as a small difference between large numbers equivalent to a few weak intermolecular interactions.[176] In this part of the thesis we examined the effect of different denaturants and salt concentrations on catalysis by DHFR.

A previous study has shown that the conformational stability for MpDHFR in urea is lower than the mesophilic and the thermophilic homologues.[60] Unlike the dimeric, thermophilic homologue from *Thermotoga maritima*,[94] no activation was observed for either MpDHFR and EcDHFR in urea. However, while the steady state rate constant is not affected when using 2 M urea, by about 3.2 M urea a 50% decrease in the steady state rate constant for MpDHFR was observed and more than 90% of the activity was lost at 5-7 M urea. The data presented here have shown that different concentrations of urea affect the rate constants of hydride transfer for the psychrophilic and the mesophilic DHFRs in a similar manner.

For all of the three enzymes, TmDHFR, EcDHFR and MpDHFR, the activity was decreased by increasing the concentration of Gdn-HCl, with TmDHFR seeming to be the most sensitive and MpDHFR the least sensitive between the three enzymes. On the other hand, an activation of EcDHFR was seen at very low concentrations of Gdn-HCl in the steady state where the rate-limiting step is the product release step.[7]

Previous studies in our group have shown that the thermal melting point of apo-MpDHFR is ~38 °C, which is lower than that of EcDHFR (T_M ~51 °C) and TmDHFR (T_M ~80 °C).[173] The thermal melting point of MpDHFR can be increased by bound ligands such as MTX,[79] and with increasing salt concentrations.[90] Under steady state conditions at neutral pH, the MpDHFR catalysed reaction was slightly enhanced by addition of salts to the reaction buffer at concentrations <0.5 M. Such enzyme activation was not observed for the mesophilic EcDHFR,[157] but a similar effect was seen for TmDHFR.[94,173] However, no salt discrimination was seen for MpDHFR, unlike TmDHFR. A previous study suggested that the moderate halophilicty for MpDHFR is perhaps a feature of the enzyme due to the habitat of the native bacterium,[90] which requires NaCl for growth.[175]

In summary, structure stability and enzyme inactivation in the steady state was seen for the mesophilic DHFR at all salt concentrations[157] and for the psychrophilic DHFR at salt concentration ≥ 0.5 M.[90] Under pre-steady state conditions both enzymes show salt independent kinetic isotope effect under the same conditions (EcDHFR at all salt concentrations and MpDHFR at salt concentration ≥ 0.5 M). The different behaviour observed for MpDHFR at salt concentrations lower than 0.5 M suggesting adaptation to the environment of its original bacterium. The loss of activity for EcDHFR and MpDHFR at high salt concentrations is most probably due to affecting enzyme electrostatic interactions rather than decreasing protein flexibility.

7

Summary & Future directions

7.1 Overall summary

Studying the role of protein dynamics in enzyme catalysis is one of the hot spots in recent enzymology. The fact that the conformational movements of proteins can be important to ligand binding and release is broadly accepted. However, the debate arises when discussing the contribution of protein motion to the reaction chemical step. While some researchers support enzymatic promoting motion models suggesting that catalysis can be enhanced by the coupling of vibrational motion to the reaction coordinate pushing the reactants into a position that efficiently compresses the reaction barrier and enhances tunnelling in hydrogen-transfer reactions,[40,46-47,177] others believe that such dynamics are not important for catalysis, but instead that the energy landscape and preorganisation within the active site is the dominant feature.[38,48-50,178]

Studying the temperature dependence of the KIE is often used to understand the relation between protein dynamics and the rate of enzymatic reaction. For better understanding of how protein motions couple to the reaction coordinate and the effect of environmental conditions on these motions in DHFR, in this thesis the hydride transfer reaction and kinetic isotope effect have been investigated for the psychrophilic MpDHFR and various variants and compared to the mesophilic EcDHFR and the dimeric and thermophilic TmDHFR.

MpDHFR is a cold adapted enzyme that was isolated from the organism *Moritella profunda*, isolated from deep sea sediments at 2 ^{o}C.[175] MpDHFR has shown the highest rate constants compared to the mesophilic and the thermophilic DHFR homologues (EcDHFR and TmDHFR respectively). However, comparing the three DHFRs at their typical operating temperatures at pH 7 shows that MpDHFR is actually a slightly poorer catalyst than EcDHFR under single turnover conditions and is equivalent to TmDHFR in the steady state. Studying the temperature dependences of the KIE on hydride transfer reaction catalysed by MpDHFR, the mesophilic and extremely studied homologue, EcDHFR[103] and the thermophilic homologue, TmDHFR[101] have shown that the origin of chemistry in the three enzymes is similar. The data was interrupted according the environmentally coupled tunnelling model.

In the steady state, TmDHFR has shown a different kinetic behaviour for the hydride transfer step than that observed for MpDHFR and EcDHFR. This can be due to dimeric properties for this enzyme. In the steady state, however, product release is the rate limiting step for MpDHFR and EcDHFR[7] at pH 7 and the chemical step is partially limited at elevated pH. The chemical step is partially rate limiting the steady state rate constants for the dimeric enzyme, TmDHFR, at pH7. Thus,

it is difficult to compare the behaviour of the steady state temperature dependence of the KIEs of the monomeric enzymes with that of the dimeric enzyme.

We have shown that impairing the occluded conformation does not affect the chemical step during catalysis by DHFR. Steady state kinetics and binding measurements in addition to evaluating a novel NMR method to study binding of NADPH to DHFR have suggested that the occluded conformation is important for EcDHFR to control the binding to $NADP^+$ and guides the enzyme to follow the steps of the catalytic cycle in a strictly ordered manner. Removal of the occluded conformation in EcDHFR causes a great decrease in the value of k_{cat} resulting from the change in the steady state rate limiting step for product release from the ternary complex E.$NADP^+$.THF instead of E.NADPH.THF. In spite of lacking the occluded conformation, MpDHFR seems to follow a similar catalytic cycle to EcDHFR at pH 7, however, it still unclear how this occurs. At low pH, the decrease in the steady-state reaction rate for MpDHFR might be due to the reaction being diverted into two parallel kinetic pathways as has been described previously for MtDHFR.[70]

A recent study by Wright and co-workers[179] is in a good agreement with our data. The study has shown that the occluded conformation is important for EcDHFR as $NADP^+$ and THF concentrations in the *Escherichia coli* cells is inhibitory. The study has shown also that human DHFR do not form the occluded conformation and instead binds to the cofactor more tightly and release it more slowly which is explaining the NMR date we reported for MpDHFR in Chapter 4. This behaviour for human DHFR was suggested to be due to the low cellular concentrations of $NADP^+$ and THF in vertebrate cells.[179] However, in this thesis we have reported the same behaviour for the bacterial DHFR from *Moritella profunda* and have shown that many others DHFRs lack a hydrogen bond donor in the position corresponding to Ser148. Therefore, the occluded conformation is unlikely to be a general characteristic for DHFR catalysis.

For further understanding of the role of loop dynamics during catalysis by DHFR, various MpDHFR and EcDHFR variants in the M20 loop and the FG loop were created and studied. Mutations in the M20 loop of EcDHFR most probaply has affected the dynamic of the loop causing the remarkable decrease in the steady state rate constants without affecting the hydride transfer step. On the other side, none of the MpDHFR variants has shown a large difference in the turnover number, suggesting that such M20 loop dynamics observed in EcDHFR do not control the catalytic cycle in MpDHFR. In contrast to the reported data from similar mutations for EcDHFR, mutation in the FG loop at positions 121 and 122 in MpDHFR did not affect the chemical step of the reaction. Instead the two

variants have shown a sharp decrease in the steady state rate constants, which suggests a change in the physical step without perturbing the chemistry of the reaction. Studying the MpDHFR-M42W variant in the future could be of great interest as the equivalent variant in EcDHFR has shown a sharp decrease in the hydride transfer rate constant and is thought to be involved in long range coupled motion in EcDHFR.[150,152]

H/D exchange experiments have suggested that the M20 loop, FG loop and GH loop may be more flexible in EcDHFR compared to MpDHFR.[96] Therefore, in light of the above findings, it is reasonable to conclude that the dynamic nature reported for the mesophilic enzyme from *Escherichia coli* is not clear for the psychrophilic homologue from *Moritella profunda* suggesting that MpDHFR is using a different mechanism to modulate the enzyme's ability to adopt different ligand complexes compared to the mesophilic enzyme EcDHFR. On basis of these findings it is important to refer that the currant enzymatic models that reveals enzyme dynamics to catalysis efficiency has become invalid. As a consequence, modifying these models has become an essential matter.

The effect of different denaturant and salt concentrations on catalysis by DHFR was also examined. The results have shown that addition of urea to the reaction buffer is affecting the chemical step of the reaction catalysed by the monomeric DHFRs (MpDHFR and EcHFR) in a similar manner and different to that catalysed by the dimeric enzyme, TmDHFR. Increasing the concentration of Gdn-HCl decreased the activity for all the DHFR homologues studied here. However, TmDHFR has shown the greatest sensitivity to Gdn-HCl followed by EcDHFR then MpDHFR. Circular dichroism spectroscopic and NMR can be used for further understanding of the effect of denaturants on structure and catalysis of DHFR

Studying salt effect on MpDHFR and EcDHFR has shown that the kinetic isotope effect does not dependent on salt concentration. The data suggests adaptation of MpDHFR to the environmental of its original bacterium *Moritella profunda*, which is a moderately halophilic organism that needs NaCl for growing and can cultured from marine broth.[175] The loss of activity for EcDHFR and MpDHFR at high salt concentrations is most probably due to affecting enzyme electrostatic interactions rather than decreasing protein flexibility. However, this cannot be confirmed in absence of structure information at various salt concentrations.

7.2 Future directions

The best evidence for the existence of an occluded conformation in MpDHFR would be from a structural technique such as crystallography or multidimensional NMR spectroscopy. The crystal structures of the apo-MpDHFR and the ternary complex MpDHFR.NADPH.MTX have been reported earlier.[62] Also, previous work in our group have determined the ^{1}H, ^{13}C and ^{15}N chemical shift assignments of MpDHFR in complex with $NADP^{+}$ and folate.[95] In the long term the crystal structure and the three dimensional solution structure of MpDHFR.folate complex or MpDHFR.MTX (as a model for the DHFR.THF complex) can be solved. These complexes show the occluded conformation in EcDHFR,[59] but will expected to be in the closed conformation in MpDHFR, similar to LcDHFR[119] which also lacks the Serine residue at position 148.

^{15}N labelling of the cofactor $NADP^{+}$ has provided valuable information of how the cofactor binds to various DHFRs through ^{1}H-^{15}N HSQC NMR spectroscopy. Such methodology can be applied to study the different EcDHFR and MpDHFR M20 loop variants, studied in chapter 5, to investigate how the M20 loop residues can affect the binding of $NADP^{+}$. This method can also be used in studies of many other nicotinamide dependent enzymes to improve our understanding of enzyme catalysis in general and may lead to advances in enzymology and other aspects of chemical catalysis in the broadest sense. Furthermore, it would be exciting to synthesise labelled DHF and THF and design a different NMR experiments to evaluate more information on how DHFR binds to different ligands.

Study of the various M20 loop and FG loop variants has shown that loop dynamic that has well established for the mesophilic enzyme from *Escherichia coli* does not control catalysis by the psychrophilic homologue from *Moritella profunda*, however, the two enzymes use the same catalytic cycle and the nature of the chemistry in both enzymes is similar. Various NMR experiments can be used to study dynamics in MpDHFR and compare it to the extensively studied enzyme (EcDHFR). It seems interesting also to study the MpDHFR-M42W variant and compare it to the equivalent variant in EcDHFR.

8

References

(1) Benkovic, S. J.; Hammes-Schiffer, S. *Science (Washington, DC, U. S.)* **2003**, *301*, 1196.
(2) Kraut, J. *Science* **1988**, *242*, 533.
(3) Radzicka, A.; Wolfenden, R. *Science* **1995**, *267*, 90.
(4) Schramm, V. L. *Annu. Rev. Biochem.* **1998**, *67*, 693.
(5) Cleland, W. W. *Annu. Rev. Biochem.* **1967**, *36*, 77.
(6) Cook, P. F.; Cleland, W. W. *Enzyme kinetics and mechanism*; Garland Publishing: London and New York, 2007.
(7) Fierke, C. A.; Johnson, K. A.; Benkovic, S. J. *Biochemistry* **1987**, *26*, 4085.
(8) Copeland, R. A.; Wiley-VCH, Inc.: 2000, p 416.
(9) Schnell, J. R.; Dyson, H. J.; Wright, P. E. *Annu. Rev. Biophys. Biomol. Struct.* **2004**, *33*, 119.
(10) Daniel, R. M.; Dunn, R. V.; Finney, J. L.; Smith, J. C. *Annu. Rev. Biophys. Biomol. Struct.* **2003**, *32*, 69.
(11) Fischer, E. *Berichte der Deutschen Chemichen Gesellschaft* **1894**, *27*, 3189.
(12) Kunz, H. *Angewandte Chemie International Edition* **2002**, *41*, 4439.
(13) Eyring, H. *J. Phys. Chem.* **1935**, *3*.
(14) Pauling, L. *Nature* **1948**, *161*, 707.
(15) Koshland, D. E. *Proceedings of the National Academy of Sciences* **1958**, *44*, 98.
(16) Bruice, T. C.; Benkovic, S. J. *Biochemistry* **2000**, *39*, 6267.
(17) Cha, Y.; Murray, C.; Klinman, J. *Science* **1989**, *243*, 1325.
(18) Henzler-Wildman, K.; Kern, D. *Nature (London, U. K.)* **2007**, *450*, 964.
(19) Eisenmesser, E. Z.; Bosco, D. A.; Akke, M.; Kern, D. *Science (Washington, DC, U. S.)* **2002**, *295*, 1520.
(20) Cleland, W. W. *J. Biol. Chem.* **2003**, *278*, 51975.
(21) Fersht, A. *Structure and mechanism in protein science. A guide to enzyme catalysis and protein folding, by A. Fersht. 1999. New York: Freeman.*; W. H. Freeman and Company: New York, 1999.
(22) Hay, S.; Pang, J.; Monaghan, P. J.; Wang, X.; Evans, R. M.; Sutcliffe, M. J.; Allemann, R. K.; Scrutton, N. S. *ChemPhysChem* **2008**, *9*, 1536.
(23) Klinman, J. P. *Chemical Physics Letters* **2009**, *471*, 179.
(24) Heisenberg, W. *Z. Physik* **1927**, *43*, 172.
(25) Kohen, A.; Klinman, J. P. *Accounts of Chemical Research* **1998**, *31*, 397.
(26) Knapp, M. J.; Klinman, J. P. *Eur. J. Biochem.* **2002**, *269*, 3113.
(27) Kohen, A.; Klinman, J. P. *Chem. Biol.* **1999**, *6*, R191.
(28) Sutcliffe, M. J.; Scrutton, N. S. *Trends Biochem. Sci. (Pers. Ed.)* **2000**, *25*, 405.
(29) Kohen, A.; Limbach, a. H.-H. *Isotope effects in chemistry and biology*; Taylor & Francis, CRC Press: Boca Raton, FL, 2006.
(30) Knapp, M. J.; Rickert, K.; Klinman, J. P. *J. Am. Chem. Soc.* **2002**, *124*, 3865.
(31) Stojković, V.; Kohen, A. *Israel Journal of Chemistry* **2009**, *49*, 163.
(32) Swain, C. G.; Stivers, E. C.; Reuwer, J. F.; Schaad, L. J. *J. Am. Chem. Soc.* **1958**, *80*, 5885.
(33) Kohen, A. In *Hydrogen-Transfer React.*; Hynes, K., Limbach, Schowen, Ed.; WILEY-VCH Verlag GmbH & Co.: Weinheim, 2007; Vol. 4, p 1311.
(34) Kohen, A. *Progress in Reaction Kinetics and Mechanism* **2003**, *28*, 119.
(35) Bell, R. P. *The Tunnel Effect in Chemistry*; Chapman and Hall: London, 1980.
(36) Moiseyev, N.; Rucker, J.; Glickman, M. H. *J. Am. Chem. Soc.* **1997**, *119*, 3853.
(37) Sutcliffe, M. J.; Scrutton, N. S. *Eur. J. Biochem.* **2002**, *269*, 3096.
(38) Antoniou, D.; Caratzoulas, S.; Kalyanaraman, C.; S. Mincer, J.; Schwartz, S. D. *Eur. J. Biochem.* **2002**, *269*, 3103.

(39) Francisco, W. A.; Knapp, M. J.; Blackburn, N. J.; Klinman, J. P. *J. Am. Chem. Soc.* **2002**, *124*, 8194.
(40) Villà, J.; Warshel, A. *The Journal of Physical Chemistry B* **2001**, *105*, 7887.
(41) Marcus, R. A. *The Journal of Physical Chemistry B* **2007**, *111*, 6643.
(42) Marcus, R. A.; Sutin, N. *Biochim Biophys Acta* **1985**, *811*, 265.
(43) Limbach, H.-H.; Schowen, K. B.; Schowen, R. L. *J. Phys. Org. Chem.* **2010**, *23*, 586.
(44) Yahashiri, A.; Howell, E. E.; Kohen, A. *ChemPhysChem* **2008**, *9*, 980.
(45) Nagel, Z. D.; Klinman, J. P. *Chemical Reviews* **2006**, *106*, 3095.
(46) Adamczyk, A. J.; Cao, J.; Kamerlin, S. C. L.; Warshel, A. *PNAS* **2011**, *108*, 14115.
(47) Loveridge, E. J.; Behiry, E. M.; Guo, J.; Allemann, R. K. *Nature Chemistry* **2012**, *4*, 292.
(48) Antoniou, D.; Basner, J.; Nunez, S.; Schwartz, S. D. *Chem. Rev. (Washington, DC, U. S.)* **2006**, *106*, 3170.
(49) Mincer, J. S.; Schwartz, S. D. *The Journal of Physical Chemistry B* **2002**, *107*, 366.
(50) Bhabha, G.; Lee, J.; Ekiert, D. C.; Gam, J.; Wilson, I. A.; Dyson, H. J.; Benkovic, S. J.; Wright, P. E. *Science (Washington, DC, U. S.)* **2011**, *332*, 234.
(51) Sirawaraporn, W. *Drug Resistance Updates* **1998**, *1*, 397.
(52) Douglas, K. T. *Medicinal Research Reviews* **1987**, *7*, 441.
(53) Schrecker, A. W.; Huennekens, F. M. *Biochem. Pharmacol.* **1964**, *13*, 731.
(54) Hitchings, G. H.; Burchall, J. J. In *Advances in Enzymology and Related Areas of Molecular Biology*; John Wiley & Sons, Inc.: 2006, p 417.
(55) Roth, B.; Cheng, C. C. In *Progress in Medicinal Chemistry*; Ellis, G. P., West, G. B., Eds.; Elsevier: 1982; Vol. Volume 19, p 269.
(56) Matthews, D. A.; Alden, R. A.; Bolin, J. T.; Freer, S. T.; Hamlin, R.; Xuong; Kraut, J.; Poe, M.; Williams, M.; Hoogsteen, K. *Science (Washington, DC, U. S.)* **1977**, *197*, 452.
(57) Bolin, J. T.; Filna, D. J.; Matthews, D. A.; Hamlin, R. C.; Kraut, J. *J. Biol. Chem.* **1982**, *257*, 13650.
(58) Bystroff, C.; Kraut, J. *Biochemistry* **1991**, *30*, 2227.
(59) Sawaya, M. R.; Kraut, J. *Biochemistry* **1997**, *36*, 586.
(60) Xu, Y.; Feller, G.; Gerday, C.; Glansdorff, N. *J. Bacteriol.* **2003**, *185*, 5519.
(61) Huber, R.; Langworthy, T.; König, H.; Thomm, M.; Woese, C.; Sleytr, U.; Stetter, K. *Arch. Microbiol.* **1986**, *144*, 324.
(62) Hay, S.; Evans, R. M.; Levy, C.; Loveridge, E. J.; Wang, X.; Leys, D.; Allemann, R. K.; Scrutton, N. S. *ChemBioChem* **2009**, *10*, 2348.
(63) Dams, T.; Auerbach, G.; Bader, G.; Jacob, U.; Ploom, T.; Huber, R.; Jaenicke, R. *J. Mol. Biol.* **2000**, *297*, 659.
(64) Maglia, G.; Javed, M. H.; Allemann, R. K. *Biochem. J.* **2003**, *374*, 529.
(65) Loveridge, E. J.; Rodriguez, R. J.; Swanwick, R. S.; Allemann, R. K. *Biochemistry* **2009**, *48*, 5922.
(66) Margosiak, S. A.; Appleman, J. R.; Santi, D. V.; Blakley, R. L. *Arch. Biochem. Biophys.* **1993**, *305*, 499.
(67) Thillet, J.; Adams, J. A.; Benkovic, S. J. *Biochemistry* **1990**, *29*, 5195.
(68) Andrews, J.; Fierke, C. A.; Birdsall, B.; Ostler, G.; Feeney, J.; Roberts, G. C. K.; Benkovic, S. J. *Biochemistry* **1989**, *28*, 5743.
(69) Appleman, J. R.; Beard, W. A.; Delcampg, T. J.; PrendergastG, N. J.; Freisheimg, J. H.; Blakley, R. L. *J Biol Chem* **1990**, *265*, 2740.
(70) Czekster, C. M.; Vandemeulebroucke, A.; Blanchard, J. S. *Biochemistry* **2011**, *50*, 7045.
(71) Cameron, C. E.; Benkovic, S. J. *Biochemistry* **1997**, *36*, 15792.
(72) Bystroff, C.; Oatley, S. J.; Kraut, J. *Biochemistry* **1990**, *29*, 3263.

(73) Li, L.; Wright, P. E.; Benkovic, S. J.; Falzone, C. J. *Biochemistry* **1992**, *31*, 7826.
(74) Falzone, C. J.; Wright, P. E.; Benkovic, S. J. *Biochemistry* **1994**, *33*, 439.
(75) Miller, G. P.; Benkovic, S. J. *Chem. Biol.* **1998**, *5*, R105.
(76) Radkiewicz, J. L.; Brooks, C. L., III *J. Am. Chem. Soc.* **2000**, *122*, 225.
(77) Osborne, M. J.; Schnell, J.; Benkovic, S. J.; Dyson, H. J.; Wright, P. E. *Biochemistry* **2001**, *40*, 9846.
(78) Osborne, M. J.; Venkitakrishnan, R. P.; Dyson, H. J.; Wright, P. E. *Protein Sci.* **2003**, *12*, 2230.
(79) Evans, R. M.; Behiry, E. M.; Tey, L.-H.; Guo, J.; Loveridge, E. J.; Allemann, R. K. *ChemBioChem* **2010**, *11*, 2010.
(80) Glasoe, P. K.; Long, F. A. *J. Phys. Chem.* **1960**, *64*, 188.
(81) Futterman, S. *J. Biol. Chem.* **1957**, *228*, 1031.
(82) Zakrzewski, S. F.; Sansone, A. M. **1971**, *18*, 728.
(83) Mathews, C. K.; Huennekens, F. M. *J. Biol. Chem.* **1960**, *235*, 3304.
(84) Jeong, S. S.; Gready, J. E. *Analytical Biochemistry* **1994**, *221*, 273.
(85) Agrawal, N.; Kohen, A. *Analytical Biochemistry* **2003**, *322*, 179.
(86) Wang, W.; McMurray, J. S. *Tetrahedron Lett.* **1999**, *40*, 2501.
(87) Zatman, L. J.; Kaplan, N. O.; Colowick, S. P. *J. Biol. Chem.* **1953**, *200*, 197.
(88) Loewus, F. A.; Vennesland, B.; Harris, D. L. *J. Am. Chem. Soc.* **1955**, *77*, 3391.
(89) Ludwig, C.; Günther, U. *BMC Bioinformatics* **2011**, *12*, 366.
(90) Evans, R. M., Cardiff University, 2009.
(91) Hata, K.; Kono, R.; Fujisawa, M.; Kitahara, R.; Kamatari, Y. O.; Akasaka, K.; Xu, Y. *Cell. Mol. Biol. (Paris, Fr., Print)* **2004**, *50*, 311.
(92) Xu, Y.; Nogi, Y.; Kato, C.; Liang, Z.; Rueger, H.-J.; De Kegel, D.; Glansdorff, N. *Int. J. Syst. Evol. Microbiol.* **2003**, *53*, 527.
(93) Loveridge, E. J.; Allemann, R. K. *Biochemistry* **2010**, *49*, 5390.
(94) Wilquet, V.; Gaspar, J. A.; van de Lande, M.; van de Casteele, M.; Legrain, C.; Meiering, E. M.; Glansdorff, N. *Eur. J. Biochem.* **1998**, *255*, 628.
(95) Loveridge, E. J.; Matthews, S. M.; Williams, C.; Whittaker, S. B.-M.; Gu¨nther, U. L.; Evans, R. M.; Dawson, W. M.; Crump, M. P.; Allemann, R. K. *Biomolecular NMR assignments* **2012**.
(96) Loveridge, E. J.; Tey, L.-H.; Behiry, E. M.; Dawson, W. M.; Evans, R. M.; Whittaker, S. B.-M.; Günther, U. L.; Williams, C.; Crump, M. P.; Allemann, R. K. *J. Am. Chem. Soc.* **2011**, *113* 20561.
(97) Allemann, R. K.; Evans, R. M.; Tey, L.-h.; Maglia, G.; Pang, J.; Rodriguez, R.; Shrimpton, P. J.; Swanwick, R. S. *Philos. Trans. R. Soc., B* **2006**, *361*, 1317.
(98) Loveridge, E. J.; Behiry, E. M.; Swanwick, R. S.; Allemann, R. K. *J. Am. Chem. Soc.* **2009**, *131*, 6926.
(99) Loveridge, E. J.; Allemann, R. K. *ChemBioChem* **2011**, *12*, 1258.
(100) Loveridge, E. J.; Evans, R. M.; Alleman, R. K. *Chem.--Eur. J.* **2008**, *14*, 10782.
(101) Maglia, G.; Allemann, R. K. *J. Am. Chem. Soc.* **2003**, *125*, 13372.
(102) Sikorski, R. S.; Wang, L.; Markham, K. A.; Rajagopalan, P. T. R.; Benkovic, S. J.; Kohen, A. *J. Am. Chem. Soc.* **2004**, *126*, 4778.
(103) Swanwick, R. S.; Maglia, G.; Tey, L.-h.; Allemann, R. K. *Biochem. J.* **2006**, *394*, 259.
(104) Boehr, D. D.; McElheny, D.; Dyson, H. J.; Wright, P. E. *Science (Washington, DC, U. S.)* **2006**, *313*, 1638.
(105) Jackson, R. C. *in J. Pharm. Sci.* ; Sirotnak, F. M., Burchall, J. J., Ensminger, W. D., and Montgomery, J. A., ed.; Academic Press: Orlando, FL, 1985.
(106) Pang, J.; Pu, J.; Gao, J.; Truhlar, D. G.; Allemann, R. K. *J. Am. Chem. Soc.* **2006**, *128*, 8015.

(107) Allemann, R. K.; Evans, R. M.; Loveridge, E. J. *Biochem. Soc. Trans.* **2009**, *37*, 349.

(108) Klareskog, L.; van der Heijde, D.; de Jager, J. P.; Gough, A.; Kalden, J.; Malaise, M.; Mola, E. M.; Pavelka, K.; Sany, J.; Settas, L.; Wajdula, J.; Pedersen, R.; Fatenejad, S.; Sanda, M. *The Lancet* **2004**, *363*, 675.

(109) Mincer, J. S.; Schwartz, S. D. *The Journal of chemical physics* **2004**, *120*, 7755.

(110) Basner, J. E.; Schwartz, S. D. *The Journal of Physical Chemistry B* **2003**, *108*, 444.

(111) Masgrau, L.; Basran, J.; Hothi, P.; Sutcliffe, M. J.; Scrutton, N. S. *Arch. Biochem. Biophys.* **2004**, *428*, 41.

(112) Dann, J. G.; Ostler, G.; Bjur, R. A.; King, R. W.; Scudder, P.; Turner, P. C.; Roberts, G. C. K.; Burgen, A. S. V.; Harding, N. G. L. *Biochem. J.* **1976**, *157*, 559.

(113) Schwartz, D. E.; Rieder, J. *Chemotherapy* **1970**, *15*, 337.

(114) Nagel, Z. D.; Klinman, J. P. *Nat. Chem. Biol.* **2009**, *5*, 543.

(115) Stojković, V.; Perissinotti, L. L.; Willmer, D.; Benkovic, S. J.; Kohen, A. *journal of american chemical society* **2012**, *134*, 1738.

(116) Narayana, N.; Matthews, D. A.; Howell, E. E.; Xuong, N.-h. *Nat Struct Mol Biol* **1995**, *2*, 1018.

(117) Loveridge, E. J.; Tey, L.-H.; Allemann, R. K. *J. Am. Chem. Soc.* **2010** *132*, 1137.

(118) Andrews, J.; Clore, G. M.; Davies, R. W.; Gronenborn, A. M.; Gronenborn, B.; Kalderon, D.; Papadopoulos, P. C.; Schaefer, S.; Sims, P. F. G.; Stancombe, R. *Gene* **1985**, *35*, 217.

(119) Gargaro, A. R.; Soteriou, A.; Frenkiel, T. A.; Bauer, C. J.; Birdsall, B.; Polshakov, V. I.; Barsukov, I. L.; Roberts, G. C. K.; Feeney, J. *J. Mol. Biol.* **1998**, *277*, 119.

(120) Feeney, J.; Birdsall, B.; Kovalevskaya, N. V.; Smurnyy, Y. D.; Peran, E. M. N.; Polshakov, V. I. *J. Biochem.* **2011**, *50*, 3609.

(121) Benkovic, S. J.; Fierke, C. A.; Naylor, A. M. *Science* **1988**, *239*, 1105.

(122) Swanwick, R. S.; Shrimpton, P. J.; Allemann, R. K. *Biochemistry* **2004**, *43*, 4119.

(123) Stone, S. R.; Morrison, J. F. *Biochemistry* **1984**, *23*, 2753.

(124) Li, L.; Benkovic, S. J. *Biochemistry* **1991**, *30*, 1470.

(125) Posner, B. A.; Li, L.; Bethell, R.; Tsuji, T.; Benkovic, S. J. *Biochemistry* **1996**, *35*, 1653.

(126) Miller, G. P.; Benkovic, S. J. *Biochemistry* **1998**, *37*, 6336.

(127) Miller, G. P.; Wahnon, D. C.; Benkovic, S. J. *Biochemistry* **2001**, *40*, 867.

(128) McElheny, D.; Schnell, J. R.; Lansing, J. C.; Dyson, H. J.; Wright, P. E. *Proc. Natl. Acad. Sci. U. S. A.* **2005**, *102*, 5032.

(129) Davies, J. F., II; Delcamp, T. J.; Prendergast, N. J.; Ashford, V. A.; Freisheim, J. H.; Kraut, J. *Biochemistry* **1990**, *29*, 9467.

(130) Kovalevskaya, N. V.; Smurnyy, Y. D.; Polshakov, V. I.; Birdsall, B.; Bradbury, A. F.; Frenkiel, T.; Feeney, J. *J. Biomol. NMR* **2005**, *33*, 69.

(131) Wang, L.; Tharp, S.; Selzer, T.; Benkovic, S. J.; Kohen, A. *Biochemistry* **2006**, *45*, 1383.

(132) Wang, L.; Goodey, N. M.; Benkovic, S. J.; Kohen, A. *Proc. Natl. Acad. Sci. U. S. A.* **2006**, *103*, 15753.

(133) Wagner, C. R.; Benkovic, S. J. *Trends Biotechnol.* **1990**, *8*, 263.

(134) Venkitakrishnan, R. P.; Zaborowski, E.; McElheny, D.; Benkovic, S. J.; Dyson, H. J.; Wright, P. E. *Biochemistry* **2004**, *43*, 16046.

(135) Hammes-Schiffer, S.; Benkovic, S. J. *Annu. Rev. Biochem.* **2006**, *75*, 519.

(136) Zaborowski, E.; Chung, J.; Kroon, G.; Dyson, H. J.; Wright, P. E. *J. Biomol. NMR* **2000**, *16*, 349.

(137) Boekelheide, N.; Miller, T. F. *Abstracts of Papers, 241st ACS National Meeting & Exposition, Anaheim, CA, United States, March 27-31, 2011*, PHYS.

(138) El Omari, K.; Liekens, S.; Bird, L. E.; Balzarini, J.; Stammers, D. K. *Mol. Pharmacol.* **2006**, *69*, 1891.

(139) Klyuyeva, A.; Tuganova, A.; Popov, K. M. *Biochemistry* **2008**, *47*, 8358.

(140) Dupre, M. L.; Broyles, J. M.; Mihic, S. J. *Brain Research* **2007**, *1152*, 1.

(141) Hong, B. S.; Senisterra, G.; Rabeh, W. M.; Vedadi, M.; Leonardi, R.; Zhang, Y.-M.; Rock, C. O.; Jackowski, S.; Park, H.-W. *J. Biol. Chem.* **2007**, *282*, 27984.

(142) Chalissery, J.; Banerjee, S.; Bandey, I.; Sen, R. *J. Mol. Biol.* **2007**, *371*, 855.

(143) Li, Z.; Lukasik, S. M.; Liu, Y.; Grembecka, J.; Bielnicka, I.; Bushweller, J. H.; Speck, N. A. *J. Mol. Biol.* **2006**, *364*, 1073.

(144) Watney, J. B.; Agarwal, P. K.; Hammes-Schiffer, S. *J. Am. Chem. Soc.* **2003**, *125*, 3745.

(145) Gekko, K.; Kunori, Y.; Takeuchi, H.; Ichihara, S.; Kodama, M. *J. Biochem.* **1994**, *116*, 34.

(146) Gekko, K.; Yamagami, K.; Kunori, Y.; Ichihara, S.; Kodama, M.; Iwakura, M. *J. Biochem.* **1993**, *113*, 74.

(147) Smal s, A. O.; Leiros, H.-K. S.; Os, V.; Willassen, N. P. In *Biotechnology Annual Review*; Elsevier: 2000; Vol. Volume 6, p 1.

(148) Brandsdal, B. O.; Smalås, A. O.; Åqvist, J. *FEBS Lett.* **2001**, *499*, 171.

(149) Thorpe, I. F.; Brooks, C. L. *The Journal of Physical Chemistry B* **2003**, *107*, 14042.

(150) Rod, T. H.; Radkiewicz, J. L.; Brooks, C. L. *Proceedings of the National Academy of Sciences* **2003**, *100*, 6980.

(151) Mauldin, R. V.; Sapienza, P. J.; Petit, C. M.; Lee, A. L. *PLoS One* **2012**, *7*.

(152) Mauldin, R. V.; Lee, A. L. *Biochemistry* **2010**, *49*, 1606.

(153) Rajagopalan, P. T. R.; Lutz, S.; Benkovic, S. J. *Biochemistry* **2002**, *41*, 12618.

(154) Kohn, W. D.; Kay, C. M.; Hodges, R. S. *J. Mol. Biol.* **1997**, *267*, 1039.

(155) Baldwin, R. L. *Biophys. J.* **1996**, *71*, 2056.

(156) Collins, K. D.; Washabaugh, M. W. *Q Rev Biophys* **1985**, *18*, 323.

(157) Wright, D. B.; Banks, D. D.; Lohman, J. R.; Hilsenbeck, J. L.; Gloss, L. M. *J. Mol. Biol.* **2002**, *323*, 327.

(158) Attri, P.; Venkatesu, P.; Lee, M.-J. *J. Phys. Chem. B* **2010**, *114*, 1471.

(159) Kaufman, B. T. *Biochem. Biophys. Res. Commun.* **1963**, *10*, 449.

(160) Kaufman, B. T.; Gardiner, R. C. *J. Biol. Chem.* **1968**, *243*, 6001.

(161) Fan, Y.-x.; Ju, M.; Zhou, J.-m.; Tsou, C.-l. *Biochim. Biophys. Acta, Protein Struct. Mol. Enzymol.* **1995**, *1252*, 151.

(162) Binbuga, B.; Boroujerdi, A. F.; Young, J. K. *Protein Sci* **2007**, *16*, 1783.

(163) Timasheff, S. N. *Biochemistry* **1992**, *31*, 9857.

(164) Makhatadze, G. I.; Privalov, P. L. *J. Mol. Biol.* **1992**, *226*, 491.

(165) Watlaufer, D. B.; Malik, S. K.; Stoller, L.; Coffin, R. L. *J. Am. Chem. Soc.* **1964**, *86*, 508.

(166) Rossky, P. J. *Proceedings of the National Academy of Sciences* **2008**, *105*, 16825.

(167) Schellman, J. A. *Biopolymers* **1987**, *26*, 549.

(168) Perry, K. M.; Onuffer, J. J.; Touchette, N. A.; Herndon, C. S.; Gittelman, M. S.; Matthews, C. R.; Chen, J. T.; Mayer, R. J.; Taira, K.; Benkovic, S. J.; et al. *Biochemistry* **1987**, *26*, 2674.

(169) Dams, T.; Jaenicke, R. *Biochemistry* **1999**, *38*, 9169.

(170) Wu, J.-W.; Wang, Z.-X.; Zhou, J.-M. *Biochem. J.* **1997**, *324*, 395.

(171) Van de Casteele, M.; Legrain, C.; Wilquet, V.; Glansdorff, N. *Gene* **1995**, *158*, 101.

(172) Fan, Y.-x.; Ju, M.; Zhou, J.-m.; Tsou, C.-l. *Biochem. J.* **1996**, *315*, 97.

(173) Maglia, G., The University of Birmingham, 2003.

(174) Miller, G. P.; Benkovic, S. J. *Biochemistry* **1998**, *37*, 6327.

(175) Xu, Y.; Nogi, Y.; Kato, C.; Liang, Z.; Rüger, H.-J.; De Kegel, D.; Glansdorff, N. *Int. J. Syst. Evol. Microbiol.* **2003**, *53*, 533.

(176) Jaenicke, R.; Schurig, H.; Beaucamp, N.; Ostendorp, R. In *Advances in Protein Chemistry*; Frederic M. Richards, D. S. E., Peter, S. K., Eds.; Academic Press: 1996; Vol. Volume 48, p 181.

(177) Scrutton, S. H. a. N. S. *Nature Chemistry* **2012**, *4*, 161.

(178) Glowacki, D. R.; Harvey, J. N.; Mulholland, A. J. *Nat Chem* **2012**, *4*, 169.

(179) Bhabha, G.; Ekiert, D. C.; Jennewein, M.; Zmasek, C. M.; Tuttle, L. M.; Kroon, G.; Dyson, H. J.; Godzik, A.; Wilson, I. A.; Wright, P. E. *Nat Struct Mol Biol* **2013**, *20*, 1243.

9

Appendix

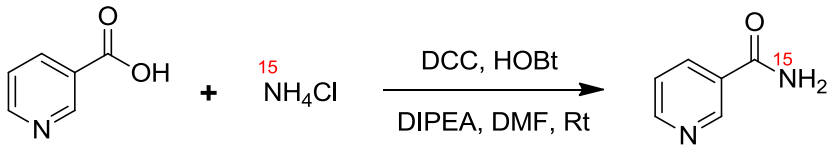

Scheme 1: Formation of ^{15}N-nicotinamide.

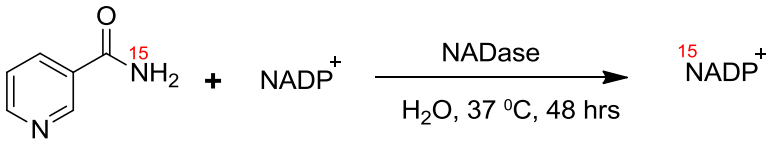

Scheme 2: Formation of ^{15}N-NADP$^+$

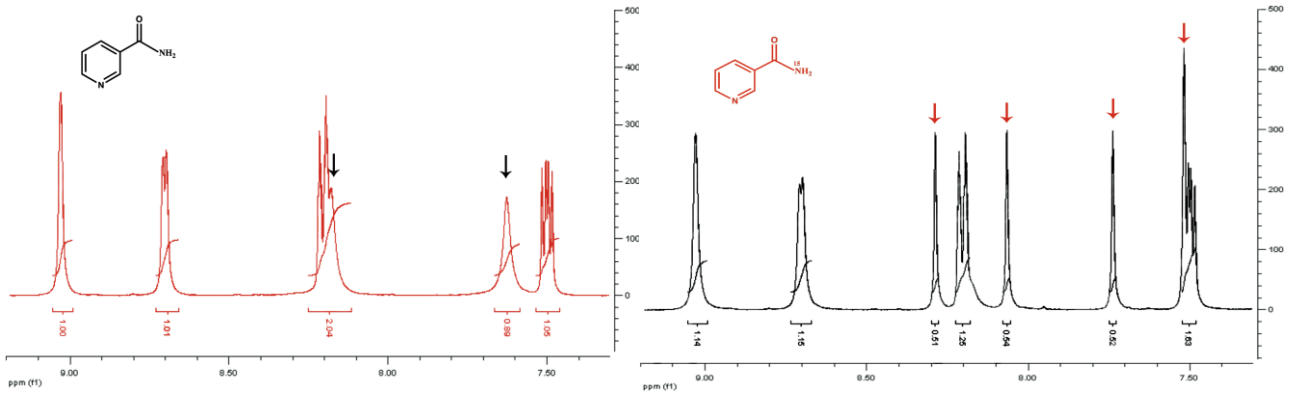

Figure I.1: ^{1}H-NMR spectra in d_6-DMSO of nicotinamide (left, red) and ^{15}N-nicotinamide (right, black). The peaks of the amide protons are indicated.

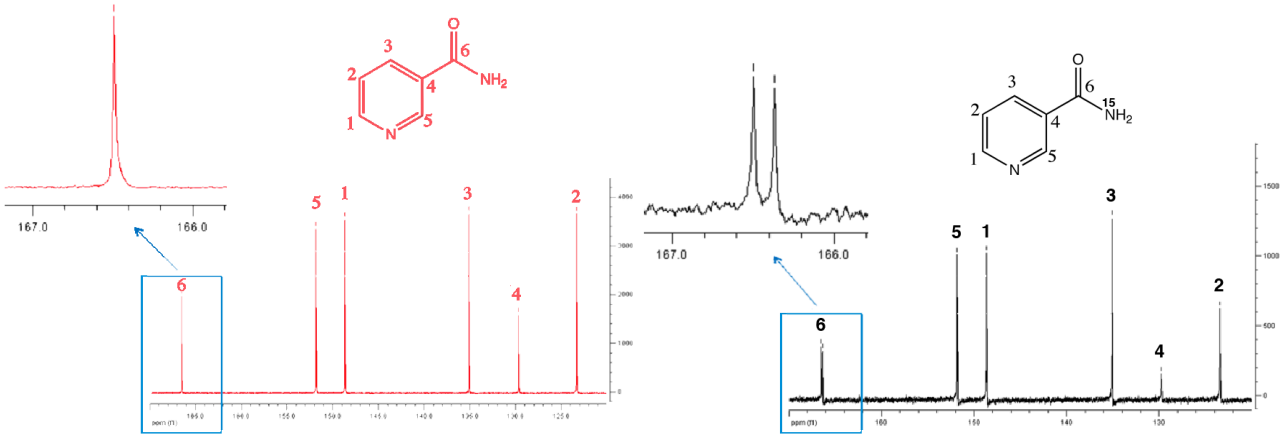

Figure I.2: ^{13}C-NMR spectra in d_6-DMSO of nicotinamide (left, red) and ^{15}N-nicotinamide (right, black), showing the splitting of the amide carbonyl peak by ^{15}N.

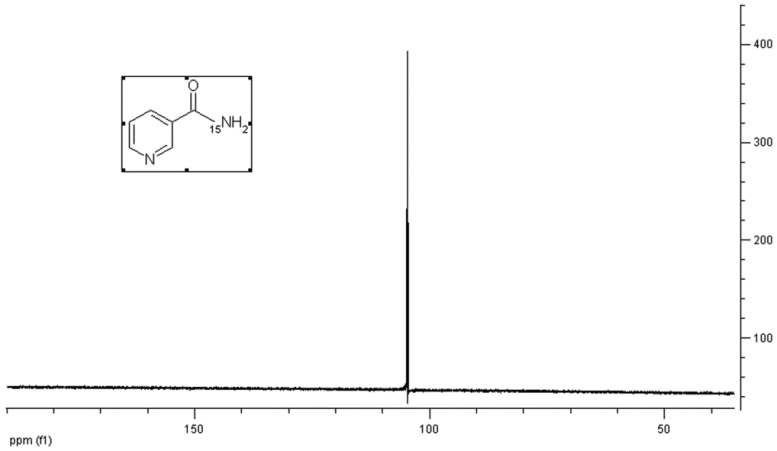

Figure I.3: ^{15}N-NMR spectrum in d_6-DMSO of ^{15}N-nicotinamide.

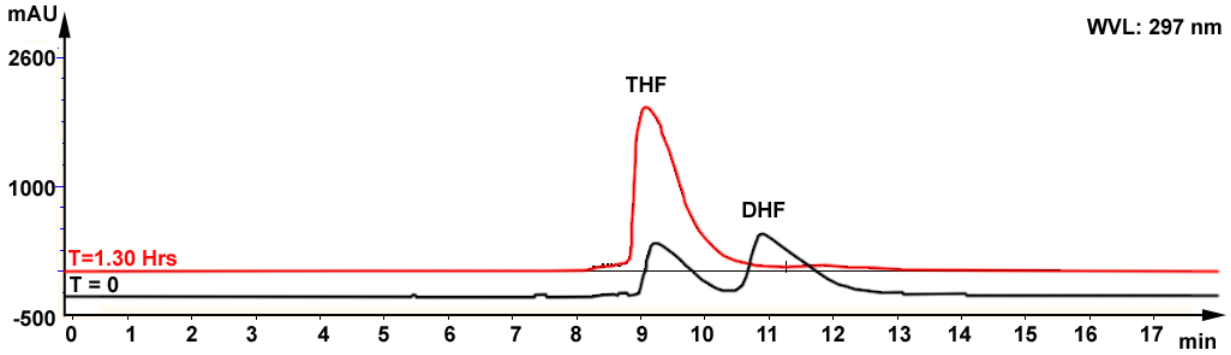

Figure I.4: FPLC trace for the preparation of tetrahydrofolate (THF) from dihydrofolate (DHF) using dihydrofolate reductase (DHFR).

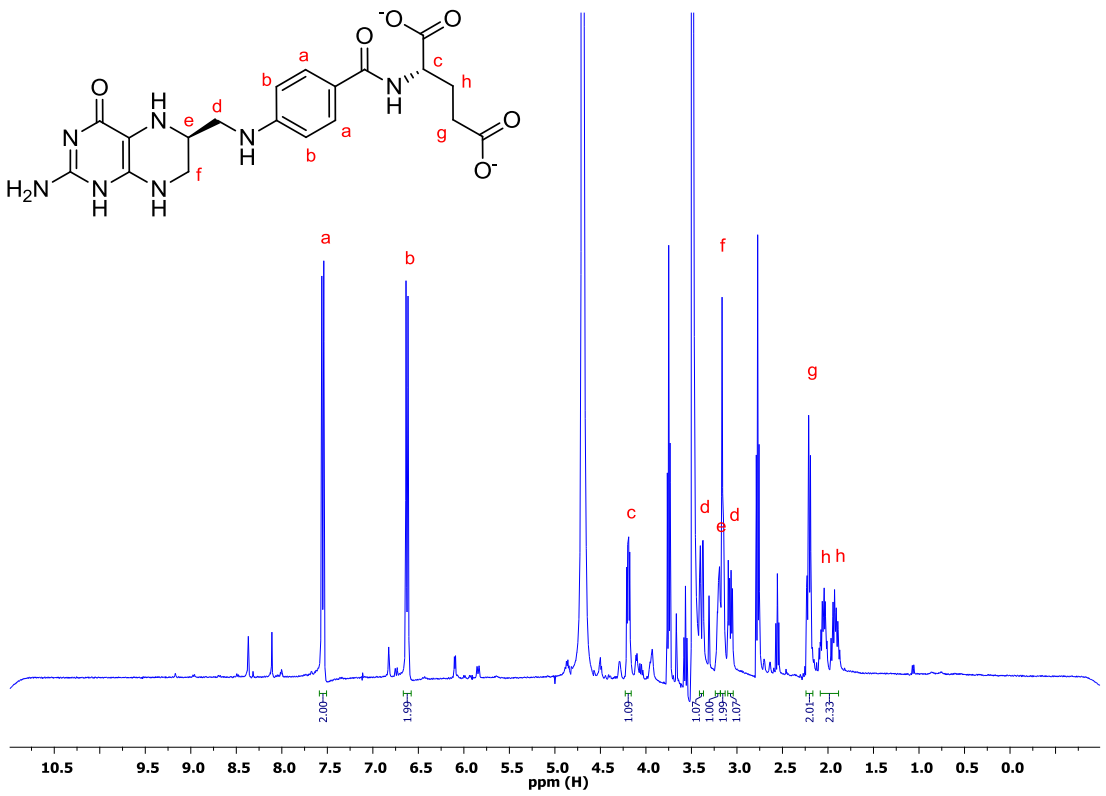

Figure I.5: ^{1}H-NMR spectrum in D_2O of tetrahydrofolate (THF).

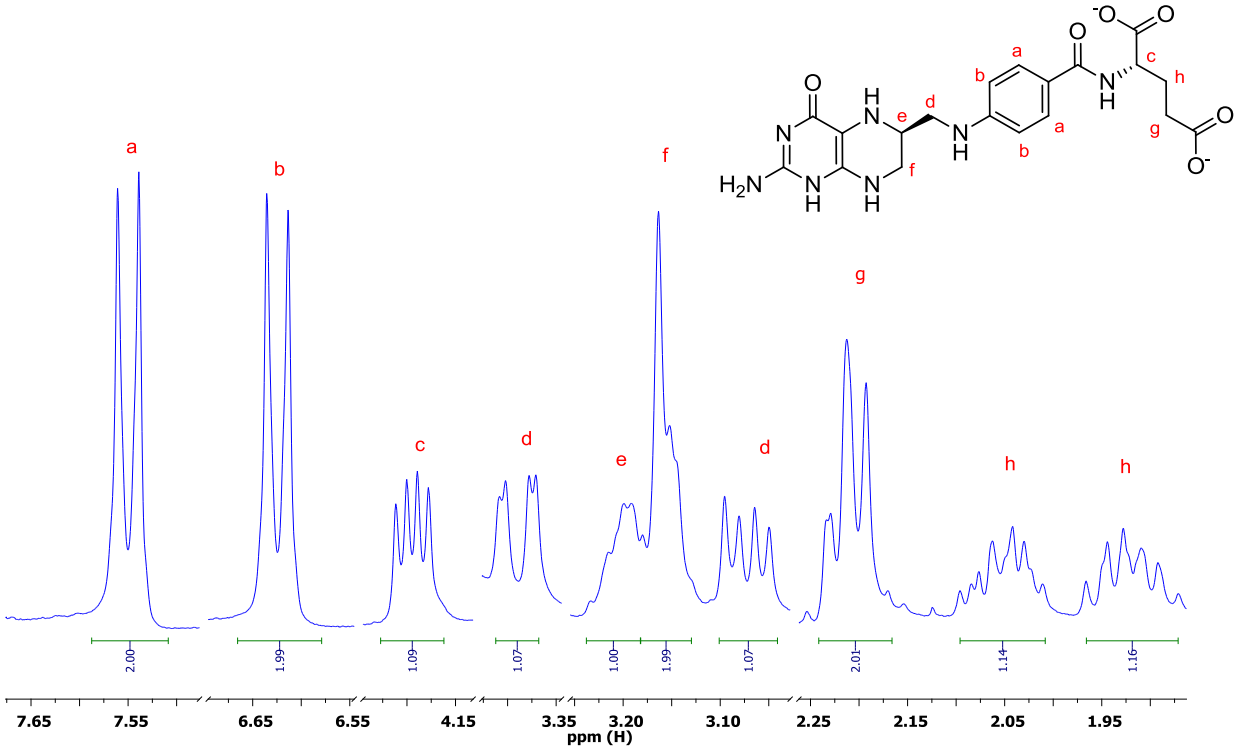

Figure I.6: Expansion of ^{1}H-NMR spectrum of tetrahydrofolate (THF) in D_2O showing the chemical structure and corresponding peak integration.

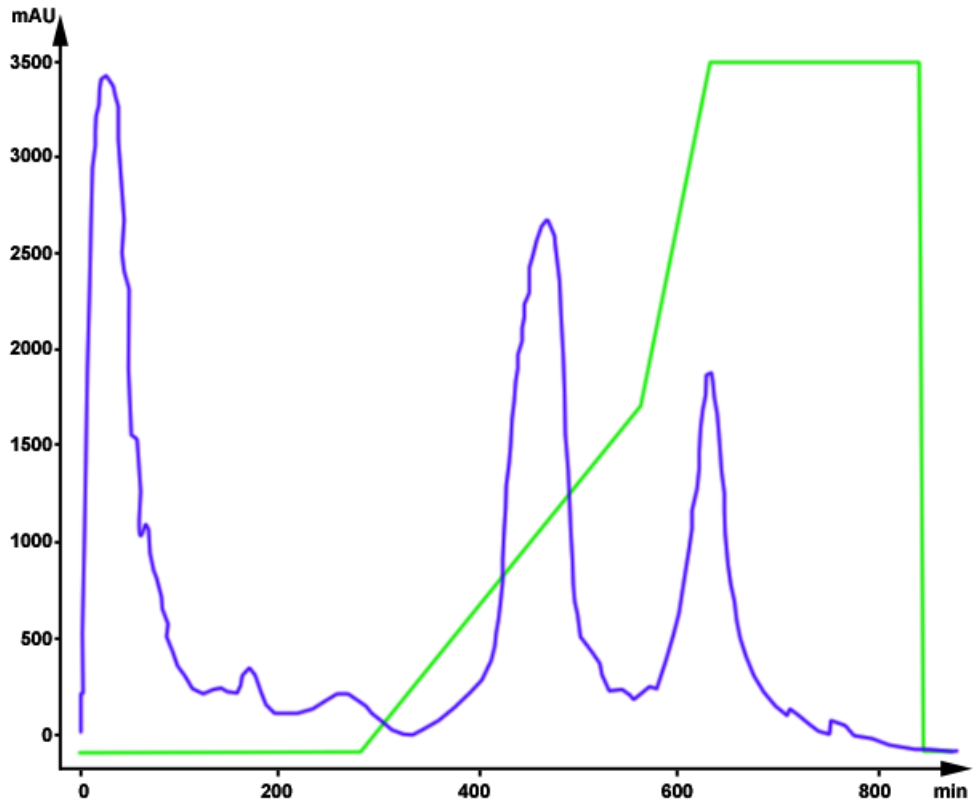

Figure I.7: FPLC trace (absorption at 280 nm, purple line) showing the elution of DHFR from Q-sepharose anion exchange resin using a 0-1 M NaCl gradient (green line).

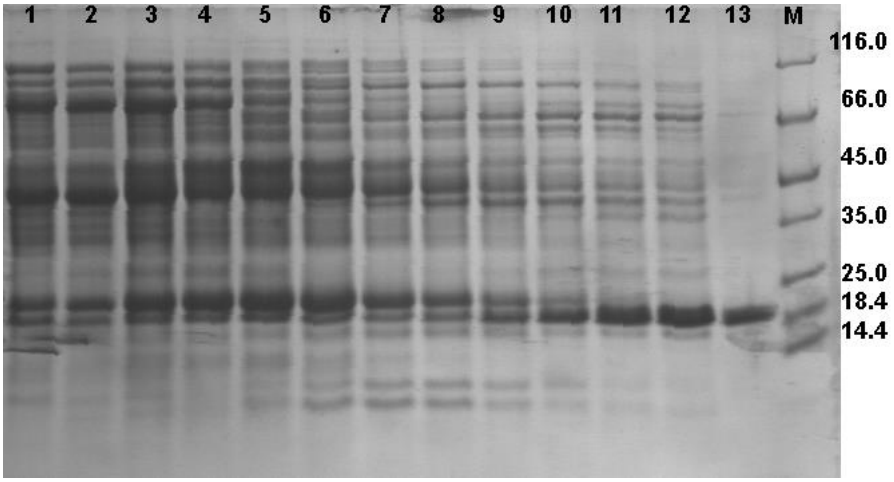

Figure I.8: 10% SDS-PAGE gel showing purification of MpDHFR. lane 1 to 12: fractions collected during Q-sepharose purification, lane 13: pure DHFR after elution from a Superdex75 size exclusion column. M: protein molecular markers shown in kDa.

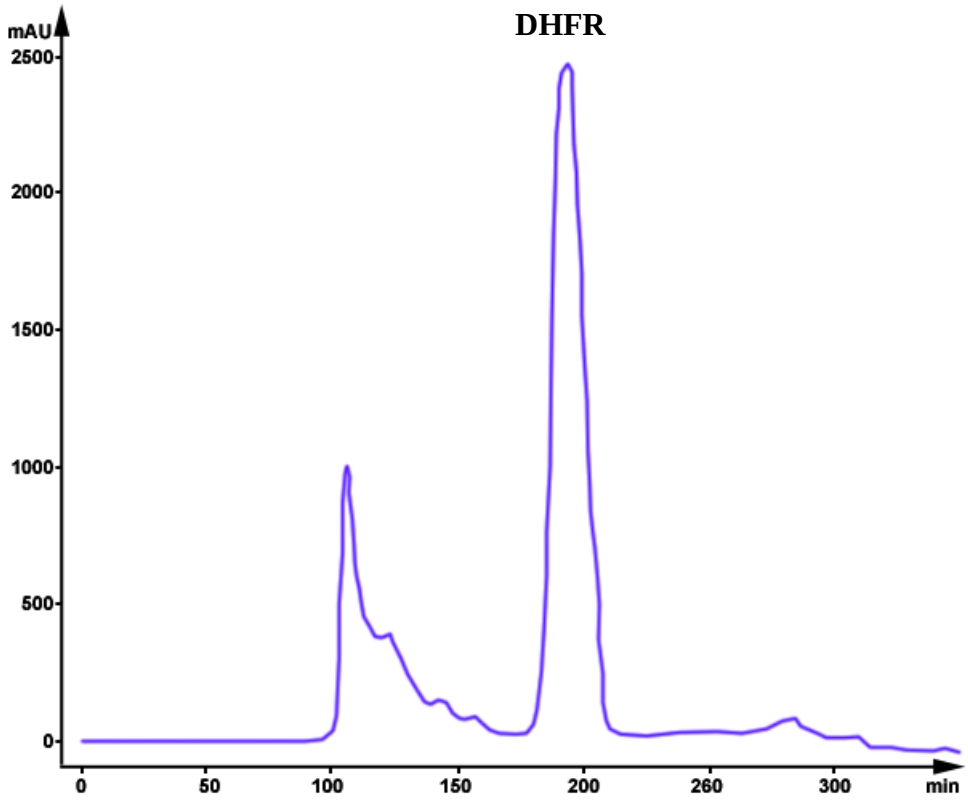

Figure I.9: FPLC trace (absorption at 280 nm) for the purification of DHFR using a Superdex75 size exclusion column.

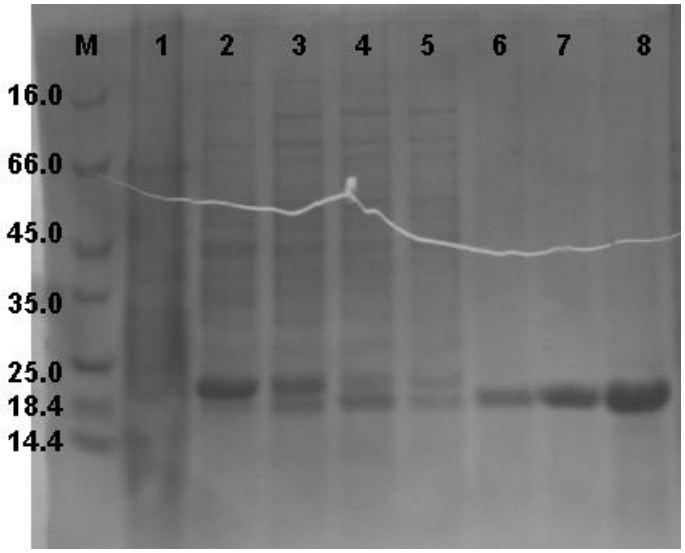

Figure I.10: 10% SDS-PAGE gel showing purification of MpDHFR. M: protein molecular markers shown in kDa, lane 1: supernatant solution, lanes 2 to 5: protein after Q-sepharose purification, lanes 6 to 8: pure DHFR after elution from the Superdex75 size exclusion column.

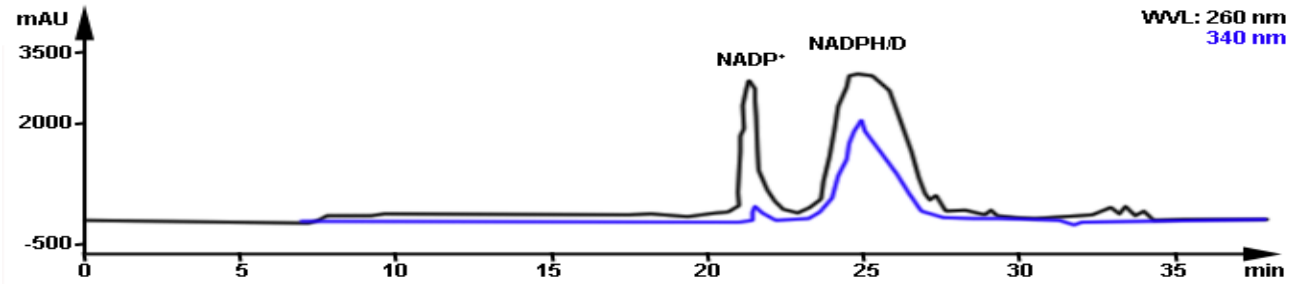

Figure I.11: FPLC trace for the preparation of reduced nicotinamide dinucleotide phosphate (NADPH/D) from the oxidized nicotinamide dinucleotide phosphate ($NADP^+$).